RICE UNIVERSITY

Dimension Controlled Self-Assembly of Perylene Based Molecules

by

Arshad S. Sayyad

A THESIS SUBMITTED
IN PARTIAL FULLFILLMENT OF THE
REQUIREMENTS FOR THE DEGREE

Doctor of Philosophy
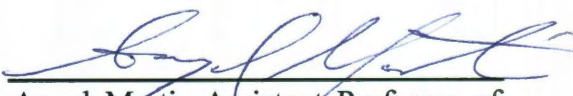
Approved, Thesis Committee:

Pulickel M. Ajayan, Chair, Benjamin
M. and Mary Greenwood Anderson
Professor in Engineering and
Professor of Mechanical Engineering
and Materials Science and Chemistry

Lon Wilson, Professor of Chemistry

Angel Marti, Assistant Professor of
Chemistry and Bioengineering

Houston, Texas

DECEMBER 2010

ABSTRACT

Dimension Controlled Self-Assembly of Perylene Based Molecules

by

Arshad S. Sayyad

Recent advances in the self-assembly of highly organized structures of organic semiconducting molecules by controlled non-covalent interactions has opened avenues for creating materials with unique optical and electrical properties. The main focus of this thesis lies in the synthesis and self-assembly of n-type perylene based organic semiconducting molecules into highly organized materials. Perylene based molecules used in this study are perylene diimide (PTCDI, two side-chains), perylene mono imide (m-PTCI, one side-chain), perylene tetracarboxylic acid (PTCA, no side-chain) and tetra-alkali metal salts of PTCA (M_4-PTCA, no side-chain), which are synthesized from the parent perylene tetracarboxylic dianhydride (PTCDA). The self-assembly of these molecules have been performed using solution processing methods (dispersion, phase-transfer, and phase-transfer at high temperature) by taking advantage of the changes in solubility of the molecules, wherein the molecular interactions are maximized to favorably allow for the formation of highly organized structures.

Dimension control (1D, 2D and 3D structures) of self-assembly has been obtained for different perylene based molecules by appropriate design of the molecule followed by controlling the conditions of assembly. In case of PTCDI, a new solution processing method phase-transfer at high temperature (2L-HT) allowed for the controlled formation of extremely long and fluorescent 1D structure. For the m-PTCI molecules the

organization by the 2L-HT method was found to result in highly organized, single-crystalline, fluorescent 2D sheets.

In the case of perylene based molecules with no side-chains two different methods have been developed for the realization of organized 1D nanostructures. The first method utilizes the chemical conversion of a highly soluble PTCA into 1D nanofibers of the parent insoluble perylene tetracarboxylic anhydride. The second method utilizes the assembly of tetra potassium salt of PTCA (K_4-PTCA) into 1D nanostructures. Furthermore, it has been demonstrated that these 1D nanostructures can be chemically converted to two different chemical species, both of which still retain the 1D morphological characteristic, though with changes in the size. Various functional self-assembled structures developed in this thesis opens up new avenues to explore structure-property-function relationships and their use in applications such as sensors, electronics and opto-electronic devices.

Acknowledgement

The past five years that I have spent at Department of Chemistry, Rice University for my doctoral studies have been a wonderful and great learning experience. I would not miss this great opportunity to express my gratitude and thanks to all those who are involved in completion of this thesis. This has always been a collective effort and many people deserve to be acknowledged.

First and foremost, I would like to sincerely thank my research advisor Prof. Pulickel M. Ajayan for his generosity and giving me an opportunity to work in his group. Above all, his considerable support, patience and direction in various ways throughout my doctoral studies helped me to successfully complete my thesis. Special thanks to Dr. Kaushik Balakrishnan, post doctoral research associate in Ajayan's research group for his enormous help especially in making of this thesis. His key advices that I received during my entire Ph.D journey has enriched me with valuable knowledge which I am sure would help me in the near future. I have benefited immensely by his continuous supervision, guidance in polishing my writing and presentation skill and various scientific discussions on the various topics in this thesis. I am heartily gratified for his contributions and effort without which it would have been hard for me to step forward.

I gratefully acknowledge Prof. Ahmad Kabbani, professor of Chemistry, Lebanese American University, who frequently visited Ajayan's research group as a visiting scholar. He has always tried to provide me with an insight on various subjects, taught me the significance of research and patiently helped me in correcting my errors. Also, he has been a great supporting factor during my ups and downs at Rice University. I thank you Dr. Ahmad T. Kabbani for your love and affection that you showed towards

me. I also wish to thank Prof. Eugene Zubarev, Associate professor of chemistry, Rice University for all his support and guidance that he provided me in the first two years of my stay at Rice University. He has been greatly instrumental in developing a scientific aptitude and problem solving skills in me which I think will benefit me for my entire life. My special thanks to all my teachers at Institute of chemical technology (Formerly known as UDCT) for their guidance and teachings. My sincere thanks to Dr. Wahegaokar for helping me to develop an interest in chemistry and directing me to UDCT for my further studies which helped me enormously to become a part of department of chemistry at Rice University.

I would also like to thank the entire team members of Ajayan's research group for creating a friendly and enthusiastic atmosphere and for various technical and scientific group discussions for shaping up my ideas. I would like to specially thank all the staff members of shared equipment authority at Rice University for providing the training on various instruments which I used for the characterization of my samples in this thesis. Additionally, I wish to thank Prof. Michael Wong and Dr. Angel Marti for their help and assistance in using the fluorescence spectrometer and Dr. Karin Keller, University of Texas, Austin for her help with the mass spectroscopy of my samples. I am grateful to all the staff members of the department of chemistry and department of mechanical engineering and material sciences for providing various services throughout my Ph.D.

Special thanks to all my special friends to whom I treasure the most. Words fall short when it comes to describe my friends and their tremendous support during my stay at Rice University. If these friends would not have patiently stood behind me during my hardships, I would have been disheartened and discouraged in completing my Ph.D.

Achin, Tilok, Sachin, Jai, Benny, Pramit, Bishnu, Anubha, Shilpi, Gaurav and Mansi, I sincerely and specially thank each one of you for incredible support and care. I would also like to thank all my cousins for admiring and cheering me which have served as a great motivation towards completion of this thesis.

I am indebted to all my family members who always played a crucial role in providing me with moral and financial support. I would wish to thank my wife for her love and all the emotional support, for helping me during difficult times and to be an important part of my life. Behind all my achievements and all the way throughout this long journey lies the dedication and hardship of the real people, my parents and my sister. I am fortunate to have them in my life. They have always been a source of inspiration and motivation during my entire career at Rice University. Special thanks to my mother for her supporting words, love and remembering me in her prayers that gave me energy to work hard. To them I dedicate this thesis. Thanks to almighty God for giving me strength and helping me to reach my goal.

Table of Contents

List of Figures

formation of perylene-3,4,9,10-tetracarboxylic-3,4,9,10-dianhydride (PTCDA) and stable

urea product. Path B: N-acylpyridinium intermediate can be formed from O-acylisourea

in presence of DPTS, which undergo reaction with their neighboring carboxylic acid

List of Schemes

List of Tables

CHAPTER 1

Self assembly of organic semiconductors

1.1. Introduction to organic semiconductors

Organic semiconductors mainly consist of organic molecules having alternating single (σ-) and double (σ- and π-) bonds leading to high degree of conjugation due to presence of π-electrons in their structure. The organic semiconductors have emerged as promising candidates for various applications in electronics and optoelectronics.[1-7] For a considerable period of time, it was believed that the conjugated organic molecules possess large intermolecular distances and hence were regarded as insulators. In 1954, the complex of bromine doped perylene was shown to have conducting properties which was believed to be possible because of presence of bromine.[8] In 1963, Siudak et al.[9] observed the conductivity in case of iodine doped polypyrrole complex but very little interest was paid towards this work. The work of organic charge transfer complexes by Heeger et al.[10,11] for both conductivity and superconductivity and McGinness et al.[12] on the conductivity of melanin based compounds further advanced the scope for the organic materials for use in electronic devices. In 1977, Heeger and co-workers published a first report on electrical conductivity in case of iodine-doped polyacetylene.[13,14] This ground breaking research in the field of conducting polymers was awarded the Nobel Prize for Chemistry in 2000. Since this discovery, a wide variety of organic semiconductors have been synthesized and have been exploited for their applications in devices such as transistors,[15] diodes,[16,17] photovoltaics[18] and sensors.[19]

Traditionally, inorganic semiconductors such as silicon (amorphous, polycrystalline or single crystalline) have been demonstrated for various electronic and optoelectronic

applications.[20-22] Inorganic semiconductors have high stability towards environment leading to increased device lifetimes.[23] They have very high charge-carrier mobility, thermal and mechanical stability.[24] Despite these advantages there are several disadvantages of inorganic semiconductors. They are expensive, brittle (cannot withstand mechanical deformation) and hence light weight flexible devices are beyond realization. Very high processing temperatures above 600°C are required and their modification of properties is very limited and restricted.[25] On the other hand, organic semiconductors hold many advantages in comparison to the inorganic semiconductors. Organic semiconductors include the ability to introduce wide range of functional groups in their structure through organic synthesis thus leading to the fine tuning of their optical and electrical properties.[26] Their solubility in wide range of solvents enables to utilize low-cost solution processing techniques for the formation of ordered structures and fabrication of devices on the flexible transparent plastic substrates at low temperature.[27-29] Efficient charge transport behavior of the various organic semiconducting materials have led to their application as organic light emitting diodes (OLED), light harvesting applications such as solar cells, field effect transistors (FET) etc.[1-7] Considerable research efforts, by appropriate design and modification of architectures, have now led to much improved performances (in comparison to the prototypes) and efficiencies (in terms of transport characteristics) close to amorphous inorganic silicon based semiconductors have been already achieved.[30]

Organic semiconductors can be classified into four categories namely small molecules, oligomers, dendrimers, and polymers.[31] Small molecules have very well defined molecular weight on the other hand polymers, which consist of monomers as the

repeating units are polydisperse and hence do not have well defined molecular weights. Oligomers and dendrimers have defined number of monomers and hence well defined molecular weights and their properties lie in between small molecules and polymers. Depending upon the majority charge carriers present in the organic semiconductors, they are classified as electron accepting materials (n-type)[32] or electron donating materials (p-type).[33] The charge carrier mobility, μ (measured in cm^2/Vs) and the conductivity, σ (measured in S/cm) determines the efficiency of charge transport through these materials. Metals have high conductivities ($\sigma \geq 10^3$ S/cm) on the other hand insulators have low conductivities ($\sigma \leq 10^{-12}$ S/cm). Semiconductors have conductivity in between metals and insulators.[34] The charge transport in organic semiconductors is not governed by the classical band theory, as found in case of inorganic semiconductors, owing to very weak coupling between adjacent organic molecules.[35,36] Though the mechanism of operation for the organic semiconducting molecules remains elusive, the phonon assisted hopping model best describes the charge transfer in most of the cases, in which the energy for hopping is provided by the lattice vibrations.[37,38] The high rate of hopping (or high charge carrier mobilities) depends on effective electronic coupling between the adjacent sites and hence in order to have high charge mobilities, a dense packing of molecules is highly desirable.[39] Some other key desirable properties include high purity of the molecules, large grain size and structural defects should be as less as possible in order to avoid trapping of the charges leading to decreased mobilities.[40] Self-assembly of active channel organic materials can be utilized to attain some of the desired properties essential for obtaining high quality, and ordered organic materials for the fabrication of devices and remains a key focus of research despite the impressive records already demonstrated.

1.2 Self-assembly of organic semiconductors

Self-assembly refers to the spontaneous organization of an appropriately designed molecule under appropriate conditions by non-covalent forces of interactions.[41-44] Essentially, the self-assembly is a bottom-up method for the realization of ordered structures and is well suited for the current fabrication techniques (such as top-down methods, e-beam and photolithography) for the device fabrication. Therefore, research on organic semiconductors has also focused heavily on the synthesis of molecules by design, which includes not only the ability for the tailored organic molecules to interact via non-covalent forces but also the ability to attain desired electrical and optical characteristics needed for device fabrication. Some of the common non-covalent interactions used for the self-assembly of organic semiconductors rely on the use of π-stacking, H-bonding, electrostatic, hydrophobic and van der Waals forces of interactions. Despite the utilization of these weak forces of interactions highly organized and stable materials have already been created. A variety of examples have been demonstrated for the self-assembly of designed active channel organic compounds in different environments such as solid (surfaces, interfaces, etc.) and solution (interface, etc.) for the organic semiconductors ranging from small molecules to polymers.[45-48] The resulting structures are also referred to as supramolecular structures because of the large number of individual units present in the final assembled structures.

Recently, supramolecular electronics that bridges the gap between the molecular electronics (having Ångstrom dimensions) and the bulk electronics (having micro- to milli-meter range) has gained a lot of importance.[49] The self-assembly has been utilized to generate ordered supramolecular structures. Often, to create ordered structures such as

one dimensional (1D) structures particularly from the small organic molecules, π-stacking interactions are utilized. It is expected that the formation of ordered structures by strong π-stacking interactions (e.g. face-to-face packing) between the planar semiconducting aromatic molecules could lead to materials with good charge transport characteristics for exploitation in device fabrication.[50,51] Essentially, the packing of the molecules within the organized structure allow for the determination of the final properties and therefore their characteristic performance. Thus, presently the research in the self-assembly of organic semiconductors focuses heavily on understanding the *structure-property-function* relationships. By comprehending such relationships it will be possible to improve the design of the molecules and their assemblies for obtaining high quality materials with desired characteristics for use in a range of applications.[48]

The increased electronic wave function coupling between the neighboring molecules in the stacks leads to an increase in bandwidth thus correlating to the increased electrical conductivity found in these materials.[52] The strong π-π interactions between these extended aromatic systems have been utilized to realize various 1D nanostructures such as nanotubes, nanoribbons, nanowires and nanofibers. The use of self-assembly to generate 1D nanostructures from functional organic materials is particularly attractive and is expected to have far reaching effects in the field of nanoscale photonics and electronics because of their extraordinary morphological and opto-electronic properties.[53] Owing to the strong electronic coupling between these molecules due to the π-π interactions, the charge transport characteristics are expected to be efficient along the long axis of the nanostructures, especially in case of 1D structures.[50,51] These 1D nanostructures have been realized for various applications like vapor sensors,[54,55]

phototransistors,[56,57] solar cells[58] and as an active channel materials for use in field effect transistors.[59,60] The morphology, properties, and therefore the characteristic transport behavior is a direct result of packing of these molecules in solid state.[61,62] Highly ordered single-crystalline nanostructures are most desirable to study various transport mechanisms,[63,64] structure-property-function relationships,[65] and effect of domain size[64,66] in microstructures which govern most the performances of these materials.

Various solution processing methods have been developed for fabricating 1D nanostructures.[48,67-69] These techniques have been utilized to self-assemble organic semiconducting molecules into highly crystalline 1D nanostructures either in solution or substrate-solution interface. Owing to the cost effectiveness and ease of processing,[70-72] there is a growing need to explore various solution processable methods leading to very uniform organic single crystal nanostructures thus exhibiting high transport characteristics.[68,73-77] The morphology and packing of the organic molecules can be tailored by realizing the self-assembly utilizing various solvents. Moreover, the self-assembled materials by solution processing can be transferred to variety of substrates for device fabrication or characterization, provided the molecular interactions are sufficiently stronger than those of the molecule-surface interactions.

In order to realize the self-assembly of polymers into 1D nanostructures by solution processing methods various side chains are attached to polymer backbone (π-rich structure). This allows for increasing the solubility mainly in organic solvents.[78] The presence of bulky side chains attached to the polymers can lead to the disruption of the planarity (of the π-conjugated backbone) and therefore have pronounced effect on formation of ordered aggregates upon self-assembly.[79-81] On the other hand linear alkyl

side chains tend to retain the planarity (of the π-conjugated backbone) and allows for obtaining ordered aggregates.[82,83] For example, the above concept has been widely demonstrated in case of the poly(3-alkylthiophene) polymers.[84,85] Similarly, well defined nanowires can be also be fabricated form block co-polymer namely poly(3-hexylthiophene)-b-poly(styrene) by π-π stacking interactions.[86,87] Similar side-chain effects have also been observed in case of oligomers, and small molecules. In all of the studies involving exclusively π-stacking of alkyl-substituted π-conjugated cores the assembly is a direct function of co-operative interaction of the lateral side-chain interdigitation (by hydrophobic interactions) and the essential π-stacking. The morphology thus depends largely on the domination of one interacting force over the other. Furthermore, H-bonding interactions along with π-stacking interactions have also been utilized for the realization of organized 1D nanostructures based on the domination or co-operative presence of the multiple interactions leading to stable structures.[47,48,88] Thus, the side chain modulation is an essential parameter for the self-assembly of organic semiconducting molecules.

The role of side chains attached to the π-conjugated small molecules has also been extensively studied for the self-assembly by solution processing.[89-93] For example, Mullen et al.[94,95] demonstrated unusual liquid crystalline behavior and high charge carrier mobility from alkyl subsitituted hexa-peri-hexabenzocoronene (HBC), a widely studied organic semiconducting molecule. In case of a C_{12}-HBC, the dodecyl side chains interdigitate amongst each other, thus enhancing the π-π interactions of the planar HBC core resulting in uniform 1D nanofibers by the slow drying of the solvent (THF).[45,46] In this study, Mullen et al. have demonstrated the side-chain substitution effects on a wide

variety and with different number of end group functionalization and their morphological traits and concomitantly their effects on the transport characteristics. Another solution processing method that has been widely used especially for HBC relies on the solvent exchange. In this process the molecules are transferred from a solvent, in which the molecules exist in homogeneously dissolved state, to another solvent in which the molecule has no solubility. This allows for the rapid interaction of the π-rich surfaces to allow for the formation of 1D structures. One of the most elegant examples for the self-assembly by design of the HBC molecule has been shown by Aida et al.[96] The amphiphilic HBC molecules having two dodecyl side chains and two triethylene glycol chains allowed for the formation of 1D nanotubes by the π-stacking and side chain interdigitation interactions.[96] The self-assembled nanotubes are realized by forming uniform solution of this amphiphilic molecule in THF at 50°C and slow cooling to 30°C. Thus, all these solution based methods based on aggregation (by precipitation) leads to the formation of ordered 1D nanostructures of planar and π-conjugated semiconducting organic molecules.

While the synthesis and self-assembly of various molecules exhibiting p-type behavior have been widely studied, the synthesis and self-assembly of n-type organic semiconducting molecules have recently started attracting attention. Chapter 2 will discuss about the synthesis and self-assembly of perylene diimides (PTCDI) which fall into a rare category of n-type organic semiconducting molecules. Several research groups have synthesized various PTCDI molecules having various functional groups in their structure and they have been further self-assembled into ordered structures based on various interactions such as metal ligand, ionic, hydrogen bonding and π-π stacking. The

ordered self-assembled structures from these molecules have been utilized for the fabrication of various electronic and opto-electronic applications.

Chapter 3 is focused on synthesis and self-assembly of planar symmetric PTCDI molecules having varying length of alkyl side chains attached to the perylene core. Various solution processing conditions such as dispersion, phase transfer at room temperature and phase transfer at high temperature (a new method developed and reported in this thesis) have been explored for controlling the size of the resultant 1D structures by self-assembly. The role of solvents and effect of the side chains attached to the PTCDI on the final morphology of the 1D structures have also been studied. The newly developed solution process namely two layer phase transfer at high temperature (2L-HT) has been utilized to generate millimeter long wires from these molecules by slow nucleation and growth process which show a very intense excimer emission. This has direct implications for applications in organic light emitting, photovoltaics and sensors.

Chapter 4 will focus on the synthesis and self-assembly of perylene monoimides (m-PTCI) having only one hydrophobic alkyl side chain attached to perylene core. The self-assembly of m-PTCI have been carried out by the newly developed two layer phase transfer method leading to the formation of highly crystalline two dimensional (2D) sheets. The optical properties of these sheets have also been studied.

3,4,9,10-Perylenetetracarboxylic dianhydride (PTCDA) represents one of the extensively studied material for organic electronics and opto-electronics applications and is the starting material for the synthesis of PTCDI. The well defined nanostructures of this material have relied on the heavy use of vapor-phase methods. However, solution

processing of such insoluble materials remains a challenge to-date. In chapter 5, chemical reaction mediated self assembly have been utilized to generate crystalline 1D nanofibers of PTCDA. For this purpose a highly soluble perylene tetracarboxylic acid (PTCA) has been converted to highly insoluble PTCDA by utilizing the carbodiimide chemistry. This particular chemical transformation wherein the system transforms from homogeneous state to an aggregated state, leads to in situ formation of 1D nanofibers of PTCDA.

In Chapter 6 the self-assembly of perylene based salts from their aqueous solutions have been explored. Various tetra alkali metal salts of perylene tetracarboxylic acid (M_4-PTCA) were utilized for self-assembly process. It was found that the self-assembly in this system is a very sensitive function of the processing conditions leading to the formation of 1D, 2D and 3D self-assembled structures. Further, the self-assembled 1D nanostructures formed in this system have been chemically modified. The changes in the morphology of these self-assembled 1D structures due to the chemical modification have been also studied.

CHAPTER 2

Synthesis and Self-Assembly of Perylene Tetracarboxylic Diimides

2.1 Introduction

Perylene tetracarboxylic diimides (PTCDI) have been widely studied owing to their high chemical, electrochemical and photochemical stability along with their ability to act as electron acceptors (*n-type*).[97] Since their use in prototype organic photovoltaic devices[3,98,99] and xerographic applications[100] these materials have formed an important class of molecules to be utilized in a variety of applications. There are very few n-type organic materials and therefore demand for these molecules is rather large. PTCDI are electron deficient and exhibit two reversible one electron reductions[97] and have been used as an electron acceptors in photoinduced charge transfer systems.[99,101-103] Electron mobility as high as 1.7 cm^2/Vs have been observed for the films deposited by vapor deposition methods of N,N'-dioctadecyl-3,4,9,10-perylene diimide.[104-106] Thus, PTCDI molecules represent the best organic electron transport materials available till date.[107]

PTCDI have a strong tendency to aggregate by π-stacking interactions and various research groups have utilized this ability to form ordered 1D structures. This self-assembly of PTCDI leads to strong electron coupling and hence results in improved charge transfer properties. This chapter will discuss the synthesis and self-assembly of PTCDI. Fabricating well defined self-assembled structures from n-type organic semiconductors opens up new areas of research to explore their use in applications such as sensors, photovoltaics (OPV), light emitting diodes (OLED) and complementary inverter devices based on Field effect transistor (FET).

2.2 Perylene tetracarboxylic diimides (PTCDI)

The perylene tetracarboxylic diimides (PTCDI) also known as perylene bisimides or perylene diimides are very important chromophores that have been explored for various applications as dyes and pigments.[108,109] This is primarily because of the exceptional properties displayed by PTCDI such as high chemical persistency, very high thermal stabilities upto $550^{\circ}C$, extremely high photostability, and weather fastness.[110] The chemical structure of a typical PTCDI molecule is shown in Figure 2.1.
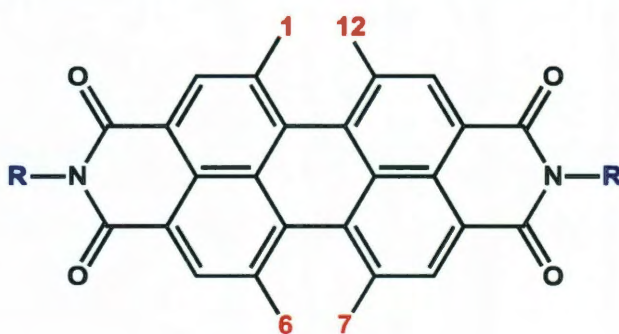
Figure 2.1 Chemical structure of a PTCDI molecule. The R-groups at the imide-N represent the different side-chains that can be attached to the perylene core. The positions 1, 6, 7 and 12 at the perylene cores (also known as bay-positions) shown in red can be functionalized to yield novel highly soluble PTCDI.

The perylene dyes were first discovered by Kardos in 1913 and utilized as vat dyes in textile industries. Later on owing to their extremely low solubilities, the research on these dyes was shifted towards their applications as high performance pigments mainly as shades of red and violet black (Figure 2.2: **2a-c**).[97,110] But most recently, owing to the high electron affinity of the PTCDI,[111] they have been explored as n-type semiconducting electronic material.[112,113] Due to their unique optical, redox and stability properties they have been explored for their applications in electrophotography or xerography.[100] The extreme insolubility of these molecules is a criterion for pigment related applications but

in order to perform chemistry with these molecules the solubility in an organic solvent is desired. Moreover, various functional groups in the form of corresponding amines can be introduced in the structure of PTCDA parent molecule resulting in the formation of more soluble PTCDI.

2.3 Synthesis of PTCDI

The condensation of the corresponding amine with the parent Perylene-3,4,9,10-tetracarboxylic dianhydride (PTCDA), 1 has been utilized for the synthesis of various PTCDI.[108,114-116] A diverse range of both aliphatic and aromatic amines can be used for this purpose. Furthermore, by adjusting the reaction conditions it is possible to synthesize symmetrical PTCDI 2, asymmetric PTCDI 6, and m-PTCI (N-mono(alkyl)-3,4,9,10-perylene tetracarboxylic monoanyhydride monoimide, 5. When only the O-positions of the parent anhydride are replaced by N- the core of the perylene structure remains planar. However, upon substitution of the bay-positions (1, 6, 7, & 12, see Figure 2.1) within the perylene core results in the loss of the planarity of the perylene cores structure.

2.3.1 Synthesis of symmetrical PTCDI

When the two substituents at the imide nitrogen are similar, the PTCDI are termed as symmetric. The reaction scheme for the synthesis of symmetric PTCDI is shown in Figure 2.2. In 1959, Langhals et al. [108,114-116] proposed the first route for the synthesis of PTCDI in which the long hydrophobic alkyl chains were introduced at the imide nitrogen which lead to the increase in the solubility of these molecules. Using this strategy various substituents comprising straight chains, branched carbon chains, phenyl groups can be attached to the ends of the dianhydride by the corresponding primary amine substitution leading to various PTCDI (2a-f). A very high solubility was observed when pure aliphatic

substituents were attached to the N-atom as compared to that obtained by attaching aromatic substituents.
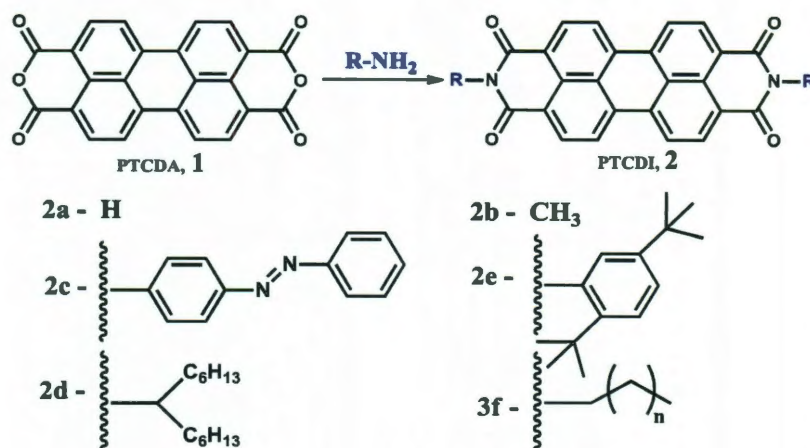
Figure 2.2 Synthesis of planar symmetrical PTCDI.

When cyclo-alkyl substituents are attached to the perylene core, the solubility of these dyes increases till five membered ring, which then decreases for the medium sized rings and then again increases drastically for large sized rings as they form parallel zig-zag chains. When two identical branched alkyl chains ('swallow-tail' substituents) are attached to the perylene core extremely high solubilities are observed in chloroform (e.g. **2d**). It has been observed that the melting point of the branched perylene diimides decreases from higher values (as observed in case of linear alkyl substituted) to less than 100°C as the length of the branched alkyl chains increases.

2.3.2 Synthesis of asymmetrical PTCDI

When the two substituents at the imide nitrogen are different, the PTCDI are termed as asymmetrical. The reaction scheme for the synthesis of asymmetric PTCDI is shown in Figure 2.3. Though the procedure for obtaining symmetric PTCDI is relatively straightforward process in which the PTCDA, **1** is condensed with excess of the primary

amine, the synthesis of non-symmetric PTCDI involves multiple reaction steps and therefore yields of the desired products are much lower than that obtained for symmetrical PTCDI.
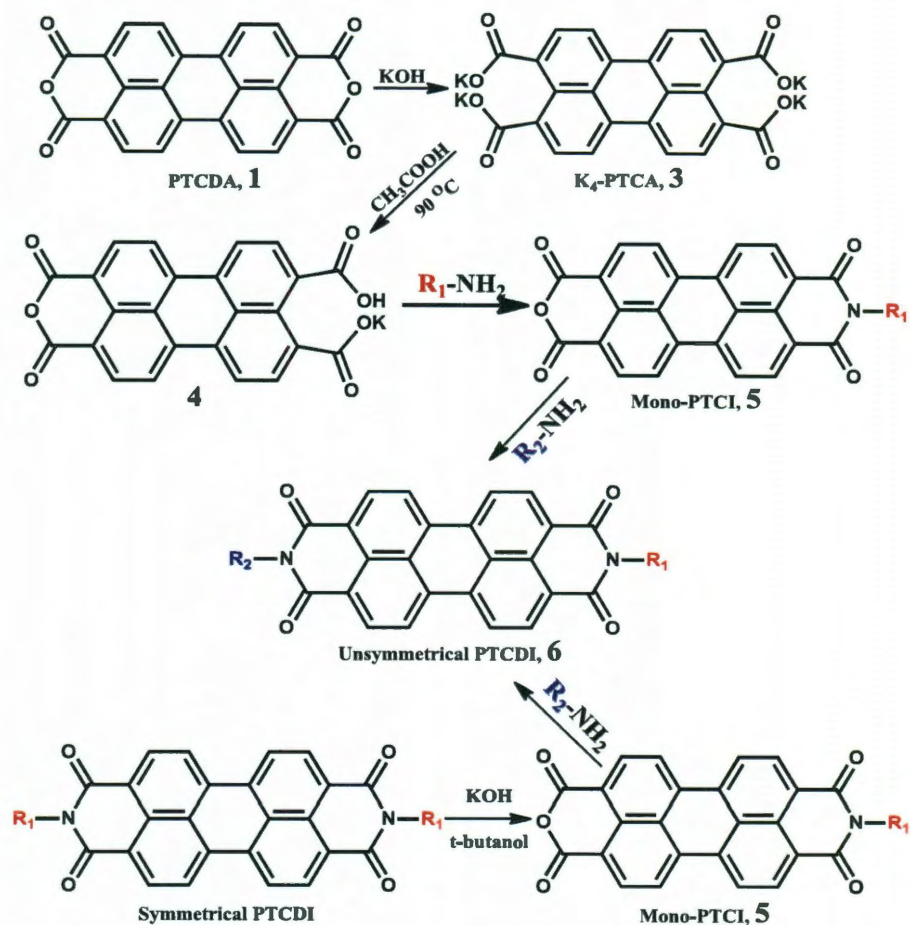
Figure 2.3 Synthesis of planar mono (**5**) and unsymmetrical (**6**) PTCDI.

Monofunctionalized dyes have been utilized for the synthesis of non-symmetrical PTCDI and complex multichromophoric architectures. It would appear straightforward to react excess of PTCDA with primary alkyl amine as minor components leading to formation of perylene monoimides (m-PTCI), **5**. But it is observed that even under controlled reaction conditions PTCDI is a major product with very small amount of

perylene monoimide. Efforts were made to synthesize asymmetric PTCDI by the condensation of PTCDA with mixture of two different primary amines. However, such reactions yield mixture of products which are rather difficult to separate.

Troster et al. [117] have developed a very elegant synthesis protocol for the synthesis of perylene monoimides, **5** (Figure 2.3). In this procedure, first PTCDA, **1** is converted to highly water miscible tetrapotassium salt, **3** by the reaction with potassium hydroxide. Slow addition of acetic acid or phosphoric acid with heating leads to the moderate acidification, thus resulting in the precipitation of the monoanhydride monopotassium salt, **4** from water. Usually acetic acid is preferred over phosphoric acid because its removal from the final product is much easier. Due to the extraordinarily high lattice energy of the perylene monoanhydride monopotassium salt, **4** it is absolutely insoluble in any solvent even at high temperatures thus leading to its removal from the acid base equilibria. This method therefore allows for synthesis of extremely pure perylene monoanhydride monopotassium salt, **4**.[118] This salt can then be coupled with various primary amines in water only at one position, **5** and subsequently the second position can be reacted with other primary amine after ring closing leading to the formation of non-symmetric PTCDI, **6**. The yields of the perylene monoimides by this strategy decreases as the hydrophobicity of the amines increases. However, reasonable yields are obtained and hence this strategy has been utilized for the preparation of asymmetric PTCDI in high yields utilizing water soluble primary amines. One major limitation of this method is that it cannot be used when extremely long and branched alkyl chains are used.

In order to form perylene monoimides in high yields utilizing hydrophobic amines, the hydrolysis of symmetrical PTCDI based upon these hydrophobic chains is

employed. Nagao and coworkers have explored a method of partial acid saponification of symmetric PTCDI in concentrated sulfuric acid at 180-200°C.[119,120] But this procedure usually requires harsh reaction conditions and hence substituents attached to the perylene core might undergo sulfonation at this temperature. Hence, to overcome this disadvantage other methods have been developed in which the symmetric PTCDI (in which one of the desired chain in the final structure) are hydrolyzed under mild conditions utilizing KOH and tertiary butanol, which upon acidification and heating result in the formation of perylene monoimide, 5.[118] Moreover, since highly hydrophobic secondary amines can be coupled to perylene core in this way, there is enhanced solubility of these monoimides. These molecules can be then further condensed with various alkyl amines thus leading to asymmetric PTCDI chromophores.

2.3.3 Synthesis of bay-substituted PTCDI

The method for realizing highly soluble perylene dyes (by disruption of the planarity) was developed by Seybold and coworkers at BASF.[121] They devised a method to introduce substituents directly in the carbocyclic scaffold which is also termed as bay-area (positions 1, 6, 7, 12, see Figure 2.1). Their approach was based on utilizing tetrachloro perylene diimide derivative, 7 as an initial precursor which can undergo nucleophilic displacement reaction by the displacement of chlorine leading to the introduction of substituents directly in the perylene core (Figure 2.4). The main drawback of this method was the formation of tri and penta substituted chloro derivates of perylene along with the tetra chloro derivative which were very difficult to separate from the reaction mixture.[122] It was possible to successfully incorporate four phenoxy groups in the bay area leading to the synthesis of tetraphenoxy perylene derivatives, 8.[121] However,

the other nucleophilic substituents were very difficult to be introduced in higher yields and single reaction product was rarely obtained. In 1997, di-bromination (at positions 1,7) of PTCDA at bay was established[123] and it was subsequently converted to the di-substituted (1,7) bay perylene derivatives.
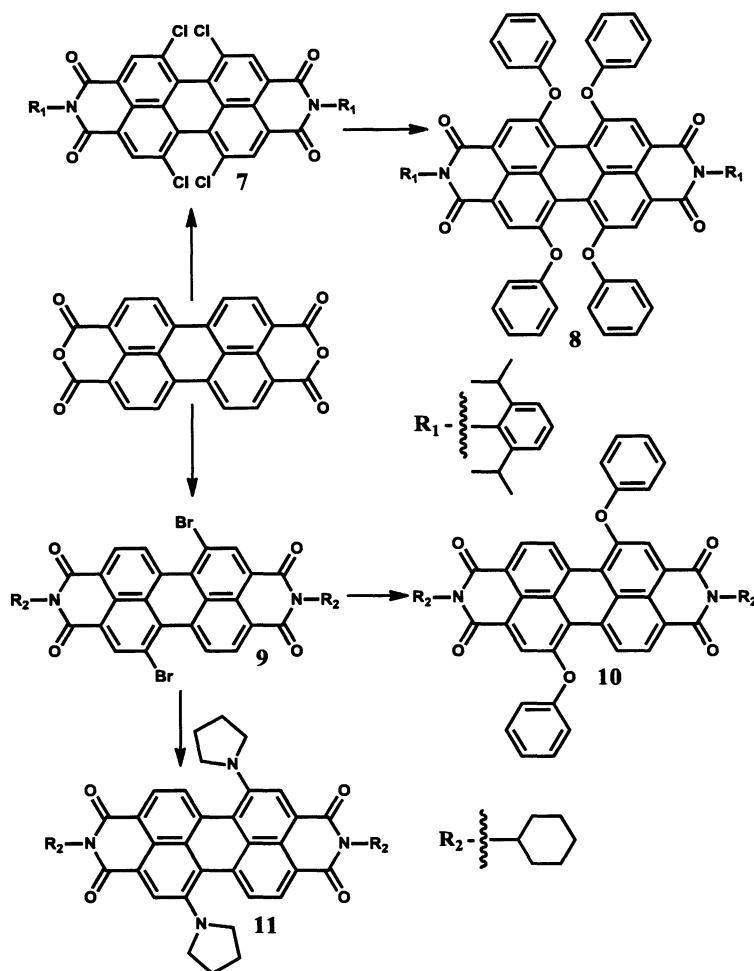
Figure 2.4 Synthesis of bay substituted PTCDI.

The major disadvantage of this method was that the product obtained after bromination was contaminated with almost three fold bromination products[124,125] and significant amount of second dibromo regioisomers, which could be detected only by high field (>400 MHz) H-NMR spectroscopy. However, recently new method has been

developed for the di-bromination of PTCDA in very high yield (> 70 %) by the addition of iodine at 80 °C.[126] It was also possible to obtain tetra bromo derivatives of PTCDA in a reasonable yield (30%) by adding additional iodine and refluxing at higher temperature for a longer period of time.[127] Since the displacement of bromine substituents with various nucleophiles like carbon, cyano, oxygen, oligothiophene and nitrogen is a very straightforward reaction, it is now possible to make wide range of bay substituted PTCDI **10, 11** in higher yields having various functional groups thus leading to very unique properties.[128-132]

Depending on the size and the number of substituents at the bay positions, the two naphthalene planes that make up the structure of perylene can be twisted about 20°-40°.[97] Various tetra- and di- substituted perylene dyes have been widely synthesized because of the relative ease of the control of substituents at the bay positions. Not only the small molecules but also various polymers can be coupled to the perylene core leading to the formation of star shaped polymers with the core comprising of perylene. These star shaped polymers have been synthesized successfully which also show very unique mechanical properties.[133] Moreover, Mullen et al.[134] have systematically investigated the introduction of the polyphenylene dendrons at the bay area of the perylene core. These higher generation polyphenylene dendrons prevented the aggregation of the perylene core by π-π interactions, thus leading to increased solubility in solution.

2.4 Optical properties of PTCDI

The absorption and emission properties of the PTCDI in homogeneous solution are completely indistinguishable for various PTCDI having the imide substituents with

wide range of functional groups and varying number of carbon atoms in the side chains. This is primarily because the nodes are present in the HOMO and LUMO of the imide nitrogen which leads to minimal coupling between the perylene core and the imide substituents (Figure 2.5a). Therefore, PTCDI are usually considered as the closed chromophoric system in which the intensity and the position of the S0-S1 transition is polarized along the long molecular axis and is independent of the imide substituents. This type of modification retains the conjugation in the perylene core and therefore these PTCDI have very high fluorescence quantum yield and very low stokes shift, especially in solution.
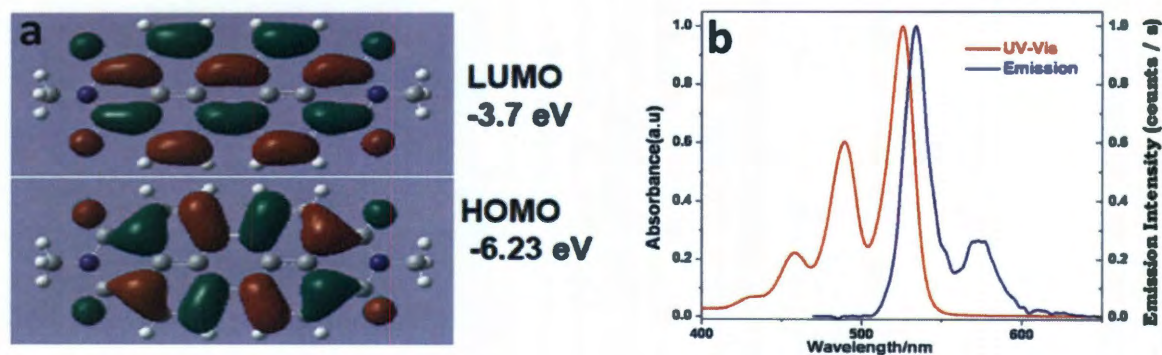
Figure 2.5 (a) HOMO and LUMO levels of Me-PTCDI as calculated by Gaussian 03. The frontier orbitals on both HOMO and LUMO for PTCDI's exhibit nodes at the imide nitrogen. **(b)** Typical UV-visible and fluorescence emission spectra of perylene diimides homogeneously dissolved in solution.

Moreover, these optical properties are independent of the environment i.e solvent in which these dyes are highly soluble and hence these dyes exhibit very little solvatochromism. The planar PTCDI show strong absorption in the visible range of 450-520 nm and the emission from the free molecules is a mirror image of the absorption spectra (Figure 2.5b). The absorption and emission spectra have very well resolved vibrational structures. The fluorescence quantum yield for these types of dyes is close to

unity even under atmospheric oxygen.[116] Thus, because of its high light fastness ability, these dyes have been utilized as standards for obtaining the quantum yield of other fluorophores. In the case of phenyl substituents at the imide nitrogen, due to the twisting of aryl groups the aggregation is prevented and solubility is increased. But due to the vibronic motions the quantum yields reduces to 70%.[122] In case of the highly electron rich alkoxyphenyl substituents (at the imide positions), the quantum yields as low as 5% have been reported due to the photoinduced electron transfer from the electron-rich phenyl substituents to the electron deficient perylene core.[135,136] The absorption spectra for these dyes cannot be tuned by just attaching alkyl/aryl chains at the imide nitrogen. However, it can be tuned either by the bay-substitution of the perylene core.

Significant changes in the absorption and emission spectrum are obtained by the functionalization of the perylene core in the bay positions (1,6,7,12).[137] For example, the substitution of two phenoxy groups at the 1,7 positions lead to a bathochromic shift of 20 nm[97] whereas, the substitution of four phenoxy groups leads to a bathochromic shift of 50 nm[137] as compared to the bay-unsubstituted PTCDI dyes and the fluorescence changes to orange and red colors, respectively. However both these substituted dyes retain their high fluorescence quantum yield, solvatochromism and photostability. When the bay positions are substituted by two electron-donating pyrrolidino groups, green colored dyes with a bathochromic shift of 160 nm and their emission properties in infrared regions are obtained.[131] This is attributed to the charge transfer due to the pyrrolidino groups which leads to pronounced solvatochromism and decrease in fluorescence quantum yield. On the other hand, introduction of the electron-withdrawing substituents at the bay positions leads to insignificant changes in the absorption and emission spectrum.

This leads to unique situation in PTCDI where in the dissolved state no solvatochromism behavior is observed, but in solid state upon aggregation a pronounced crystallochromy can be observed, leading to crystals with different shades of color ranging from red to black.[138,139] Kazmaier et al.[140] has derived an empirical relation between the absorbance maxima and the different offsets (transverse and longitudinal) in the packing of the PTCDI, which results in the crystallochromy. Upon aggregation of the PTCDI molecules in poor solvents pronounced changes occur in the optical absorbance spectra.[141,142] In some cases, it has been found that a new absorption band appears at longer wavelength (crystal phase) upon aggregation in certain solvents and concomitantly a decrease in the absorbance of the 0-0 peak and increase of the 0-1 and 0-2 transitions. These optical characteristics have been associated with the strong co-facial packing of the perylene cores.

2.5 Structural properties of PTCDI

PTCDI dyes having small substituents such as H, -CH$_3$ attached at the imide positions are extremely insoluble and tend to form several single-crystals. The X-ray diffraction of these crystals confirmed the extreme planarity of the perylene core.[139] From the bond length calculations, PTCDI are considered to be composed of two naphthalene half units each of which is attached to an imide unit and the naphthalene units are connected by two C sp^2- C sp^2 single bonds.[97] Upon substitution of the bay areas, there is introduction of sterical strain thus resulting in a twisting of the naphthalene units.[143] This twisting behavior was first observed for the tetrachloro-substituted perylene bisimides in which the torsional angle was determined as 37° whereas a smaller torsional angle of 25° was observed in case of tetraphenoxy-substituted diazadibenzoperylene derivative.[144,145]

Owing to such a distortion, the solubility of these dyes is drastically improved but the planarity of the perylene core is destroyed and therefore considerable constraints exist in packing of these dyes in solid states or in molecular aggregates. Marks and coworkers have utilized the crystallography and electronic structure calculations to study the distortion in case of bay substituted PTCDI.[146] The studies indicate that there exists a correlation between the electron mobilities and the distortion due to the functionalization of perylene core. The core twisted perylene diimides exhibit a distorted packing whereas the planar PTCDI exhibit co-facial packing. Hence, the study of packing behavior of various PTCDI is necessary in order to optimize the transport characteristics which determine efficiencies for the performance of various electronic and optoelectronic devices based on these materials.

2.6 Packing behavior of PTCDI – Effects on optical properties upon aggregation
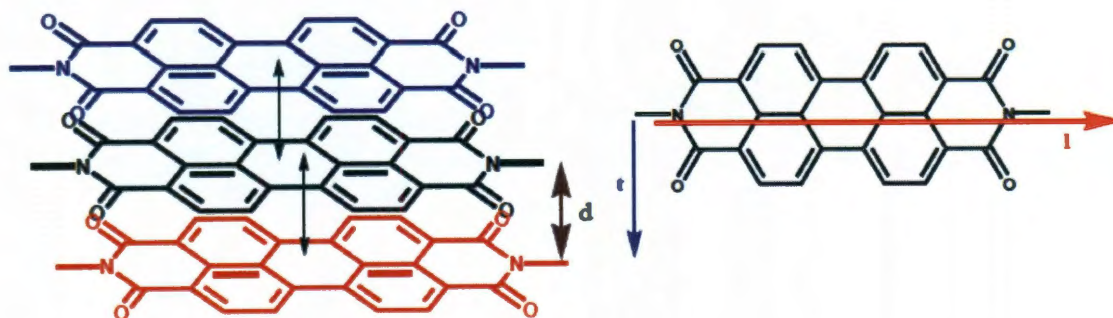
Figure 2.6 The ideal co-facial packing for perylene diimides with three PTCDI units stacked one over other by π-π interactions is shown in left. The distance between the two adjacent perylene diimide core is represented as d (π-stacking distance). The lateral (l) and transverse (t) offsets observed in the packing of perylene diimides.

The alkyl or aryl substituted PTCDI show almost similar optical properties in homogeneously dissolved state, but in the aggregated state their properties vary as the

packing of the perylene cores is different for different alkyl substituted (linear, branched, bulky) PTCDI. This difference in the packing behavior leads to various colored pigments having varying optical properties. The crystal structures of 18 different PTCDI pigments that differ only in the substituents attached to the perylene core have been extensively studied by Graser, Hadicke and Klebe at BASF.[138] Zugenmaier et al.[147] have reported the crystal structure of six more derivatives. All these studies reveal that the PTCDI exhibit planar geometry and they are arranged in stacks corresponds to the π–π interactions between the perylene having parallel orientation of these dyes at a distance of between 3.34 and 3.55 Å. This distance corresponds to the distance between the perylene cores which is similar to that observed between the graphene layers in the graphite. However, in case of PTCDI with bulky substituents (at the N- position) or the ones that lead to core twisting (bay position), π-stacking distances up to 4.3 Å is observed. This increase in distance is because of the introduction of longitudinal and transverse offsets to allow for the stabilization of the energy of the aggregates leading to distorted or weak packing of perylene cores (Figure 2.6).[97,143,148] Thus, the nature of the substituents attached to the imide nitrogen dictate the offsets incorporated in the packing of the PTCDI. Moreover, the rotation offsets in a few phenyl substituted PTCDI result in screw type packing.[147]

Kazmaier and Hoffmann have further studied these crystallochromic effects on 1D infinite stacks of these dyes as a function of these two offsets based on extended Huckel calculations.[140] It was also found that a small change in the conformation of the side chains of the PTCDI (trans to gauge) leads to the significant changes in the longitudinal and transverse offsets. A direct consequence of such change in the

configuration results in a change in the absorption maxima from 559 nm for gauge conformation to 610 nm for trans conformation.

2.7 Self-assembly of PTCDI

The advancement and the flexibility in the synthesis of PTCDI, to allow for desired side-chain to be attached to the perylene at various positions, has allowed for realizing a wide range of PTCDI molecule with unique size, shape and solubility. The planar PTCDI molecules show strong propensity to aggregate by π-stacking interactions. The resulting aggregates often show ordered crystalline structures as seen by the X-ray diffraction of the crystals grown for a range of PTCDI. Also, the ability to show crystallochromic effects due the differences in packing because of side chain modulation allows for tuning the optical properties. The major goals of self-assembly of PTCDI molecules are obtaining well defined morphological structures that are highly ordered such as 1D structure which is well suited for use in application. Such stringent requirements therefore demand the synthesis and assembly of wide range of PTCDI molecules with programmed molecular interactions. Some of the non-covalent interactions that have been widely utilized for the realization of such structures are mentioned below.

2.7.1 π-π interaction based self-assembly

The self assembly of various symmetrical, asymmetrical PTCDI and perylene monoimides by π-stacking interactions has been studied by various groups. The chemical structures of these various PTCDI are mentioned in Figure 2.7 In order to understand the side chain effects on the self-assembly, Balakrishnan et al.[142] studied the self-assembly of two planar PTCDI molecules having linear, **13** and branched alkyl chains, **14**. They found

that owing to the minimal steric hindrance and strong π-π stacking between perylene backbones in case of linear side chain PTCDI, very uniform 1D nanobelts could be realized. On the other hand, owing to the bulky side chain, there is significant distortion in packing of the perylene core leading to the formation of 0D particles.[141] The interdigitation of side chains between the PTCDI due to the hydrophobic interactions also govern this type of self-assembly. All these assemblies were characterized by SEM, TEM, DSC, XRD and fluorescence microscopy.

Further Che et al.[149] demonstrated ultralong fibers self-assembled from an amphiphilic asymmetrical PTCDI, **15** having polyoxyethylene on one end and hydrophobic branched alkyl chain, hexylheptyl, attached to the perylene core. They found that the π-stacking interactions between the perylene cores could be maximized in the water/ethanol solvent mixture. These ultralong fibers also show good electrical response upon doping with an electron donor such as hydrazine implying the long range charge migration due to efficient π electron delocalization over the entire length of the fibers. Highly fluorescent fibers were also fabricated by π-π interactions of perylene monoimide, **17** having only one bulky side chain attached to the perylene core by a slow solvent vapor diffusion process in a closed container which behaved as an efficient sensor for detection of volatile organic compounds (VOC) (e.g. amines), again based on the principle of electron transfer from the VOC to the perylene core.[150] Single crystalline organic nanobelts were also reported by Che et al.[151] by the solvent phase transfer self-assembly of PTCDI, **16** having cyclohexyl groups at the imide nitrogen which was essentially driven by the π-π interactions.
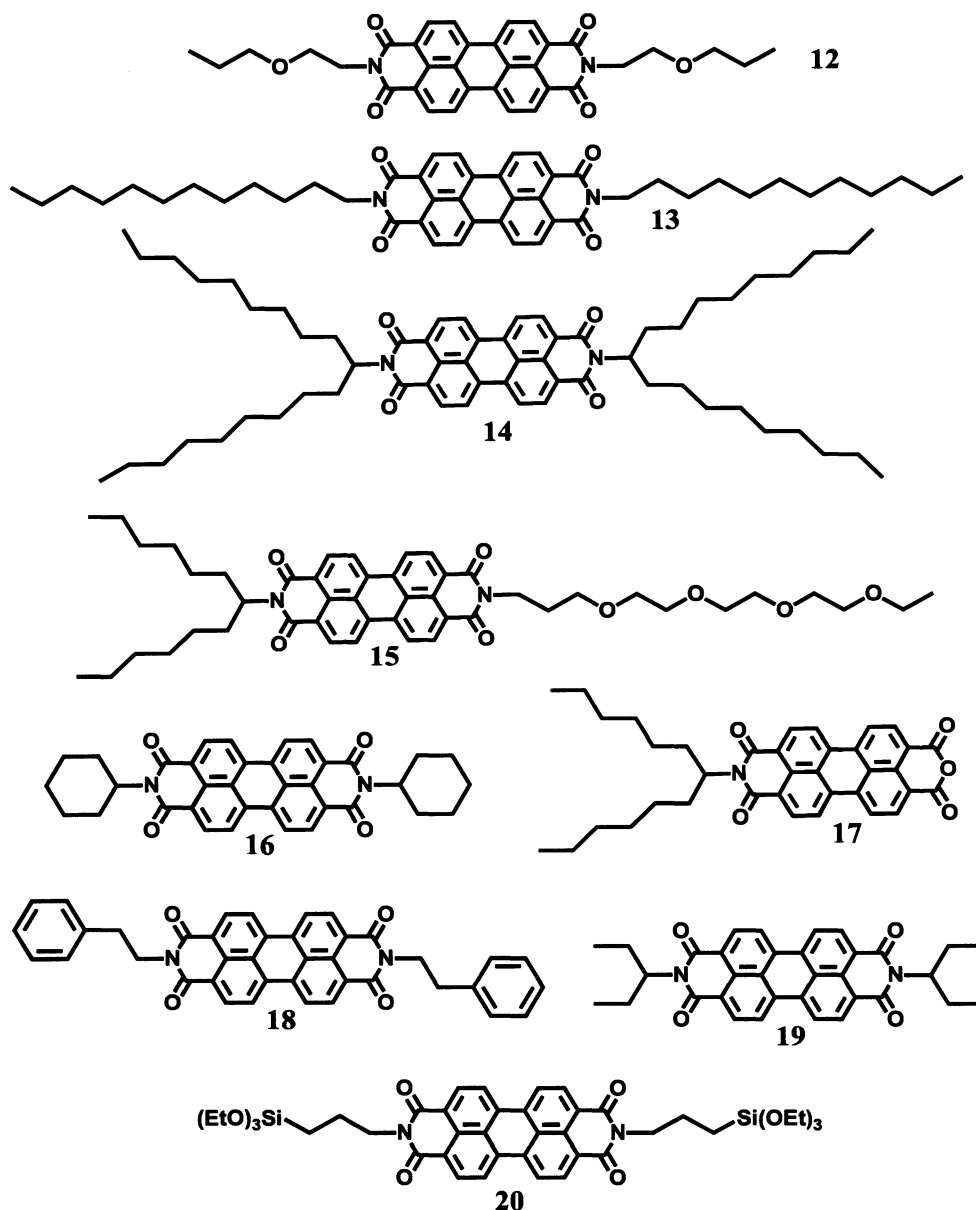
Figure 2.7 Structures of various planar symmetrical, unsymmetrical PTCDI and perylene monoimides employed for the self-assembly by π-π interactions.

Datar et al.[152] and Mullen et al.[153] have utilized the solvent vapor annealing method on the films of PTCDI on surface for the self-assembly of planar PTCDI **12** and **19** into highly ordered supramolecular architectures by π-π interactions on various substrates. Briseno et al.[67] have studied the self-assembly of symmetrical PTCDI having

varying side chain length at the imide nitrogen by a modified phase transfer method. They found that as the length of the side chain increases, the rate of aggregation by π-π interactions and side chain interdigitation increases, leading to more number of nuclei and hence the resulting diameter of the 1D fiber decreases. They utilized these 1D fibers along with the p-type nanowires of hexathiapentacene[68] to form complimentary invertors. Bao et al.[154] have fabricated the single crystalline 1D nanofibers of N,N-bis(2-phenylethyl)-perylene-3,4,9,10-tetracarboxylic diimide, **18** by either adding a small amount of methanol to the hot homogeneous solution of this PTCDI in toluene or dispersing a concentrated homogeneous solution of the PTCDI in huge excess of methanol. In the former case large diameter and length of fibers are obtained due to slow nucleation and growth whereas in the latter case small diameter and length of fibers are observed. They reported highest charge carrier mobility of 1.4 cm^2/Vs from the single wire of this n-channel organic semiconducting molecules.

Luo et al.[155] have studied the self-assembly of PTCDI, **20** having (propyl)triethoxysilane groups at the imide nitrogen. They found that the solvophobic interactions of the perylene core and the solvophilic interactions of the (propyl)triethoxysilane parts in the acetone/petroleum ether mixed solvents drives the self assembly into tubular, crystalline 1D nanotubes by π-π interactions. Further, Lu et al.[156] demonstrated that by controlling the kinetics of self-assembly (rate of solvent drying, concentration, solvent composition) of PTCDI, **20** bearing (propyl)triethoxysilane parts, various morphologies like micro-tubes, macro-fibers, hollow spheres, to dense spheres could be obtained by hierarchical assembly in solution. Recently, Ren et al.[157] have studied the self-assembly of hybrid organic-inorganic molecules based on PTCDI, which

comprised of oligosilsesquioxane nanoparticles covalently attached to imide nitrogen via a rigid 1,4-phenylene linkage. Despite the presence of bulky nanoparticle substituents at the imide nitrogen, these hybrid molecules self-assembled into single crystalline nanobelts by π-π interactions on various substrates upon evaporation of its THF solution. Yu et al.[158] have recently studied the self -assembly of PTCDI molecule having permethyl-*b*-cyclodextrins attached at the imide nitrogen via π–π stacking interactions into 1D fluorescent nanorods that have been explored for sensing applications.

2.7.2 Hydrogen bonding based self-assembly

The control of specificity and directionality of the hydrogen bonding interactions between the two interacting species have recently attracted lot of attention for creating supramolecular structures. The structures of various PTCDI and complimentary hydrogen bonding molecules employed for the hydrogen bond directed self-assembly are mentioned in Figure 2.8. The self-assembly of PTCDI, **21** having two –CO-NH-CO-sequence with a NH hydrogen bond donor (D) and two CO hydrogen bond acceptors (A) thus leading to A-D-A sequence which can form hydrogen bond with various donor acceptor sequence have been widely studied. Wurthner et al.[159] has studied the self assembly of bay substituted PTCDI, **21a** having such A-D-A sequence at imide nitrogen that can undergo two self-complimentary hydrogen bonding amongst each other in organic solvents. Owing to presence of bulky substituents in bay position, perylene core twisting is observed leading to the slipped arrangement. There also exists secondary π-π interaction amongst the slipped perylene cores leading to highly fluorescent helically twisted supramolecular polymer exhibiting J-type packing. They have further synthesized bay substituted PTCDI, **21b** having such A-D-A sequence and studied its ability to

undergo hydrogen bonding with complimentary ditopic dialkyl melamines, **29**.[160] The triple hydrogen bonded complex are very rigid and hence these hydrogen bonded supramolecular chains also undergo π-π interactions between perylene core and alkyl side chain interactions present in melamines in aliphatic solvents like methylcyclohexane leading to formation of highly fluorescent and extremely photostable self assembled nanostructures.
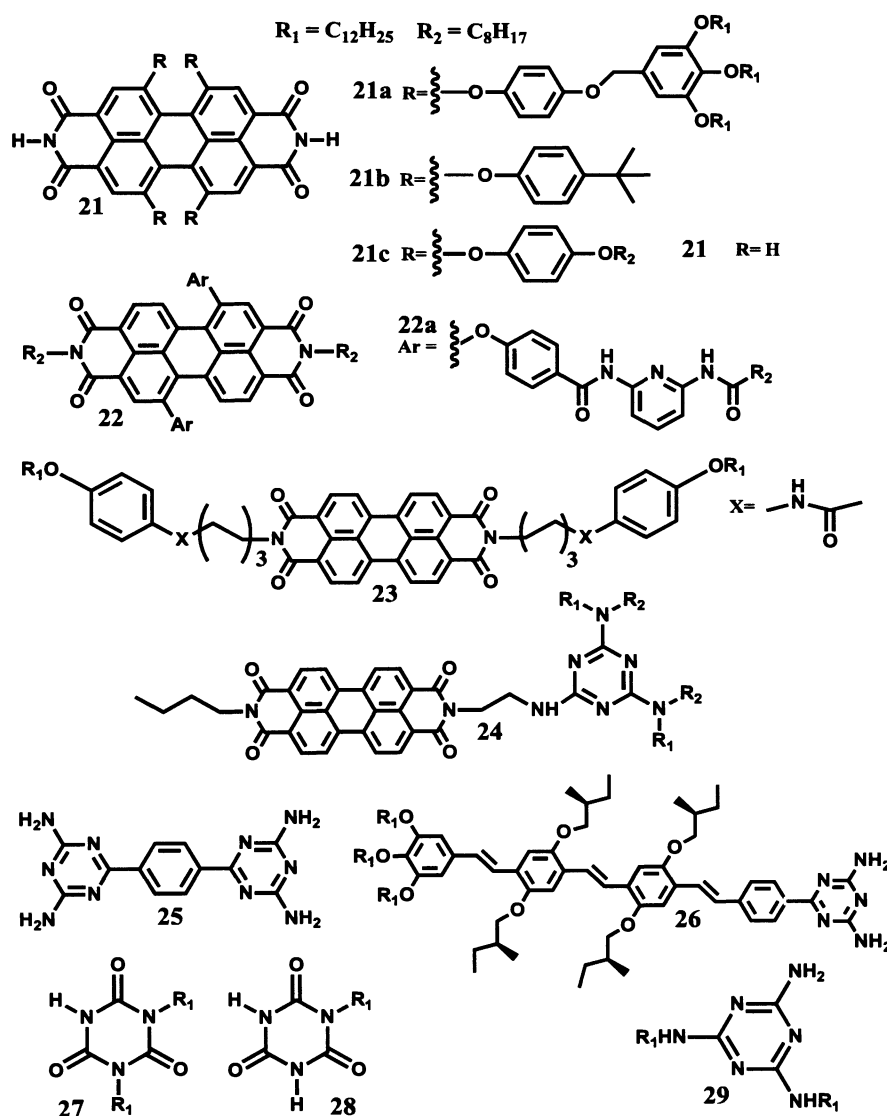
Figure 2.8 Structures of various PTCDI and complimentary hydrogen bonding molecules employed for the hydrogen bond directed self-assembly.

Recently, Liu et al.[161] has illustrated the self-assembly of bay substituted perylene diimides, **21c** having the A-D-A sequence mentioned above with the fullerene derivative bearing a 2,6-diacylaminopyridine units for their potential light harvesting applications by the efficient energy and electron transfer. It was found that these perylene diimides undergo strong hydrogen bonding interactions in chloroform and leads to the formation of spherical ball like assemblies. Further, they have also synthesized another PTCDI derivative, **22a** having two N-(6-dodecanoylamino-pyridin-2-yl)-benzamide groups at the bay positions which can undergo triple hydrogen bonding interactions with another PTCDI derivative, **21c** having the A-D-A sequence mentioned above leading to formation of long 1D nanofibers from chloroform solution.[162] In addition to hydrogen bonding interactions, π-π interactions were have also shown to be responsible for the formation of such 1D morphology. Marta et al.[163] have also demonstrated the substrate templated self-assembly, by the triple hydrogen bonding interactions between 1,4-bis-(2,4-diamino-1,3,5,-triazine)-benzene, **25** and 3,4,9,10-perylenetetracarboxylic diimides, **21d** having such A-D-A sequence, leading to the formation of periodic bicomponent wires and ribbons.[163]

Meijer et al.[164] have reported the synthesis of electron donor-acceptor-donor triads comprised of oligo(p-phenylene vinylene) (OPV) and central PTCDI which are connected by the chiral linkers incorporating amide bonds. This molecule was shown to undergo hydrogen bonded self assembly due to the presence of amide groups in toluene. Further, Meijer and Wurthner extended this concept and demonstrated the hierarchical self assembly of bay substituted PTCDI derivative, **21b** having an appropriate functional group at the imide nitrogen that can undergo triple hydrogen bonding with two

diaminotriazine functionalized oligo(p-phenylene vinylene), **26** and further π-π interactions leading to the formation of chiral fibers.[103] It was found that even though the donor acceptor chromophores form distorted J-aggregation, the fluorescence of the resulting chiral assemblies is completely quenched. This has been attributed to a very strong photoinduced electron charge transfer between the donor and acceptor present in the structure of the fibers. Liu, et al.[165] has demonstrated the self-assembly of PTCDI having bis-urea groups attached at the two bay positions, **22a** leading to the formation of rod like superstructures. The main driving forces for the formation of such superstructures was found to be hydrogen bonding interactions and π-π stacking interactions which were determined by the NMR, fluorescence spectra and FTIR. Asha et al.[166] have studied the liquid crystalline behavior of perylene bisimides having ester and amide linkages, **23** which are terminated by the monododecyloxy phenyl, or tridodecyloxy phenyl units at the imide nitrogen. It was found that owing to the presence of amide linkage in monododecyloxy phenyl terminated PTCDI the π-π interactions were enhanced by the additional hydrogen bonding leading to H aggregation and hence formation of long 1D nanostructures from toluene. On the other hand, owing to the absence of hydrogen bonding interactions in corresponding ester series, J aggregation was observed leading to leaf like patterns. Moreover, due to the bulky nature of the tridodecyloxy linkages, both the ester and amide series of the tridodecyloxy phenyl terminated PTCDI failed to produce ordered 1D aggregates. Recently, Wurthner et al.[167] have demonstrated the conversion of H-type to J-type packing in case of core unsubstituted PTCDI. They achieved this conversion by the hydrogen bond directed complexation of unsymmetrically substituted PTCDI, **24** having melamine units at the

imide nitrogen with appropriate cyanuric acid derivatives, **27, 28** both in solution as well as solid state. Moreover, this transformation was found to be reversible at an appropriate temperature.

2.7.3 Metal Ligand based self-assembly

With a view to form photoluminescent polymers by utilizing the concept of supramolecular polymerization by complexation between the metal ion and photoactive building blocks, Wurthner et al.[168] have synthesized PTCDI dyes having terpyridine receptor units. They studied the complexation of these dyes with octahedrally coordinating metal ions like Zn^{2+} and Fe^{2+} (Figure 2.9). In order to have efficient binding with the metal ions, the aggregation of the PTCDI must be prevented. Hence, appropriate functionalization of PTCDI and in some cases the corresponding metal ion was desired so as to form coordinate bonds in one common solvent system.[97] By appropriately controlling the structure of PTCDI and ratio of the metal ion to the perylene bisimides, dimers and polymers could also be realized.
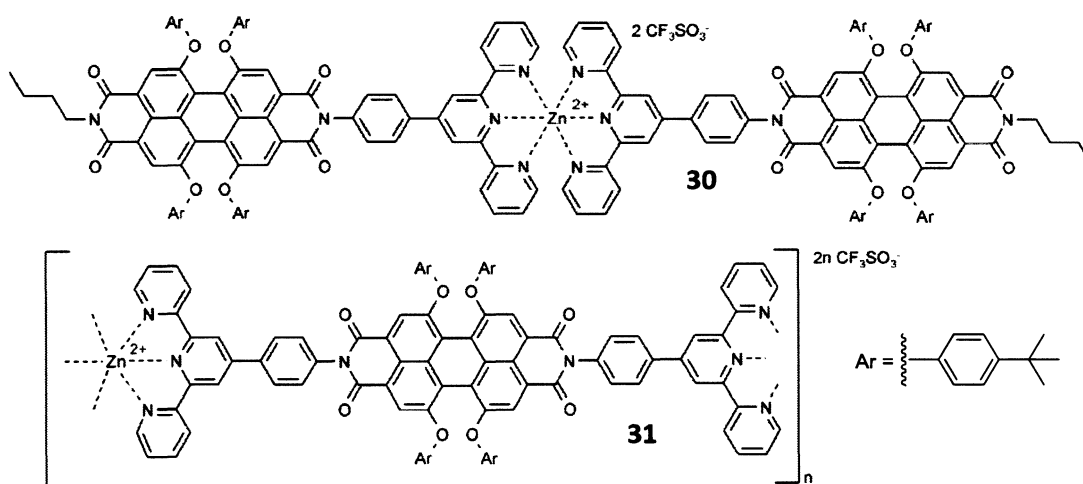
Figure 2.9 Supramolecular polymers by the metal ligand based self-assembly of PTCDI.

Moreover, it was found that fluorescent dimers and polymers could be formed by utilizing Zn^{2+} ions and this complexation was reversible, whereas the fluorescence was quenched drastically in case of dimers and polymers when Fe^{2+} was employed and the complexation was completely irreversible. Thus, it can concluded that the formation of fluorescent supramolecular polymers from PTCDI dyes with terpyridine receptors is metal directed and hence exhibits different photophysical properties. In order to further enhance the metal-ligand coordination and reduce the π-π aggregation which leads to precipitation and formation of mesophases, various diazadibenzoperylene having first to third generation dendrons attached to the bay positions have been utilized to form metal directed coordination polymers.[169]
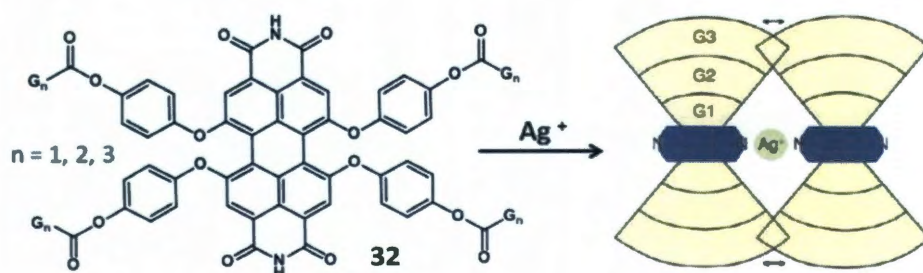
Figure 2.10 Supramolecular polymers formed by metal ligand interaction of the dendronized diaza PTCDI based building blocks.

It was found that dendronized diaza perylene blocks can be polymerized by Ag^+ ion leading to rigid rod polymers (Figure 2.10). This polymerization was dependant on generation of dendrimer attached and hence only first and second generation dendrimers afforded highly ordered polymers whereas the third generation dendrimers led to the shielding of the aza coordination site by the dendritic wedges leading to no polymerization.

M = Pt / Pd

Ar =

Ar =

33
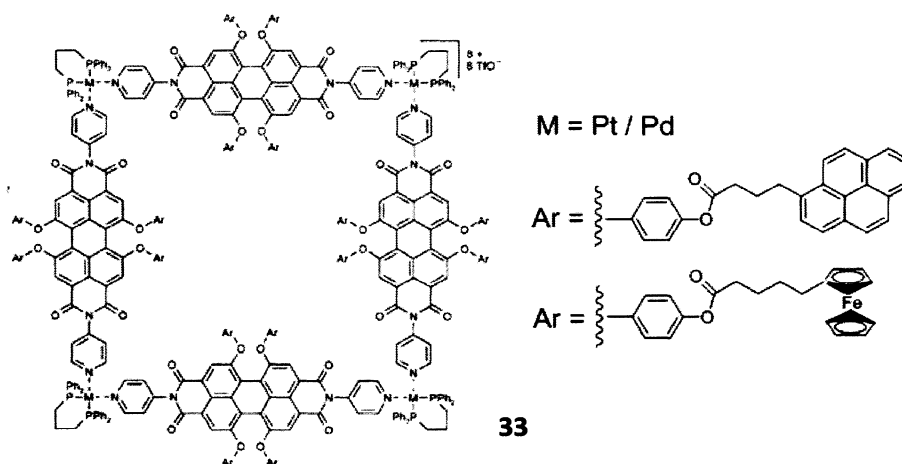
Figure 2.11 Metallosupramolecular squares based on PTCDI with various functionality.

By utilizing the metallosupramolecular strategy, more interesting macromolecular structures such as metallosupramolecular squares have been created which are comprised of perylene bispyridyl imides containing four ferrocenyl moieties attached at the four bay positions(Figure 2.11).[170] The pyridyl groups at the imide nitrogen of PTCDI's can coordinate with the Pt(II) complex which serves as the angular building block leading to the metal directed macromolecular square structures having redox active functional units (Ferrocene) organized in three dimensional space. Similarly, 4-dimethylamino-1,8-napthalimide was introduced at the four bay positions of the N,N'-bispyridyl PTCDI and they were self assembled by utilizing Pd(II) complex thus leading to supramolecular squares having sixteen dimethylaminonaphthalimide antennas and walls comprising of PTCDI (Figure 2.11).[171] These aminonapthalimide antennas can transfer the light energy to the perylene cores by the FRET mechanism leading to emission from perylene entities irrespective of excitation wavelength and these squares exhibited very high fluorescence quantum yields. These metallosupramolecular squares have additionally been explored

for various other applications such as molecular recognition to incorporate various guest molecules, catalysis, electrochemical sensing, photoluminescence etc.

2.7.4 Ionic self-assembly:
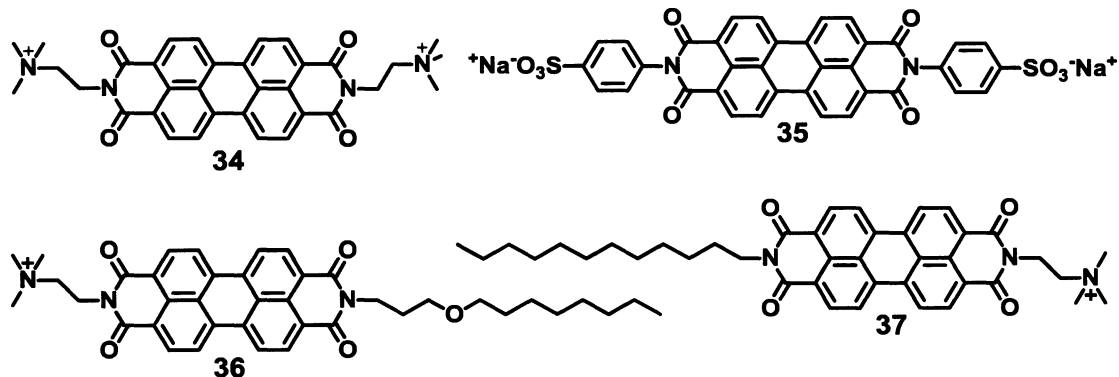
Figure 2.12 Structures of PTCDI utilized for ionic self-assembly.

The ionic self-assembly is a process in which two oppositely charged species undergo electrostatic interactions leading to ordered aggregates. Water soluble PTCDI having different ionic side chains attached to the perylene cores are shown in Figure 2.12. Faul et al.[172] has developed a method for the synthesis of complexes by electrostatic interaction between the anionic surfactants (dihexadecyl phosphate) and the cationic *N,N'*-bis(ethylenetrimethylammonium)perylenediimide,**34**. This complex has shown the formation of highly ordered thermotropic liquid-crystalline materials by utilizing this ionic self assembly which has been characterized by DSC and temperature dependant XRD. Further, by utilizing the same cationic *N,N'*-bis(ethylenetrimethylammonium)perylenediimide,**34** having two charges and anionic copper–phthalocyanine tetrasulfonate having four charges, ionic self-assembly has been utilized to create a new class of supramolecular polymers.[173] The one dimensional chains

of polymers are formed by the charge transfer and π-π interactions and the whole structure is stabilized by the electrostatic coulomb coupling leading to the helical packing in the polymer stacks. The polymer chains were characterized by the TEM and XRD. Further, they have also studied the ionic self assembly of two different cationic chiral surfactants having one and two charged headgroups respectively with the anionic PTCDI.[174] The resulting self-assembled structures yield chiral assemblies which have been characterized by CD spectroscopy and XRD indicating the formation of lamellar helical structures.

Additionally, optically active supramolecular complexes are obtained by electrostatic interactions between a chiral anion based on biological material- adenosine triphosphate and N,N'-bis(propylenetrimethylammonium)perylenediimide.[175] Other secondary interactions such as the π-π interactions between the perylene cores and hydrophobic interactions are also responsible for formation of such superstructures which were characterized by CD spectroscopy, DLS, NMR, SEM. The cationic asymmetrically substituted PTCDI namely (N-(Dodecyl)-N'-(2-(trimethylammonio)-ethyl)perylene-3,4,9,10-tetracarboxylic diimide iodide),**37** and anionic poly(acrylate) were separately drop casted from homogeneous solutions on substrate and dried leading to composite films comprised of semiordered, sub-micrometer sized clusters of PTCDI and polyelectrolyte bilayers.[176] These films exhibited diode like behavior in p-n junction hetorojunction devices and yielded photocurrent upon illumination with visible light. However, due to the discontinuity in the films, the performances of these devices were limited. In order to overcome these limitations, efforts were made to prepare PTCDI-polyelectrolyte thin films by sequential deposition utilizing a modified asymmetric

PTCDI, **36** having long chain ether which has increased solubility in water.[177] The resulting films showed larger domains of formation of curved nanofibers which are formed due to sequential deposition resulting in effective solvent annealing of the materials due to repeated deposition and slow growth of the PTCDI along the polyelectrolyte backbone. These fibers are comprised of parallel π-stacked PTCDI assemblies which are sandwiched between polyelectrolyte regions. These films are characterized by AFM and optical microscopic techniques and expected to have higher conversion efficiencies in flexible organic thin film solar cells.

2.8 Conclusions

The various organized assemblies obtained so far highlight the unique possibility of tuning optical and electrical properties by appropriately designing the molecules and carrying out the self-assembly process in different solution based methods. However, a major challenge that still attracts considerable attention especially for the formation of organized assemblies relies on the control of the formation of morphologically organized ordered structures in a reliable manner and with great consistency. It has been previously found that in some cases the side chain substitution can lead to wide size distribution of the resulting wires and finding new solution based methods to create more uniform structures are still lagging. Furthermore, statistics relevant to the size distributions are also not shown in most cases, though is apparent from the morphological evaluations. It is therefore critical to understand the reasons for the formation of wide size distribution and to control the organization by appropriate solvent conditions.

Chapter 3

Self-assembly of long fluorescent wires from PTCDI

3.1 Introduction

With the observation of photo-conductivity from PTCDI,[178] and a large library of soluble variants now available,[97,108,115] these molecules have emerged as promising candidates for sensing and opto-electronic applications (photo-voltaic). The rationally designed and synthesized PTCDI have been used as functional building blocks to construct square[179] and hexagonal[97] supramolecular structures, 1D nanostructures such as nanobelts,[67,141,142,180] nanocolloidal suspensions,[181] and vesicular nanocapsules.[182] With the recent observation of fluorescence emission in the aggregated states of PTCDI coupled to the ability of tuning fluorescence emission over the wavelength range spanning the visible region, the emphasis has therefore been towards realization of fluorescent structures that can be useful for pH sensing,[182] fluid array immunoassay,[181] and sensing of volatile organic chemicals such as aniline.[158,183] The unique 1D assemblies constructed by the successful self-assembly of π-conjugated materials represent a first and critical step towards realization of new functional materials.[184] Already, several interesting organized 1D assemblies from PTCDI using solution based processing have been demonstrated.[180] Such solution based methods have yielded organized 1D assemblies predominantly by the favored π-stacking interactions amongst the π-rich surfaces. Most recent calculations by Ratner et al.[185] and Bredas et al.[186] on a wide range of PTCDI derivatives (more than 30 combined) reveal that the molecular packing driven by π-stacking interactions is expected to have pronounced effects on the charge-transport characteristics and the 1D geometry is the most favorable for the charge-transport[98,185,186].

N,N'-di(pentyl)-perylene-3,4,9,10-tetracarboxylic diimide, **38**

N,N'-di(octyl)-perylene-3,4,9,10-tetracarboxylic diimide, **39**

N,N'-di(dodecyl)-perylene-3,4,9,10-tetracarboxylic diimide, **40**
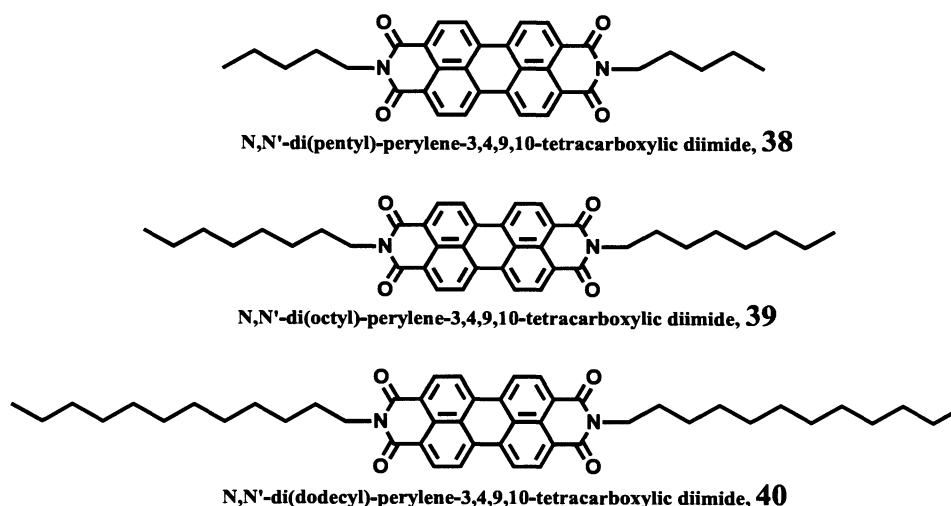
Figure 3.1 Chemical structures of the PTCDI employed for 1D self-assembly using the 2L-HT method.

The three linear alkyl substituted PTCDI used in this work to obtain self-assembled wires are shown in Figure 3.1. It has been previously shown that the resulting assemblies, particularly, from the linear alkyl substituted PTCDI are found to be 1D nanostructures and are primarily driven by non-covalent interactions such as π-stacking and alkyl side-chain interdigitation.[67,141,142] Almost in all the cases so far the 1D structures form tend to agglomerate together and form belt like structures.[67] For better understanding of the fundamental electrical and optical properties associated with the 1D structures it is essential to obtain individual 1D structures such as belts and wires in a reliable manner with extreme consistency in the dimensions of these assembled materials.[69,151] Herein, we show that it is, indeed, possible to create extremely large 1D wire like structures in a very controlled manner by adopting a modified phase-transfer method, namely, the *phase-transfer at high temperature* (2L-HT). Moreover, the 1D structures grown using the 2L-HT method show very intense excimer like emission from the aggregated state.

It is interesting to note that these self-assembled materials show intense fluorescence behavior despite the organization of the PTCDI molecules being primarily driven by π-stacking interactions. Until recently, such strong fluorescence behavior from aggregated states of PTCDI was hereto unknown. The previous studies on the assemblies of the 1D nanobelts show that there is significant quenching of the free molecule emission and almost no fluorescence emission is observed from these assemblies.[142] However, it was shown that from the disordered aggregated films of **40**, cast from homogeneous chloroform solutions, only very weak excimeric emission could be observed implying a co-facial arrangement of the perylene cores within the stacks.[141] In the same study the authors have further demonstrated that it was possible to tune the fluorescence emission (green to red) of the ill-defined assemblies, created by extremely distorted packing between the perylene cores, from swallow type (branched alkyl) PTCDI.[141] Recent studies[187-190] support this behavior and now it is generally accepted that only weak emission is observed from the strongly aggregated π-stacking (co-facial arrangement) while reasonable to strong excimeric emission can be detected from the weakly π-stacked (or distorted) aggregates. In a series of carefully carried out experiments, Wurthner et al.[188] have shown that by mixing two separate aggregates, one H- and other J-type PTCDI, it is indeed possible to co-aggregate the J-type within the H-type till equal concentrations (1:1). Above this critical concentration the J-type packing was preferred because of energetic reasons. Based on such a behavior, we hypothesize that it must be possible to have both strong and weak coupling of the PTCDI molecules within a **single wire**, by some means of organization, leading to unique 1D structure with unique emissive behavior. Thus, we explore, firstly, the formation of the wires with both

strong and weak coupling of the PTCDI molecules by using a novel solution processing method (2L-HT) and then examine the unique fluorescence behavior from these assembled wires.

3.2 Synthesis of PTCDI

The PTCDI molecules shown in Figure 3.2 were synthesized by the strategy which involved the condensation of PTCDA, **1** with an aliphatic amine under an argon atmosphere at 140 $^\circ$C using imidazole as a solvent (Scheme 1). The resulting PTCDI after purification was characterized by NMR spectroscopy.
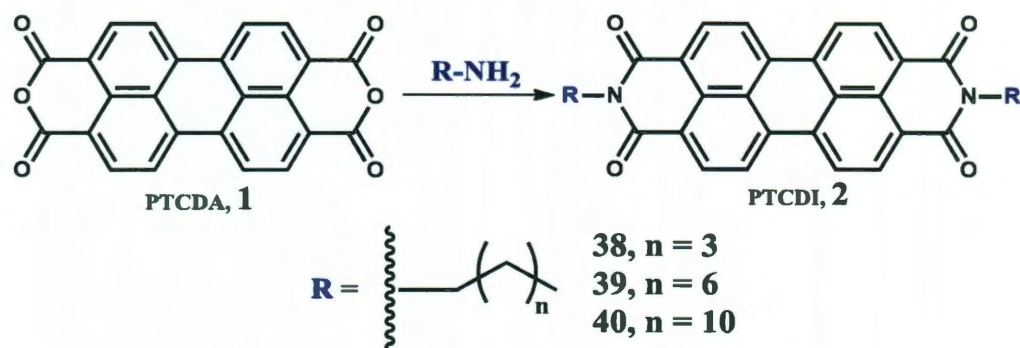
Figure 3.2 Synthesis of planar symmetrical PTCDI used in this study.

All chemical used in this study were used as received from the supplier. PTCDI **39** was commercially purchased from Aldrich while **38** and **40** were synthesized by known procedures. A detailed description of the synthesis and characterization of these two PTCDI is discussed below. All the solvents employed in the synthesis and the 2L-HT method were used as received from the supplier. In order to determine the purity, ^{1}H-NMR was performed in CDCl$_3$ solutions using a 400 MHz Bruker NMR spectrometer.

3.2.1 N,N'-di(pentyl)-perylene-3,4,9,10 tetracarboxylic diimide (38)

2 g (5.09 mmol) of perylene-3,4,9,10-tetracarboxylic dianhydride (PTCDA), 8 g (0.1175 mol) imidazole and 3.5 ml amylamine were placed in a three necked flask. One of the ends of the three neck flask was connected to a water condenser, Argon gas was purged into the reaction mixture using the second inlet and the third inlet was sealed with a rubber stopper. The flask was then purged with Argon for 10 min at room temperature so as to remove all the air trapped in the system and then immersed in the oil bath at 140 $^{\circ}$ C. The reaction mixture was stirred at this temperature in the argon atmosphere. The imidazole starts melting and the reaction is initiated. The reaction mixture was kept stirring at 140 $^{\circ}$C for 3 h to ensure the completion of the condensation reaction between the amine and the anhydride. The reaction mixture was then cooled to room temperature resulting in the solidification of the reaction mixture. Separately, 2M HCl (500 ml) and Ethanol (150 ml) were mixed together and the contents of the flask were then transferred to this solution. The entire solution was allowed to stir overnight at room temperature. The resulting dark maroon colored solid was then filtered and washed thoroughly with water until the pH of the washings turned neutral. The solid was further washed with ethanol so as to remove excess amyl amine. The solid powder was then dried at 100 $^{\circ}$C for 2 h to result give compound **38**. Yield: 93%.

^{1}H-NMR (CDCl3): δ = 0.945 (t, 6H, 2CH3), 1.401 (m, 8H, 18CH2), 1.78 (m, 4H, 2β-CH2), 4.22 (t, 4H, 2α-CH2), 8.65 (m, 8H, perylene).

3.2.2 N, N'-di(dodecyl)-perylene-3,4,9,10-tetracarboxylic diimide (40)

1 g (2.54 mmol) of perylene-3,4,9,10-tetracarboxylic dianhydride (PTCDA), 4 g (0.0587 mol) imidazole and 2.83 g dodecylamine, were placed in a three necked flask.

One of the ends of the three neck flask was connected to a water condenser, Argon gas was purged into the reaction mixture using the second inlet and the third inlet was sealed with a rubber stopper. The flask was then purged with Argon for 10 min at room temperature so as to remove all the air trapped in the system and then immersed in the oil bath at 140 ^{o}C. The reaction mixture was stirred at this temperature in the argon atmosphere. The imidazole starts melting and the reaction is initiated. The reaction mixture was kept stirring at 140 ^{o}C for 3 h to ensure the completion of the condensation reaction between the amine and the anhydride. The reaction mixture was then cooled to room temperature resulting in the solidification of the reaction mixture. Separately, 2M HCl (300 ml) and Ethanol (100 ml) were mixed together and the contents of the flask were then transferred to this solution. The entire solution was then stirred overnight at room temperature. The resulting dark maroon colored solid was then filtered and washed thoroughly with water until the pH of the washings turned neutral. The solid was further washed with ethanol so as to remove excess dodecyl amine. The solid powder was then dried at 100 ^{o}C for 2 h to give compound **40**. Yield: 95%.

^{1}H-NMR (CDCl3): δ = 0.882 (t, 6H, 2CH3), 1.392 (m, 36H, 18CH2), 1.77 (m, 4H, 2β-CH2), 4.22 (t, 4H, 2α-CH2), 8.64 (m, 8H, perylene).

3.3 Optical properties of PTCDI

Very dilute solutions with ~1.0 μM concentrations in different solvents were used for observing the spectral features associated with the three PTCDI. Solution based UV-Visible spectroscopy was performed on a Shimadzu spectrometer. Steady-state solution fluorescence emission spectra were obtained on FluoroMax-3, Horiba Jobin Yvon.

The homogeneously dissolved PTCDI molecules show very similar absorbance and emission spectra since the nodes are present at the imide nitrogen in both the HOMO and LUMO[115]. As an example, the absorption and emission spectra of **39** in chloroform are shown in Figure 3.3. Both **38** and **40,** show very similar absorbance and emission behavior in chloroform because of the aforementioned reason.
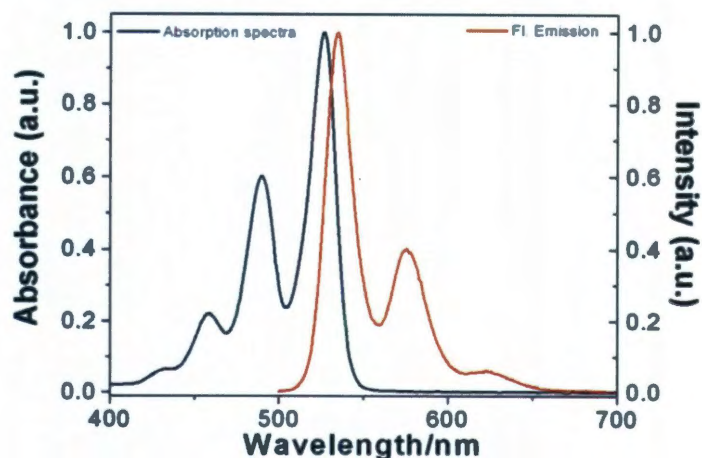
Figure 3.3 The UV-Visible absorption and emission spectra of **39** in chloroforom. The excitation wavelength or obtaining the emission spectra is 480 nm.

This leads to unique situation in PTCDI where in the dissolved state no solvatochromism behavior is observed but in solid state upon aggregation a pronounced crystallochromy can be observed, leading to crystals with different shades of color ranging from red to black[138]. Kazmaier et al.[140] has derived an empirical relation between the absorbance maxima and the different offsets (transverse and longitudinal) in the packing of the PTCDI, which results in the crystallochromy. Upon aggregation of the PTCDI molecules in poor solvents pronounced changes occur in the optical absorbance spectra[67,141]. In some cases it has been found that a new absorption band appears at longer wavelength (crystal phase) upon aggregation in certain solvents and concomitantly a

decrease in the absorbance of the 0-0 peak and increase of the 0-1 and 0-2 transitions. These optical characteristics have been associated with the strong co-facial packing of the perylene cores. In all of the three PTCDI studied in this work we observed the formation of crystal phase at longer wavelength (560-580 nm) and a concomitant increase in the 0-1 transitions in comparison to the 0-0 transition in the absorbance spectra in three different solvents upon aggregation as shown in Figure 3.4. The three solvents that we found to be suitable for the formation of aggregates from the homogenous chloroform solution were methanol, hexane and cyclohexane. A simple dispersion of the PTCDI molecules in chloroform to any one of these solvent leads to the aggregation and is usually complete within minutes (rapid). Thus, we chose these three solvents as the aggregating solvent for carrying out the assembly by the 2L-HT.
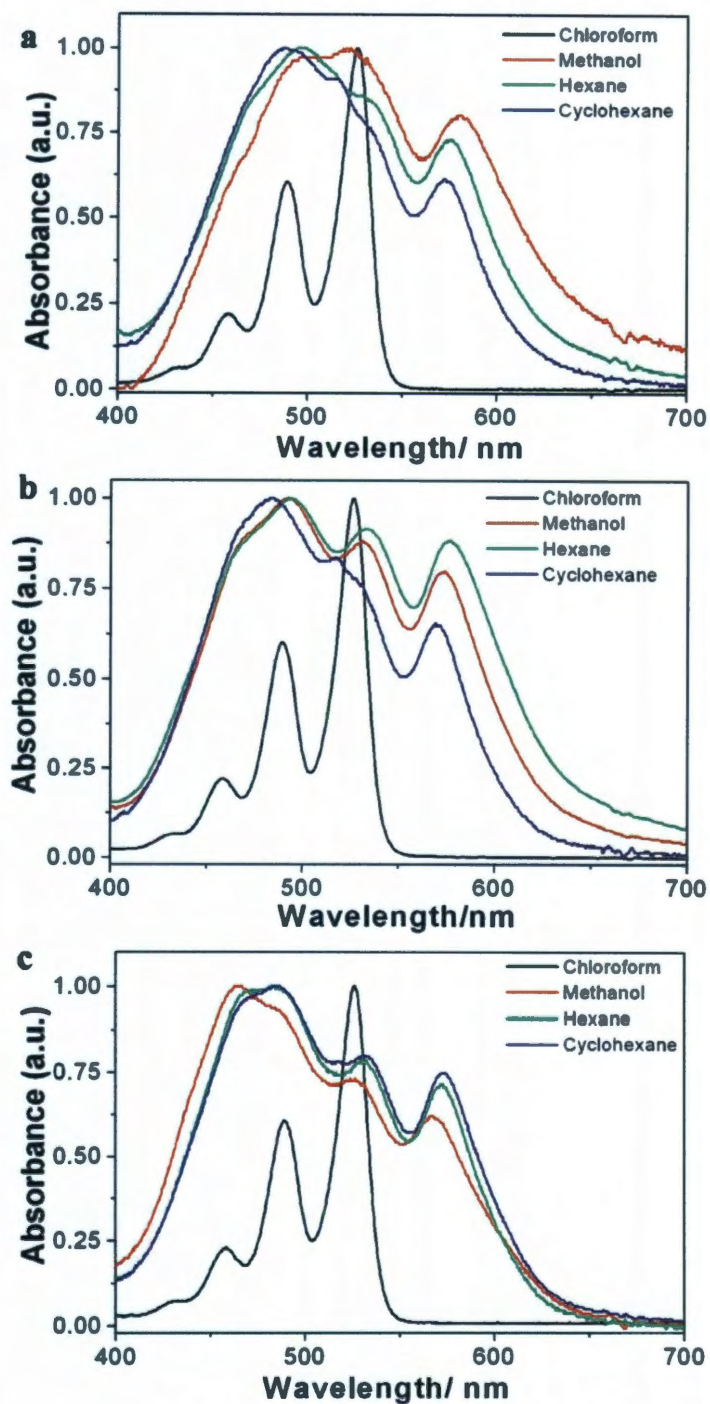
Figure 3.4 UV-Visible absorption spectra of **38** (top), **39** (middle), and **40** (bottom) in different solvents. 10 μl of 0.4 mM homogeneous solution of PTCDI in chloroform was rapidly injected in methanol, hexane and cyclohexane and the spectra were recorded in these solvents. The appearance of new peak at long wavelengths along with decrease of 0-0 transition and increase of 0-1 transition implies strong electronic coupling between the PTCDI molecules.

3.4 Self-assembly of PTCDI by room temperature solution processing

In order to study the self-assembly of PTCDI, a stock solution of each of the PTCDI was prepared in chloroform (0.4 mM, by slight heating). The solvents in which aggregation occurred were identified by performing UV-visible experiments as mentioned above. Methanol, hexane and cyclohexane were found to be suitable solvents for carrying out the self-assembly.

3.4.1 Dispersion and two layer (2L) phase transfer methods

In order to study the self-assembly by dispersion, a small amount of stock solution of an appropriate PTCDI was rapidly injected in a large excess of an appropriate non-solvent (methanol, hexane or cyclohexane). The red color aggregates were formed within 30 minutes. This process is depicted in Scheme 3.1a. The red colored aggregates were then cast on TEM grids and were examined for their morphology.
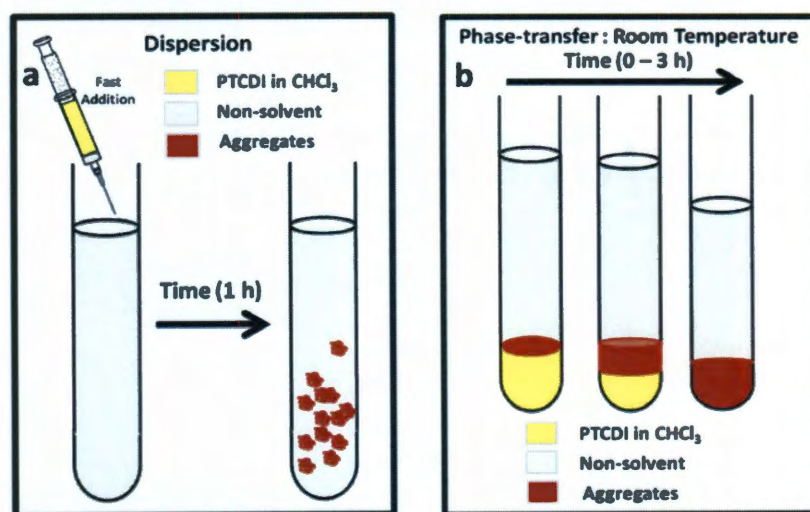
Scheme 3.1 The schematic illustration of (a) dispersion and (b) two layer room temperature (2L-RT) methods for the self-assembly of PTCDI.

In case of two layer phase transfer method (2L-RT), a small amount of an appropriate stock solution of PTCDI in chloroform was placed in small glass tube. This was then followed by the careful addition of an appropriate non-solvent (methanol, hexane or cyclohexane) on the top of the chloroform solution without disturbing the lower layer of chloroform. The aggregation took place at the interface of the chloroform and the non-solvent and there was appearance of red band within first 30 minutes. This red band slowly grew in size and in 3 h the entire yellow color solution of PTCDI in chloroform turned into red colored aggregates. This was confirmed by the absence of fluorescence emission from the free molecules of PTCDI in stock solution by a hand held UV lamp. This process is depicted in scheme 3.1b. The samples were then dried on the silicon wafer and examined by SEM.

3.4.2 Morphology of aggregates by dispersion and 2L-RT method

The dispersion and 2L-RT methods were carried out in three different solvents (methanol, hexane and cyclohexane) for each of the molecule used in this study to construct the aggregates. The as prepared aggregates in the solutions were directly spread on silicon or oxidized silicon substrates. After the evaporation of the solvents a light sputtering of the aggregates with gold is performed to allow for morphological evaluations under high vacuum and operating voltage conditions.

In case of dispersion of the individual PTCDI stock solution in an appropriate non-solvent, very uniform 1D fibers of very small diameter (in the range of few nm) and few micron length were observed by the TEM. Dispersion being a fast aggregating process, large number of uniform nuclei are rapidly generated and the free molecules of PTCDI aggregate on these nuclei resulting in small diameter and few micron long

uniform fibers. The morpholgy of the aggregates of **39** formed by utilizing all the three non-solvents is shown in figure 2.5. 30 nm, 120 nm and 130 nm diameter uniform 1D fibers result from methanol, hexane and cyclohexane as an aggregating solvent respectively. Similarly, an increase in diameter of the fibers with change in solvent from methanol to hexane to cyclohexane for **38**, and **40** was also observed which implies that the rate of aggregation is faster in methanol followed by hexane and then cyclohexane.
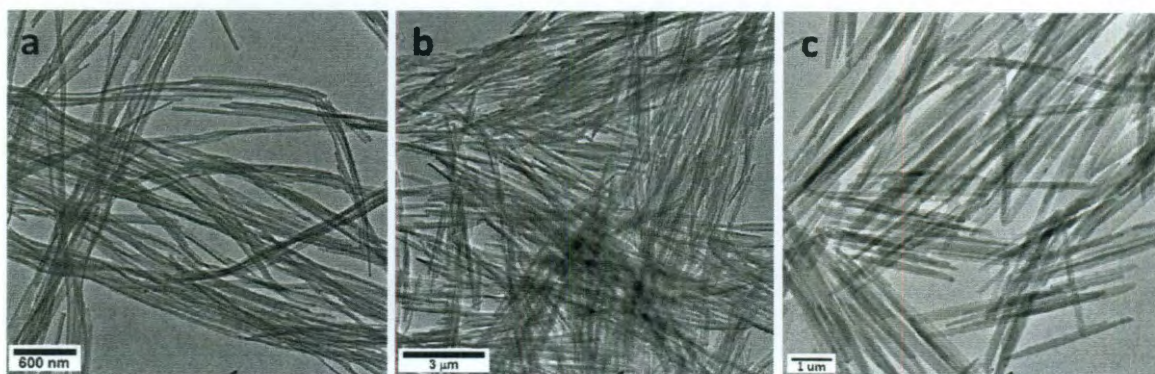
Figure 3.5 TEM images of fibers of **39** obtained by dispersion of homogeneous stock solution of **39** in (a) methanol, (b) hexane and (c) cyclohexane.

In case of 2L-RT of the individual PTCDI stock solution in methanol and hexane, there was large size distribution in the 1D self-assembled structures. There was formation of belt and wire like assemblies. The diameter of the 1D structures ranged from few nm to few microns and lengths were observed to be from few microns to a millimeter. On the other hand, cyclohexane led to very uniform diameter 1D belts from **38**, **39** and **40**. The 2L-RT, being a slow procees of aggregation at the interface of two solvents, large number of non-uniform nuclei are formed at the interface and the free molecules of PTCDI aggregate on these nuclei resulting in large size distribution. It appears that cyclohexane leads to formation of very uniform 1D belts at the interface due to slow nucleation and growth whereas methanol and hexane leads to large size distribution due to fast and non-

uniform growth. The morpholgy of the aggregates of **39** formed by utilizing all the three non-solvents is shown in figure 2.6. A wide size distribution is clearly evident when methanol and hexane were used as non-solvents whereas a narrow size distribution results when cyclohexane was used as aggregating solvent.
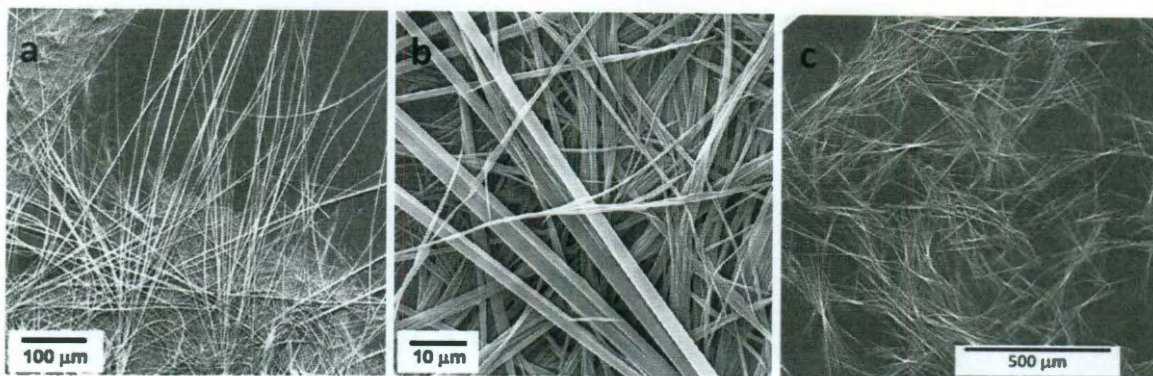
Figure 3.6 SEM images of fibers of **39** obtained by two layer room temperature of homogeneous stock solution of **39** with (a) methanol, (b) hexane and (c) cyclohexane.

Thus, 2L-RT leads to large size distribution in the morphology of 1D structures. In order to study the effect of temperature, which can control the rate of nucleation and growth, on the self-assembly by two layer phase transfer method, a slightly modified two layer phase transfer at high temperature (2L-HT) method was developed.

3.4 Self-assembly by phase transfer high temperature method (2L-HT)

The 2L-HT method developed here is an extension of the previously developed room temperature phase-transfer. A schematic depiction of the 2L-HT process is shown in Scheme 3.2. We take advantage of the previously developed phase-transfer method by carrying out the process at temperatures close to the boiling point of the chloroform solvent, in which the PTCDI molecules remain homogeneously dissolved but due to presence of a layer of poor solvent, there is very slow nucleation. The process for the formation of the assemblies of **38** in cyclohexane is described for ease of understanding.

The same protocol is followed for all PTCDI in other solvents as well. Typically, the 2L-HT process was carried out at 60 $^{\circ}$C (unless otherwise mentioned).
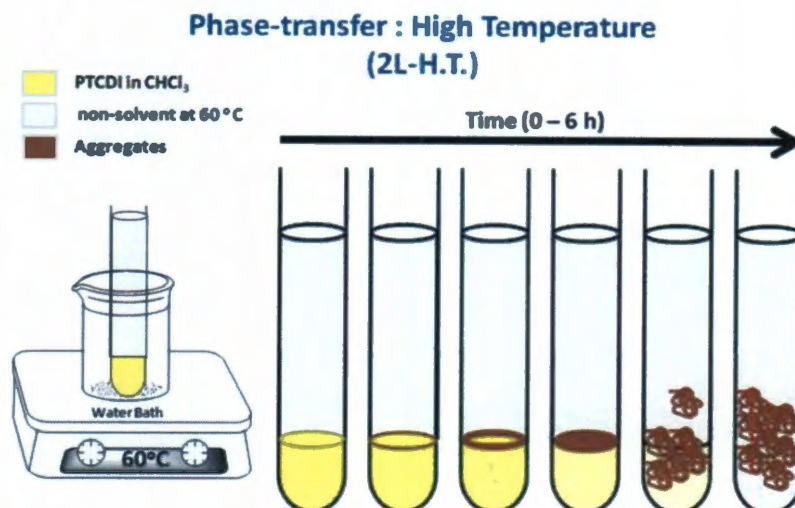
Scheme 3.2 The schematic illustration of different stages involved in the 2L-HT method (b). The 2L-HT method is carried out typically at 60 $^{\circ}$C (in a water bath), wherein the dissolved molecules of PTCDI in chloroform are thermally equilibrated for few minutes. Separately, in a tube the aggregating solvent is also equilibrated at the same temperature. After this the aggregating solvent is carefully added atop the dissolved PTCDI chloroform solution. Because of the high temperature in the 2L-HT method and the differences in the polarity of the two different solvents, the aggregation of the PTCDI dyes takes much longer for the initiation (and also completion) than when carried out at room temperature. Usually, the aggregation leading to the formation of the 1D assembly takes about 6-8 h for completion.

In a water bath set at 60 $^{\circ}$C, one testing tube filled with cyclohexane was allowed to equilibrate for 5-10 minutes. Another testing tube filled with about 0.3 mL of **38** in chloroform was allowed to equilibrate for about 2 min. in the same water bath, following which about 4 mL of the pre-equilibrated cyclohexane was carefully transferred (using pipette) atop the chloroform solution of **38**. It was ensured during this stage that no mixing of the two solvents occurs. The volume of the aggregating solvent (cyclohexane) was maintained at large excess (10:1 v/v). The assembly of the molecules was carried out

by maintaining the temperature at 60 ^{o}C throughout the growth process. In order to maintain the large volume of the aggregating solvent, the thermally pre-equilibrated aggregating solvent was periodically added once a slight notable change in the volume was noticed to maintain the 10:1 volume ratio without disturbing the two layers. Because the process is carried out at higher temperature than room temperature (usually 60 ^{o}C), the PTCDI molecules tend to remain soluble for extended periods of time. However, after a certain time period (30 min. in case of methanol, and hexane and 3 h in case of cyclohexane) a small red band can be observed at the interface of the two solvents indicating the initiation of the aggregation (nucleation). Over time this red band can then be seen to increase in size followed by the observation of needle shaped red aggregates (growth). After about (2 h in case of methanol, and hexane and 5 h in case of cyclohexane) it can be seen that a few of the needle shaped structures seem to float inside the tube while most of them are still present at the interface. At this point (~2-5 h) still considerable amount of free molecules remain in the solvent mixture (green emission seen in the bottom portion of the tube, UV-hand held lamp, 365 nm). The assembling process is further continued at the desired temperature until almost no (or detectable change of) free molecule emission can be observed. Already, at this stage in solution (i.e. at the completion of assembly process) it can be observed that the needle shaped aggregates show bright red fluorescence emission upon UV-light excitation (365 nm). The aggregates are then examined for their characteristic morphology using microscopic methods. The notable difference in the different solvents was in the time required for the formation of aggregates and completion of the 2L-HT process in each case.

3.6 Scanning electron microscopy (SEM) of the aggregates

The newly developed 2L-HT was carried out in three different solvents (methanol, hexane and cyclohexane) for each of the molecule used in this study to construct the aggregates. FEI Quanta ESEM with field emission gun under vacuum and operating voltage of 20 kV was used for the morphological investigation. The as prepared wires in the solutions using 2L-HT method were directly spread on silicon substrates. After the evaporation of the solvents the fluorescent wires were left behind on the substrate. A light sputtering of the wires with gold is performed to allow for morphological evaluations under high vacuum and operating voltage conditions.

3.6.1 Cyclohexane as aggregating solvent
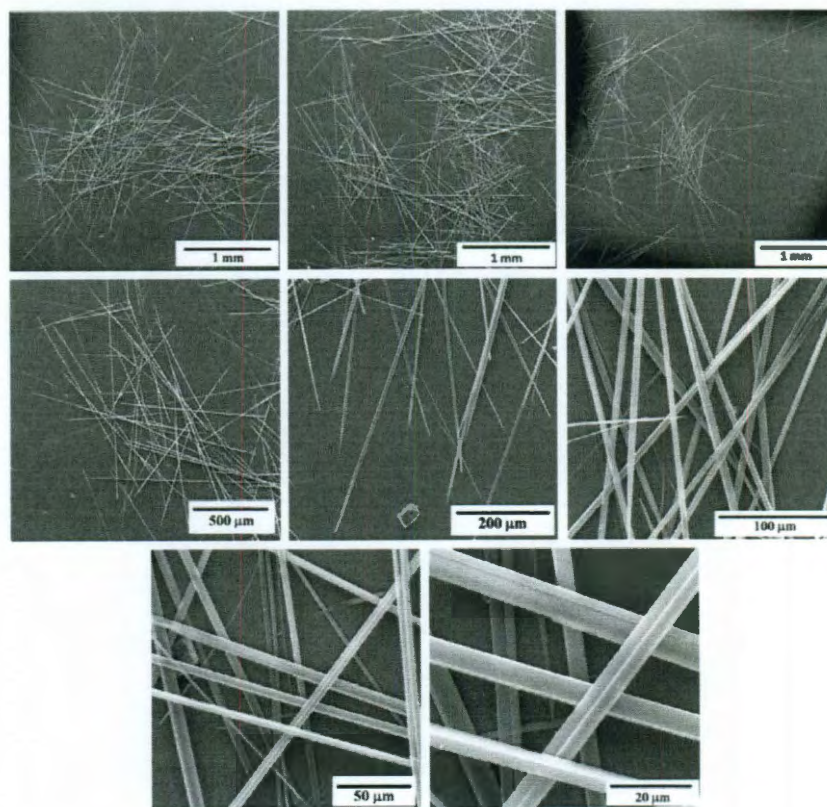
Figure 3.7 SEM images of the wires resulting from the 2L-HT processing of **38** in cyclohexane at 60 $^\circ$C.
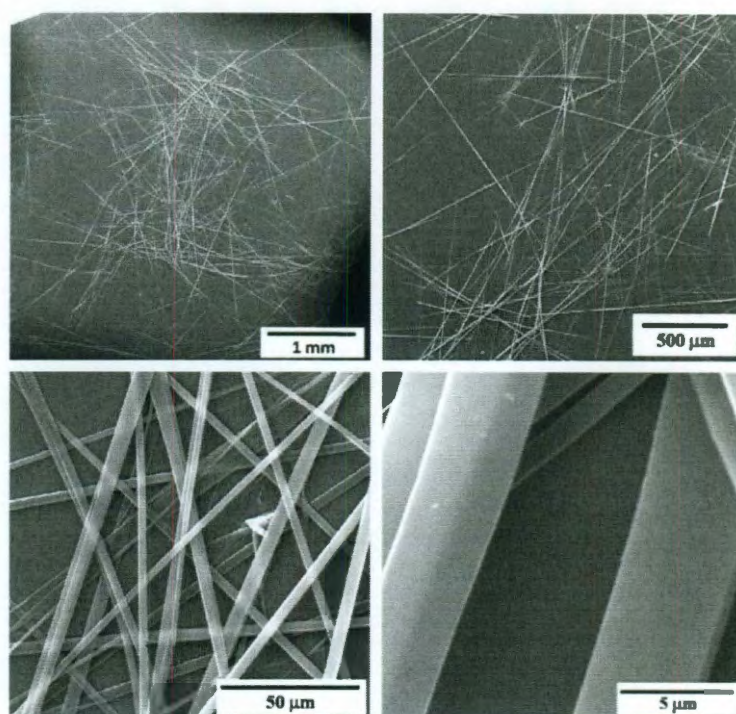
Figure 3.8 SEM images of the wires resulting from the 2L-HT processing of **39** in cyclohexane at 60 °C.
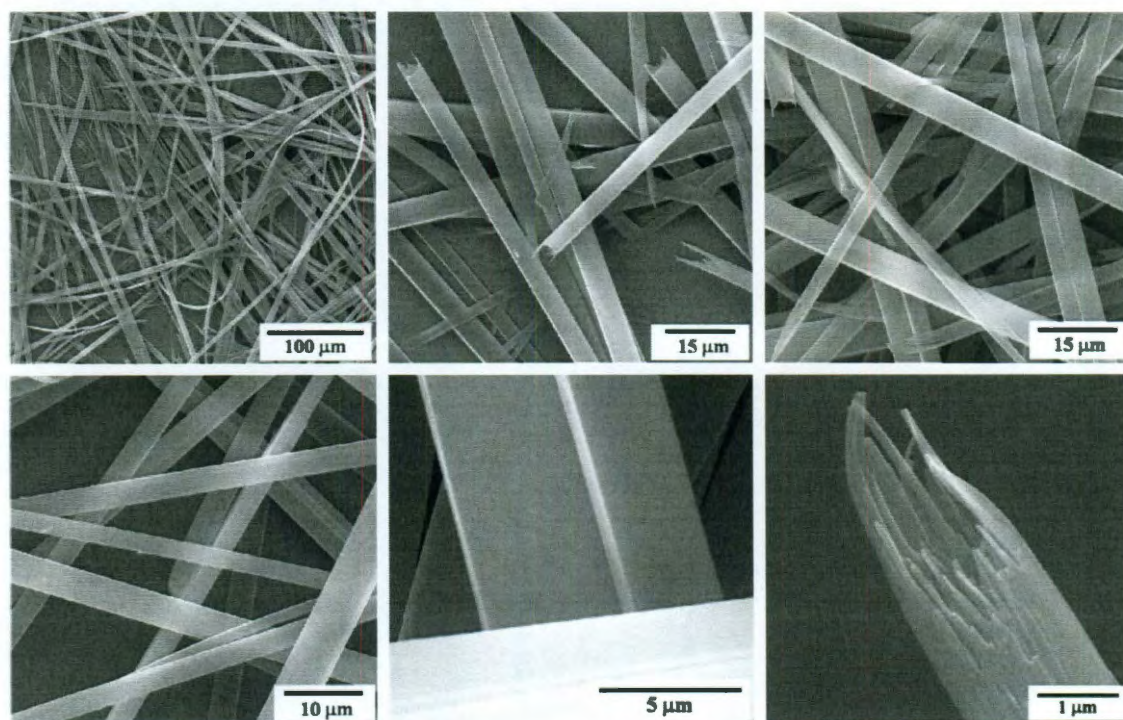
Figure 3.9 SEM images of the wires resulting from the 2L-HT processing of **40** in cyclohexane at 60 °C.

Figure 3.7, 3.8 and 3.9 shows the SEM images of the resulting aggregates using cyclohexane as the aggregating solvent from **38, 39** and **40**, respectively. When using cyclohexane as the aggregating solvent, in case of **38,** and **39** it is apparent from the low magnification images that **wire** like structures with lengths exceeding **1 mm** and widths of several microns are formed. While **40** tends to mostly form **wire** like structures with maximum lengths around 575 μm.

3.6.2 Hexane and methanol as aggregating solvents

For **38**, the largest lengths (~1 mm, average), and correspondingly the widths and heights, of the wires are observed when the 2L-HT processing is carried out in cyclohexane as the aggregating solvent while hexane produces most of the wires (more than 95 %, see Figure 3.11) having lengths ~250 μm, much shorter than cyclohexane. It is interesting to note that when methanol is used as the aggregating solvent the wires of **38** tends to bundle up rather strongly and significant distribution in the overall size (length, width and height) is observed (Figure 3.10). For **39**, cyclohexane produces the best quality of wires in comparison to those formed in methanol (see Figure 3.12), and hexane (see Figure 3.13). The overall size distribution of the wires for **39** is much more narrow in cyclohexane in comparison to methanol and hexane. For **40**, the best quality of wires is formed when the 2L-HT is carried out in hexane (see Figure 3.15) in comparison to those in cyclohexane or methanol (see Figure 3.14). In cyclohexane and methanol, in addition to the wire like structures a few belt like structures are also apparent. Also, the ends of the wires have different morphology depending on the aggregating solvent used. The ends of the wires formed from **38** and **39** are always tapered irrespective of the aggregating solvent used while **40** shows two distinct end structures depending on the

aggregating solvent used. The wires formed from **40** in hexane and cyclohexane have abrupt endings with several small wires bundled and protruding at the edges of the while in methanol slightly tapered rectangular edges are apparent. In all of the three PTCDI, 2L-HT processing creates structures with notable increase in the heights of the wires when compared with the morphology of the resulting aggregates using previously processing techniques (i.e. phase-transfer at room temperature).

The size distribution (lengths and widths) resulting for each of the PTCDI in the three solvents employed for the 2L-HT processing at 60 °C is summarized in Table 3.1. The value of the widths and lengths shown for each of the case has been estimated by averaging the results obtained for over atleast 10 measurements. Since, size distribution is apparent relative standard deviation (r.s.d, expressed in %) was calculated for each of the case. From Table 3.1 it is clear that the largest size distributions (% r.s.d) can be found in **39**, irrespective of the solvent used. When methanol is used as the aggregating solvent a trend of decreasing widths for the corresponding increase in the side-chain length can be obtained. Such a trend has previously been noted for comparable increase in the side-chain length for the nanobelts that were formed[67].

Table 3.1 Size distribution (width and length) along with emission wavelength maxima from the wires formed from the PTCDI using 2L-HT.

	2L-HT-Solvent								
	Cyclohexane			Hexane			Methanol		
	W/μm (± x%)	L/mm (± x %)	λ_{em} (nm)	W/μm (± x %)	L/μm (± x %)	λ_{em} (nm)	W/nm (± x %)	L/μm (± x %)	λ_{em} (nm)
38	6.3 (±29)	1.0 (± 33)	684, 653[a]	2.7 (±32)	265 (±41)	682, 650[a]	950 (±55)	> 500	685, 650[a]
39	2.5 (±40)	1.5 (± 28)	647 * 675*	3.1 (±90)	642 (±57)	645* 677*	923 (±40)	N.A.	646* 674*
40	4.0 (±35)	0.6 (± 31)	663	1.7 (±44)	450 (±27)	660	891 (±29)	> 40	658

W and L correspond to the width and length of the wire, respectively; x% = relative standard deviation (calculated as standard deviation/ average *100) λ_{em}= fluorescence emission (wavelengths);a= shoulder peak;*=almost similar intensity.
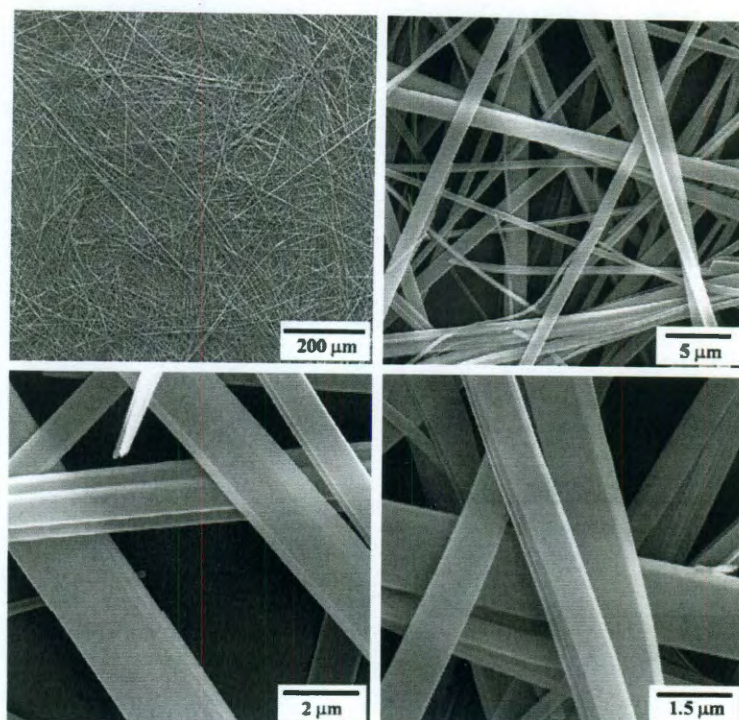
Figure 3.10 SEM images of the wires resulting from the 2L-HT processing of **38** in methanol at 60 $^{\circ}$C.
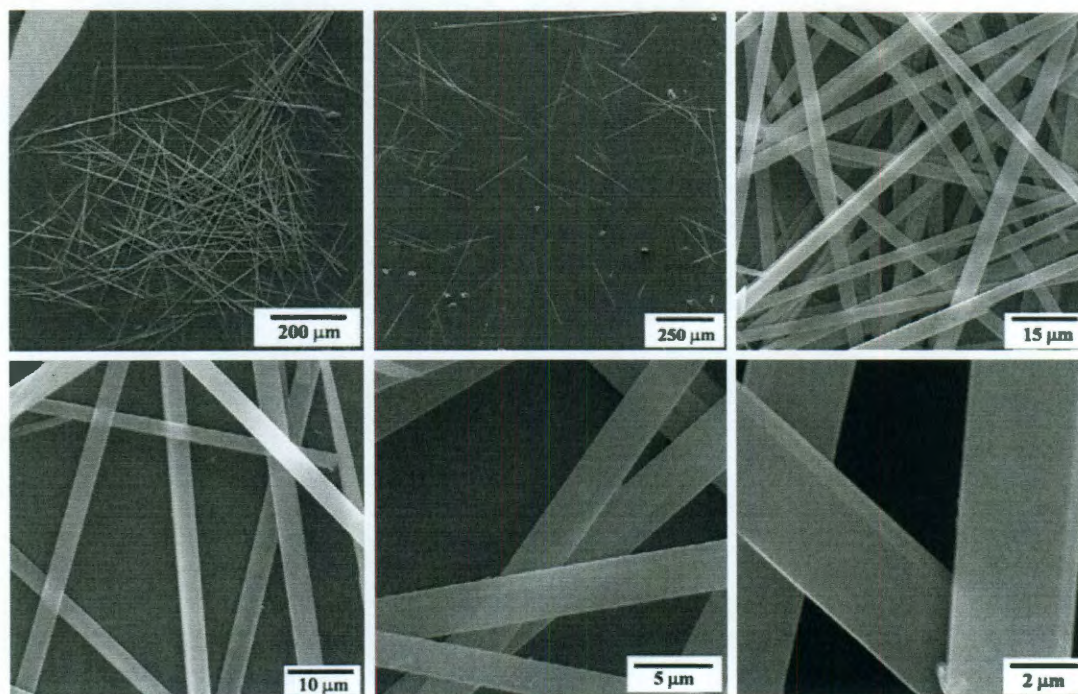
Figure 3.11 SEM images of the wires resulting from the 2L-HT processing of **38** in hexane at 60 $^{\circ}$C.
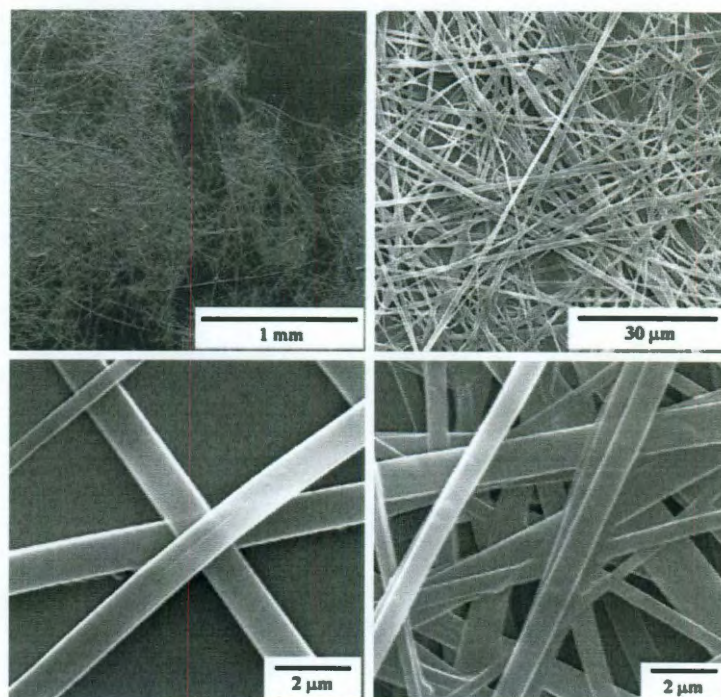
Figure 3.12 SEM images of the wires resulting from the 2L-HT processing of **39** in methanol at 60 °C.
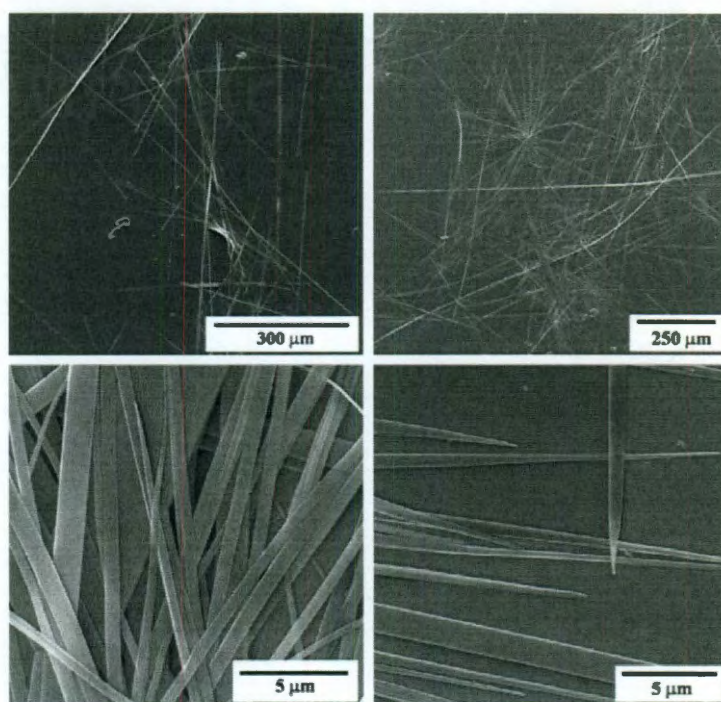
Figure 3.13 SEM images of the wires resulting from the 2L-HT processing of **39** in hexane at 60 °C.
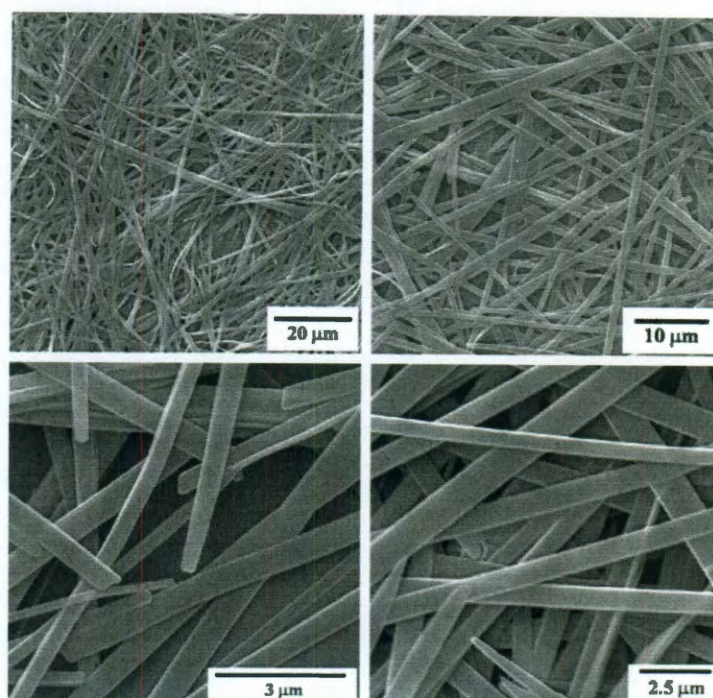
Figure 3.14 SEM images of the wires resulting from the 2L-HT processing of **40** in methanol at 60 $^{\circ}$C.
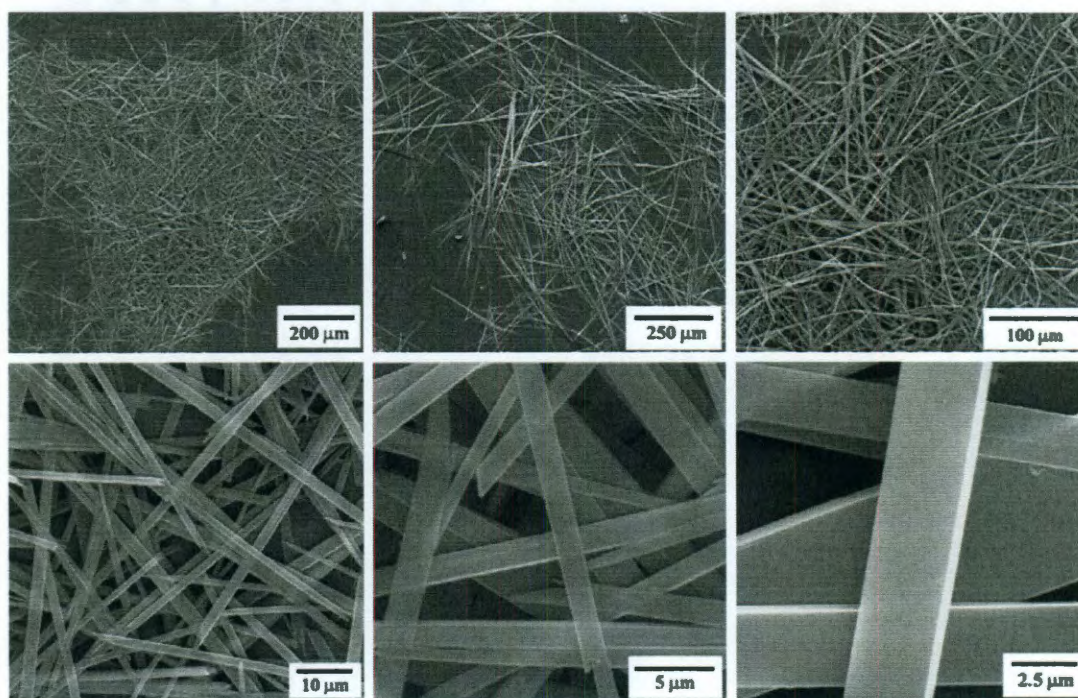
Figure 3.15 SEM images of the wires resulting from the 2L-HT processing of **40** in hexane at 60 $^{\circ}$C.

3.7 Effect of temperature on growth of PTCDI wires
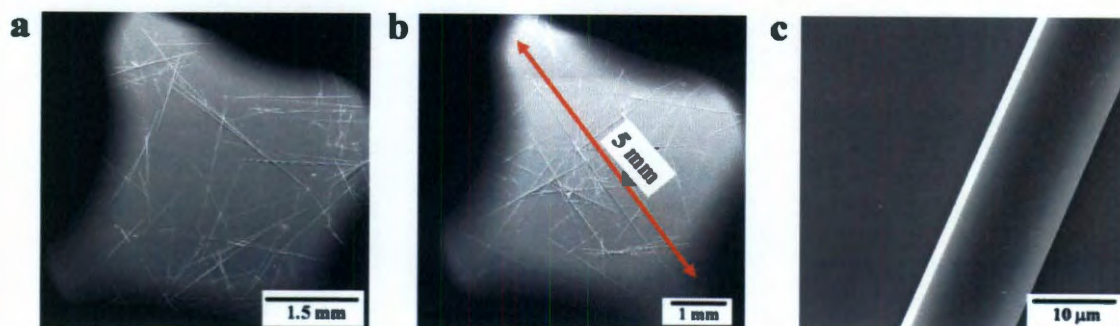
Figure 3.16 SEM images showing the large size distribution from the wires of **39** grown from cyclohexane at 70 ^{o}C.

In order to understand the role of temperature for the growth of single PTCDI wires using the 2L-HT method both lower and higher temperature conditions were used. It was found that 60 ^{o}C is the most optimal temperature for the controlled growth of the wires. Lowering the temperature between 40-55 ^{o}C only prolonged the growth and even after 10-12 h there was significant presence of the free molecules, while higher temperature, though allowed for the completion of the 2L-HT process in lesser time that 60 ^{o}C, often resulted in much more distribution in the size of the wires (in comparison to those obtained at 60 ^{o}C). Except for **39**, there was no notable change in the resulting morphology in regards to the size of the 1D assembly. For the wires grown at 70 ^{o}C for **39**, a large notable increase in the overall dimensions of the wires could be observed (Figure 3.16). Most of the wires had lengths (2-5 mm) much larger than the mean distribution shown in Table-1. Increasing the temperature more than 70 ^{o}C results in rapid evaporation of the solvents, concomitant mixing, and thus offers no control in terms of organization.

3.8 Plausible mechanism for the formation of 1D wires of PTCDI

One major observation for the assemblies grown using 2L-HT method is that the structure in **38** and **39** result in individual **wires** with extremely long lengths (in mm) when compared to those formed in **40** (a few belts and agglomeration of the wires can be seen). In the 2L-HT method, growth of the structures are primarily facilitated at the interface of the two solvents at an equilibrated temperature. Because of the increased solubility of the PTCDI molecules in chloroform solvent, very few and uniform nucleating seeds can be expected to be formed at the interface, and therefore few and extremely large structures result (in terms of overall dimensions of the wire) because of the constant addition of the aggregates to the already present nuclei (seeds). Since, the 2L-HT process is extremely slow there is sufficient time for the molecules at the interface to organize and re-organize by π-stacking and alkyl chain interdigitation interactions with the seeds in an energetically favorable manner to yield wire like structure. Both growth kinetics and thermodynamic considerations play a vital role in driving the formation of the long wires observed in **38**, and **39**. This case is particularly true in cyclohexane as the initiation and the completion of the aggregation using 2L-HT takes much longer in comparison to those in hexane and methanol, thereby resulting in much longer wires in cyclohexane. Along with the observations mentioned above and the nature of the 2L-HT process some insight into the mechanism for the formation of extended, straight structures can be gained. Two simple plausible mechanisms based on the shape and sizes of the initial seeds formed are proposed.

(i) *Molecular stacking in a controlled manner:* In this first case it is assumed that the initial nucleating seeds formed have the same widths as those of the final resulting wires

and allow fresh additions only along the long axis of the seed at the interface. At the interface, there is constant dissolution and re-precipitation of the PTCDI molecules leading to situations wherein energy optimized packing of the molecules are adopted, and consequently the constant addition of the molecules along the long axis leads to the formation of the large number of individual wires.

(ii) *Small fibers aggregating to form large wire*: Another plausible route is that upon aggregation, initially, intermingled fibers with small dimensions are formed immediately at the interface of the two solvents. This situation cannot be excluded as intermingled belt like structures are often seen in assemblies when rapid aggregation is carried out. As fresh molecules are constantly aggregated atop this surface there is significant reorganization of the aggregates, promoted further by the temperature conditions, leading to much larger structures (in terms of overall dimensions, as is observed in this report). In both the plausible cases mentioned above the orientation of the molecules within the wires are extremely hard to envision without use of prior knowledge of the crystal structure, energy, and geometry minimized structures present, and have hence been excluded from the discussion of the plausible mechanism even though they are expected to promote a favored seed shape and size.

Moreover, it is likely that more than one such geometry optimized structure exists (discussed below) leading to highly fluorescent wires with tapered ends. Further investigation is required to obtain the detailed knowledge of the molecular packing within the wires and is presently beyond the scope of this report. It is likely that within a single-wire two or more inequivalent stacks are present. Such an inequivalent stacks within the PTCDI crystals have recently been observed.[185]

3.9 Pick and place of PTCDI wires

Upon completion of the 2L-HT process the wires were spread onto a whatmann filter paper and the solvent was allowed to evaporate off completely (Figure 3.17). The largest visible individual wire was then picked up using the tweezers and could be held on the tweezers for a long time, implying that these wires have reasonabale mechanical stability. The wire could then placed onto the desired substate, for example, to prove the feasability of the pick and place, we placed these wires on oxidized silicon substrate as shown in Figure 3.17. This operation was repeated for a few more wires. It was easier to work with the wires of **38** grown at 60 $^{\circ}$C and wires of **39** grown at 70 $^{\circ}$C, owing primarily to large lengths associated with the wires. After light sputtering with gold under vacuum the wires were investigated using SEM. Notably, the wires were not lost during the sputtering operation under vacuum. The locations where the wire was held with the tweezers shows a slight amount of damage. This is useful and critical information when real-time devices are attempted from these materials. Three differnet wires were held at differnet positions. Two were held at the ends and one was held at the centre and placed on to the oxidized substrate. Some of the image identifying the damages are shown in Figure 3.19.

Additionally, a single wire of **39**, held in the tweezers could be photo-excited using a hand held UV-lamp (low intensity, 375 nm) and intense emission could be observed with naked eye (Figure 3.17 b). Such intense fluorescence emission from ordered assembly of PTCDI is expected to have large impact in opto-electronic devices. Pick and place along with the intense fluorescence emission behavior could also be achieved for the wires of **38** grown at 60 $^{\circ}$C (Figure 3.18).
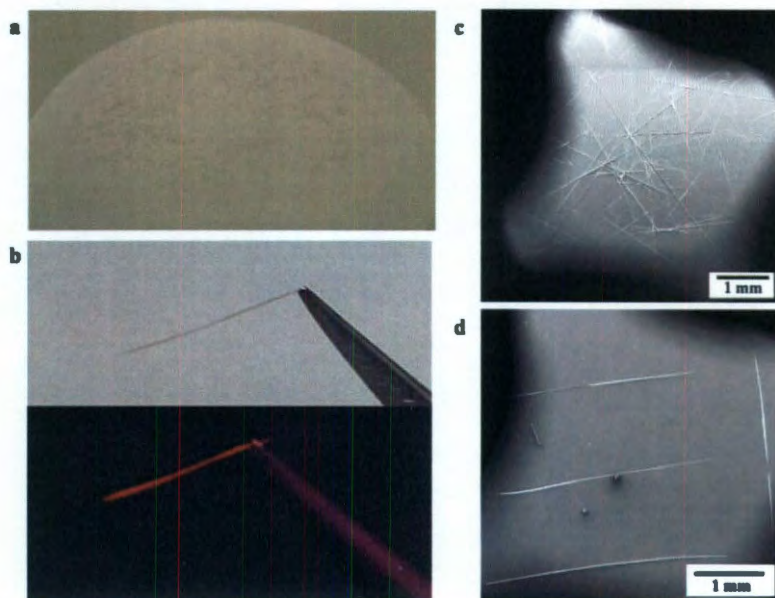
Figure 3.17 To test whether these large wires can be individually picked up, the as grown wires in cyclohexane were spread onto a whatmann filter paper. Upon evaporation of the solvent a large number of individual wires were readily visible (a). The SEM image of the spread wires on silicon substrate (c). An individual wire was then picked up using the tweezers (b, top panel) and could then be placed on desired surface, thus, establishing pick and place route for convenient fabrication of desired device. SEM imaging of the wires obtained by pick and place route for the wires of **39** (grown at 70 $^\circ$C) (d), again, highlighting that the overall size increase of the wires grown at 70 $^\circ$C in comparison to the wires grown at 60 $^\circ$C. Intense fluorescent emission from a single-wire of **39** held in the tweezers upon photo-excitation using a hand held UV-lamp (b, bottom panel).
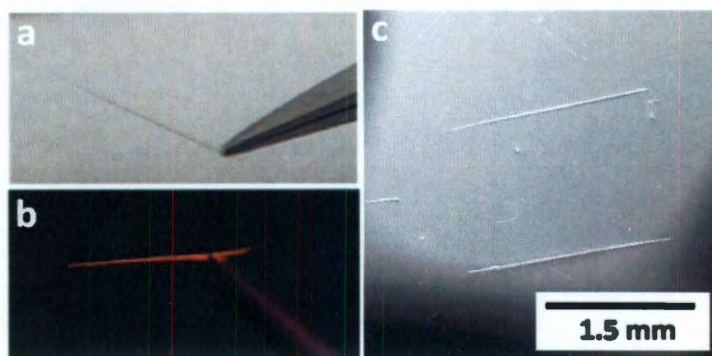
Figure 3.18. A single wire of **38** held using tweezers, **a** and its fluorescence emission, **b** upon excitation with a UV-hand held lamp (365 nm). SEM images showing the two large single wires of **38** placed on oxidized silicon substrate using the pick and place method, **c**.
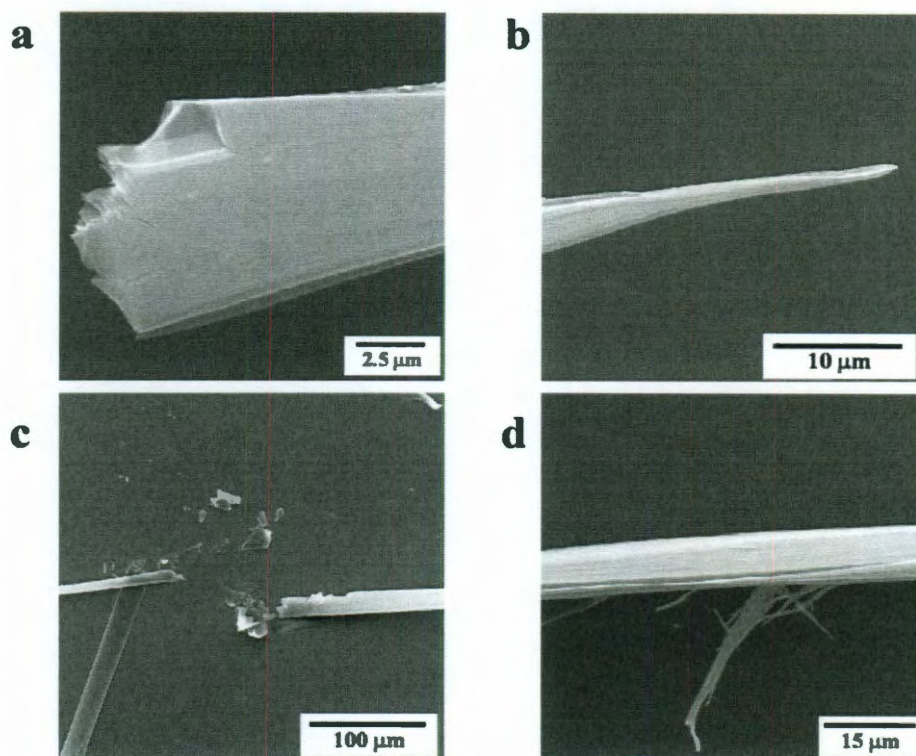
Figure 3.19 Broken ends of the wires held using the tweezers. Only the places that were held by the tweezers show a slight damage. Three wires of **39** were held by tweezers at different positions. Two of the wires held the ends are shown in a-c, while the wire held at the center is shown in d.

3.10 Optical properties of PTCDI wires

The wires of **38, 39, 40** were cast from their cyclohexane solutions after the 2L-HT process was complete on to pre-cleaned, and cut glass substrate. The dimensions of the cut glass was carefully tailored to fit diagonally (at an angle of 45°) within a polystyrene (P.S.) cuvette. The P.S. cuvette, with the sample on glass, is then placed within the specimen holder in the FluoroMax-3, Horiba Jobin Yvon. The glass containing the wires directly faces the excitation source and concomitantly the emission is then collected by the detector, which is at 90° to the excitation source. Two separate blank

measurements were performed using just the P.S. cuvette and glass + P.S. cuvette, to ensure that there is no interfearance with the real fluoresence signals of the wires. For carrying out the ensemble fluoresence emission measurements from the wires, atleast 2-3 different areas were excited using differnet wavelengths (480-600 nm) and the data was collected upto 800 nm and analyzed. The excitation wavelength range of 480-600 nm was chosen because both the free molecule and the aggregates could be excited.
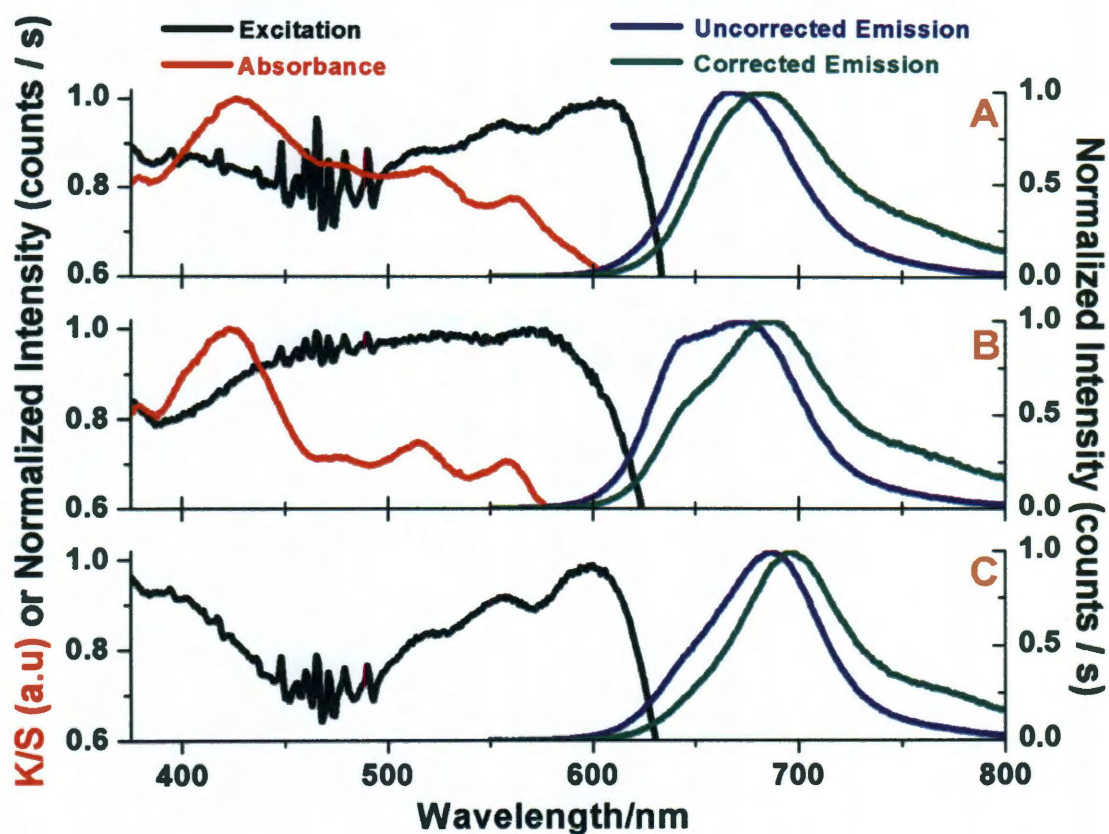
Figure 3.20 Solid state ensemble emission, excitation and absorption spectra from the 1D aggregates of **38**(C), **39**(B), and **40**(A).

Figure 3.20 (A,B and C) shows the ensemble solid state fluorescence emission spectra from the PTCDI wires aggregated from cyclohexane using 2L-HT at 60 $^{\circ}$C. For all the three PTCDI, the aggregates were excited at different wavelengths (450-600 nm)

to ensure that spectral features observed are real and representative of the sample. It is interesting to note that for the wires of both **38**, and **39**, two distinct emission peaks (structured vibronic states) could be observed while for **40**, only a single strong emission peak with maximum wavelength centered at 667 nm (red shift of 132 nm in comparison to the free molecule emission (535nm)) was observed when the respective wires were excited between 480-580 nm. For **38**, a small shoulder peak arises at 653 nm and maximum intensity at 684 nm, implying red shift of 118 nm, and 149 nm, respectively in comparison to the free molecule. For **39**, two peaks at 647 nm, and 675 nm (red shift of 112 nm, and 140 nm, respectively with free molecule emission, with almost equal intensity could be observed. No new emission peaks could be observed when the wires were excited with wavelengths of 600 nm or more in all of PTCDI. Moreover, two distinct vibronic features observed in the emission spectra of the wires could be observed in both the solid-state UV-Visible spectra and the excitation spectra. This suggests that the intense emission in this case is obtained from the aggregated state of PTCDI and is an excimeric emission.

The observation of two peaks in the emission spectra further corroborates that there are possibly at least two different π-stacking patterns involved in the formation of the wires.[189] Moreover, the large red shifts observed in the emission spectra of the wires in comparison to the free molecule emission implies that closely packed excitonic states might provide new pathways for allowing the excimer like emission from the aggregates, due of the large offsets introduced because of energetically favored assembly.[187] Therefore, both weak and strong coupling of the PTCDI molecules should be present in

the wires to allow for not only the formation of 1D wires but also strong emissive behavior, which is unknown for such linear alkyl-chain assemblies.

In general, it is unusual to see such intense emission from the self-assembled 1D structures of PTCDI, particularly, for the chemical structures used in this study, because of the strong π-π stacking involved.[141,187] Very few reports on the strong emission from the ordered aggregates of PTCDI in solid state have only been recently observed,[151,158,191,192] because for the aggregates in the solid state there are multiple quenching pathways,[187,193] while, the high fluorescence quantum yields are well known for the PTCDI family of dyes in solution. Generally, the side-chains that hinder the aggregation of the perylene core result in the dyes with high quantum yield.[115] Only recently, have the assemblies of core-twisted (bay substituted) PTCDI been shown to form fluorescent aggregates in solution state.[187,194] Additionally, it has been shown that fluorescent organogels are possible in bay-substituted PTCDI (core-twisted PTCDI).[191] Despite the 1D morphology, a large rotational and longitudinal offset was found in the aggregates of the PTCDI with the bulky side-chains,[187,188,195] thus, allowing for the electronic transitions from the ground state to both the lower and excited energy states and concomitantly the observation of fluorescence emission from these aggregates. Again, such carefully carried out experiments support our results here that it is possible to organize the PTCDI molecules in anisotropic 1D wire like structure with different π-stacking d-spacings.[185,188]

It is possible that in the initial formed seeds a certain preferred packing (with defined offsets) exists and the constant addition of fresh molecules to the aggregates results in significant reorganization of the stacks with new offsets being introduced.

Thereby, the final resulting wire gets formed because of, perhaps, two or more closely associated and energetically favored π-stacking and side-chain interdigitations. Of the two or more different π-stacking interactions that drive the wire formation, at least one is most likely the strong π-stacking interactions (H-type), while the other(s) are weakly coupled PTCDI molecules (J-type); the co-aggregation of these two types exist within the framework of each other leading to highly fluorescent and extremely long wires. It is therefore noteworthy that in our case macroscopically anisotropic structures such as wires result, despite the disorder at nanoscale (unequal π-stacking interactions).

3.11 X-ray diffraction of the wires of PTCDI

The as prepared wires in the solutions using 2L-HT method were directly spread on to glass substrates and were concentrated to a pre-defined region by directing the solutions (containing the wires), by blowing them carefully with an empty glass pipette (bulb attached). Once a certain desired thickness of the film composed of these wires was apparent in the pre-defined region the samples were allowed to completely dry in hood for a few hours. The samples were then mounted onto the sample area within the diffractometer for ensemble wire measurement and analysis. X-ray diffraction was carried out for the wires deposited on to glass substrates in the range of 3- 30° with scan rates (usually 0.25-0.5 ^{o}/min) using a Rigaku D-max Ultimate II configured with a θ-2θ goniometer. The source of the X-ray is Cu-Kα having wavelength of 1.5418 Å.
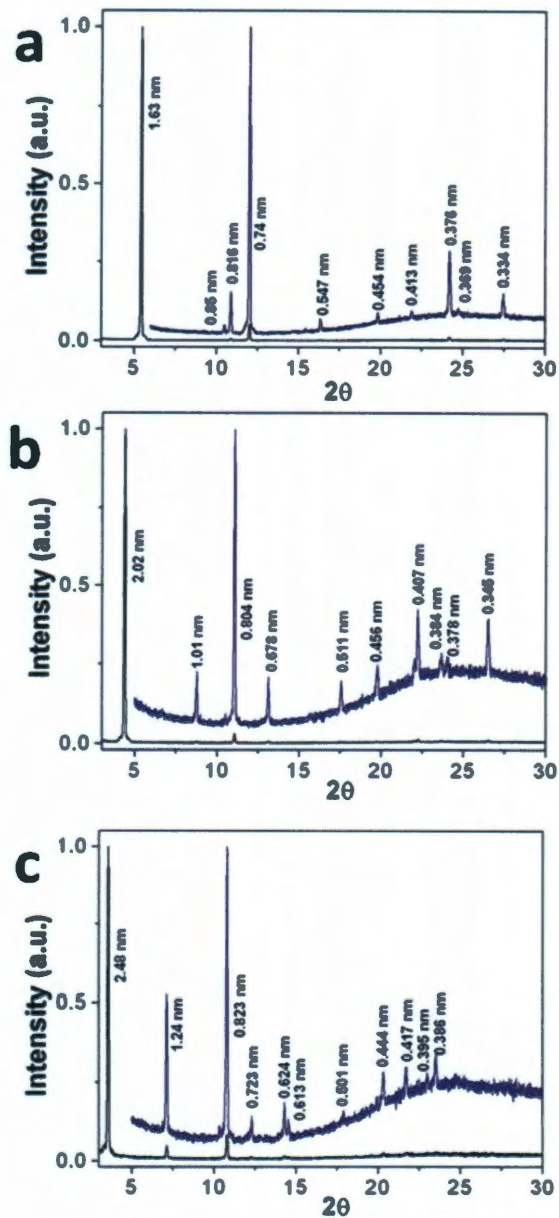
Figure 3.21 The ensemble XRD patterns obtained for **38**(a), **39**(b), and **40**(c).

The ensemble XRD patterns were recorded by casting an entire batch of the wires made using the 2L-HT of PTCDI in cyclohexane onto glass substrates. The XRD patterns for each of the PTCDI shows that indeed highly crystalline wires have been formed (Figure 3.21). The large intensity of the primary molecular peak obscured much of the

other relevant peaks present in the sample (the first peak in each case). Hence, separate θ-2θ scans were carried out beyond the main peaks to obtain meaningful XRD patterns. For the 2L-HT grown wires it is clear that in the d-spacing range of 0.335 – 0.45 nm a few peaks appear. It is well known that for perfect co-facial type packing a d-spacing of 0.335 nm is expected while generally, peaks from 0.34 -0.37 nm represent good co-facial arrangement of the molecules within the stacks and d-spacing from 0.37-0.45 nm have been shown to result in distorted packing of the molecule within the stacks.[186,189] Recently, Liu et al.[158] have shown that for their highly fluorescent PTCDI assemblies a largely distorted d-spacing of about 0.4 nm was observed. In our cases except for **40**, there is an observable peak at 0.334 nm for **38**, and 0.345 nm for **39**, indicating close contact of the molecules. Furthermore, three more peaks with d-spacing of 0.376 nm and 0.369 nm are clearly present in **38** which can be assigned to the slipped arrangement of the molecules within the stacks leading to the fluorescent wires. Similar observation could also be made in the wires of **39**, wherein, in addition to aforementioned 0.345 nm peak three additional peaks at 0.378 nm, and 0.384 nm could be seen. However, for **40**, only the peaks in the d-spacings of 0.386 nm, 0.395 nm and 0.417 nm could be observed. These structural features coupled with the fluorescence emission and observed morphology lead to interesting structure-property co-relations. For both **38** and **39**, there are both close contact and distorted π-stacking interactions driving the extremely straight wire formation, while for **40**, only distorted packing drives the self-assembly process. Moreover, the distorted packing does not allow for extremely large lengths of wires of **40**, while wires of **38** and **39** with large lengths could be easily constructed by the 2L-HT method. Additionally, the observation of two emission peaks can be attributed to the two

different spacing's present in both **38**, and **39** (both close contact and distorted) while a single Gaussian shaped emission peak for **40** can be attributed to the excitonic peak owing to the distorted packing.

3.12 Conclusions

In summary, extremely long and fluorescent wires from linear alkyl substituted PTCDI have been demonstrated using the novel solution processed 2L-HT method. This is the first report of the novel solution processing method (2L-HT) which allows for the formation of wire structure with lengths of the individual wires on the order of a few millimeters. Two or more distinct packing behavior seems to drive the formation of fluorescent wires. Moreover, given the large lengths of the wire, single wire could be easily picked and placed at desired location to expedite the use of such structures in fabrication of devices. The intense emission observed from the wires is expected to have diverse use, from studying the fundamental aspects of the emission to fabrication of devices. Further work is currently underway to identify the organization of the PTCDI molecules within the wires to enable advancement of these self-assembled materials for device applications.

Chapter 4

Synthesis and self-assembly of perylene-3,4,9,10-tetracarboxylic monoanhydride monoimides

4.1 ISntroduction

Self-assembly has been used as an efficient tool to fabricate organized functional materials by the bottom-up strategy. The ability to create self-assembled structures with well defined morphologies is essential for the applications of nanomaterials. The physical properties of the organic nanostructures depend not only on the constituent molecules but also on the size, dimension and crystallinity of the nanostructures. Various 1D structures from PTCDI molecules such as nanofibers, nanorods, nanowires and nanoribbons have already been fabricated (discussed in chapter 2) and have been utilized in functional devices such as sensors, optical waveguides, lasers and field effect transistors. Though 0D[181] and 1D[67,141,142,149] organic nanostructures based on these organic small molecules have been studied, the 2D self-assembly of these molecules still remains a major challenge. There have been several research efforts on controlling the arrangement of organic molecules on substrates.[196-198] This 2D self-assembly depends largely on the appropriate molecular building blocks which controls the directional interactions between the predesigned molecules and the specific substrate in an appropriate environment. Hence, the substrate plays a crucial role in arrangement of molecules by self-assembly. Moreover, external environmental parameters such as irradiation by light[199], electric and magnetic fields[200], time[201], concentration[202], temperature[203,204] also plays a critical role in these supramolecular self assemblies. Generating well defined nanostructures by solution processing has recently received large attention. Thus, the role of substrate governing the self-assembly is completely eliminated. Moreover, the solution processed supramolecular

assemblies can be transferred to variety of substrates depending on the intended application. Though there are very few reports on surfactant mediated two dimensional (2D) self-assembly of perylene with well defined shape[205], to the best of our knowledge the 2D self-assembly of perylene monoimides (m-PTCI) have never been explored. The fabrication of 2D sheets of m-PTCI opens new avenues to study the structure-property-function associated with this new class of materials.

4.2 Synthesis of m-PTCI

The structures of m-PTCI molecules used in this study are shown in Figure 4.2. These molecules with varying number of carbon atoms in the alkyl side chain were synthesized according to a previously reported procedure.[117] The synthetic scheme is depicted in figure 4.1
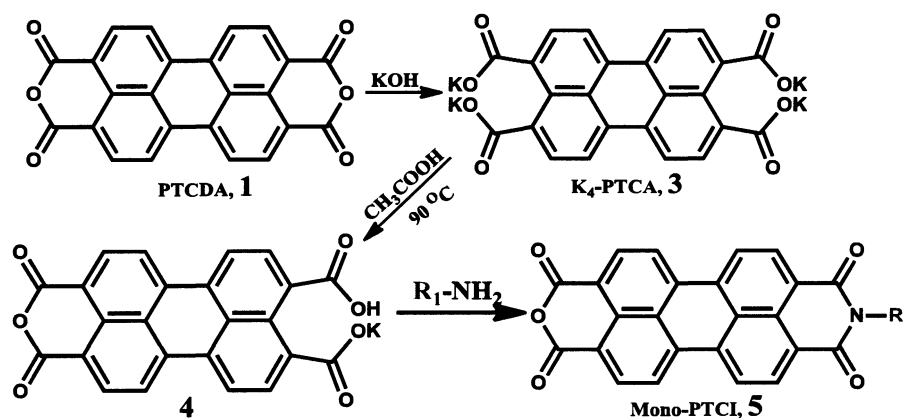
Figure 4.1 Scheme for the synthesis of m-PTCI.

Briefly, this involves the synthesis of perylene-3,4,9,10-tetracarboxylic acid monoanhydride monopotassium salt, 4 which has only one anhydride side accessible for the reaction with long alkyl chain amine. The product of this reaction is then isolated and subsequently the other open side is closed leading to the formation of m-PTCI, 5. Alkyl

amines with varying number of carbon atoms can be attached to the perylene core leading

to various m-PTCI with varying length of side chain. All these m-PTCI having only one

alkyl side chains have limited solubility in chloroform or dichloromethane and have very

strong tendency to aggregate thus making it difficult to characterize this product by ^1H

NMR. However, the mass spectroscopy was utilized to determine the purity of these

products which showed a 100% relative abundance peak corresponding to the appropriate

molecular weight of the corresponding m-PTCI.

N-mono(pentyl)-3,4,9,10-perylenetetracarboxylic monoanhydride monoimide, **41**

N-mono(octyl)-3,4,9,10-perylenetetracarboxylic monoanhydride monoimide, **42**

N-mono(decyl)-3,4,9,10-perylenetetracarboxylic monoanhydride monoimide, **43**

N-mono(dodecyl)-3,4,9,10-perylenetetracarboxylic monoanhydride monoimide, **44**
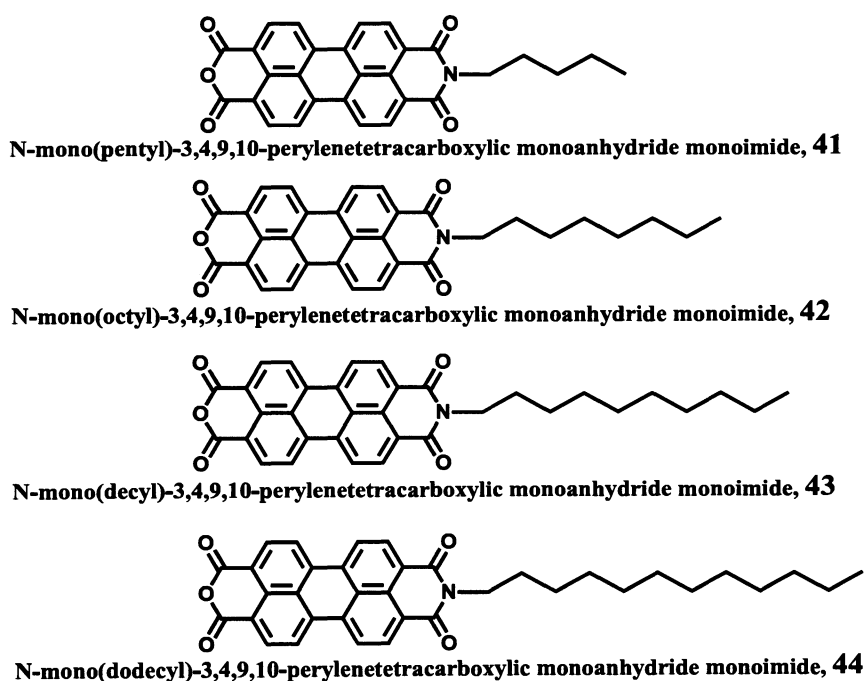
Figure 4.2 Chemical structures of the m-PTCI employed for 2D self-assembly.

(a) Synthesis of perylene-3,4,9,10-tetracarboxylic acid monoanhydride monopotassium salt :

2 g (5.09 mmoles) of perylene-3,4,9,10-tetracarboxylic acid dianhydride (PTCDA) was added to a solution of 1.7 g of KOH in 300 ml water and the resulting

mixture was heated at 90°C for 1 h with stirring to form a clear fluorescent green solution of tetrapotassium salt of perylene tetracarboxylic acid (K_4-PTCA). The resulting solution was filtered using a 0.2 µm pore size filter paper to remove any unreacted PTCDA if any. The filtrate was maintained at 90°C on hot plate. Separately, a solution of 2 ml glacial acetic acid in 18 ml water was prepared and the resulting solution was added dropwise to the 300 ml K_4-PTCA solution in water at 90°C with stirring. Highly water insoluble bordeaux colored precipitate started appearing with the addition of acetic acid at 90°C. This dispersion was allowed to stir further for 1 h at 90°C when all the fluorescent green solution of K_4-PTCA gets completely converted to bordeaux colored perylene-3,4,9,10-tetracarboxylic acid monoanhydride monopotassium salt. The resulting suspension was filtered using a 0.2 µm pore size filter paper. The bordeaux colored solid cake was obtained on filter paper which was given several washings with water to remove any unreacted K_4-PTCA if any. The solid cake was dried in vaccum oven at 120°C. Yield : 2.2 g, 99%

(b) Synthesis of N-(alkyl)-3,4,9,10-perylenetetracarboxylic monoanhydride monoimide

1 g (2.2 mmoles) of Perylene-3,4,9,10-tetracarboxylic acid monoanhydride monopotassium salt was weighed in a 30 ml glass vial. 4 molar ratio of an appropriate amine as mentioned in the Table 4.1 below, 6 ml water and 6 ml n-propanol was then added to this vial and the vial was briefly sonicated so as to uniformly disperse all the reactants. The vial was then placed on stir plate and allowed to stir vigorously at room temperature for 4 h. The color of the reaction mixture turned slowly from green to red in

the course of 4 h. This vial containing the reaction mixture was then stirred vigorously at 90°C for 2 h by immersing it in a hot oil bath. The color of the reaction mixture turned violet. After 2 h, the reaction mixture is allowed to cool and transferred in 500 ml 10% HCl and stirred overnight at room temperature. The red colored precipitate is then filtered to obtain a maroon red colored cake. This cake is washed with water until the pH of the filtrate is neutral. Then the cake was washed with ethanol several times so as to remove excess unreacted amine. The solid cake was then transferred in a 500 ml round bottom flask. To this was added 100 ml of 10% KOH solution in water and the resulting dispersion was heated at 90°C for 1 hour. This led to formation of dark reddish green solution and some precipitate. Then 100 ml of 8% KCl solution in water was added to this homogeneous solution which lead to the precipitation of potassium salt of the final monoimides product leaving behind a fluorescent green solution of K$_4$-PTCA formed due to the presence of trace amount of unreacted perylene-3,4,9,10-tetracarboxylic acid monoanhydride monopotassium salt. This dispersion was then filtered so that the solid cake was formed on the filter paper and green colored filtrate of K$_4$-PTCA was collected at the bottom. The cake was given several washings with 5% KCl solution in water till the color of the filtrate was colorless. This ensured that all the salt of PTCA was completely removed. The cake on the filter paper was then dissolved in 300 ml water which led to the formation of dark violet colored solution and some small amount of precipitate. This solution was then carefully filtered using a 0.2 μm pore size filter paper so as to obtain a clear violet filtrate. This filtrate was then acidified with 150 ml of 20% HCl and the resulting dispersion was stirred overnight at room temperature. The mixture was then filtered using a 0.2 μm pore size filter paper to obtain a maroon red colored

cake on the filter paper. This cake was then given several washings with water and ethanol so that the pH of the filtrate is neutral. The solid cake was dried in vacuum over at 120°C.

Perylene-3,4,9,10-tetracarboxylic Acid Monoanhydride Monopotassium Salt	Amine	Yield
1g	Amylamine, 0.9 g (1.2 ml)	0.830 g (80 %)
1g	Octylamine, 1.3 g (1.7 ml)	0.920 g (82 %)
1g	Decylamine, 1.6 g (2.0 ml)	0.940 g (79 %)
1g	Dodecylamine, 1.9 g	1.1 g (88 %)

Table 4.1 Ratio of amine and perylene-3,4,9,10-tetracarboxylic acid monoanhydride monopotassium salt employed for the synthesis of m-PTCI and the yield of the reaction.

4.3 Optical properties of m-PTCI
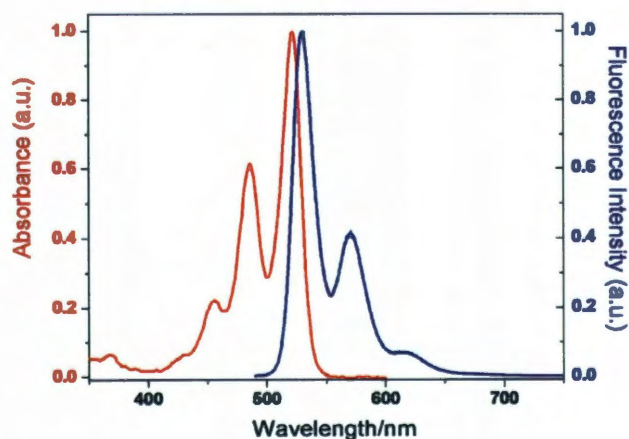
Figure 4.3 The UV-Visible absorption and emission spectra of **41** in chloroforom. The excitation wavelength for obtaining the emission spectra is 480 nm.

The homogeneously dissolved m-PTCI molecules show very similar absorbance and emission spectra as those shown by PTCDI (Figure 3.3, Chapter 3), since the nodes are present at the imide nitrogen in both the HOMO and LUMO.[115] Figure 4.3 shows the absorption and emission spectra of **41** in chloroform. The other m-PTCI **42, 43, 44** shows the similar absorption and emission spectrum in chloroform.

However, upon aggregation of the m-PTCI molecules in a poor solvent such as hexane, a new absorption band appears at the longer wavelength and there is decrease in 0-0 peak and increase in the intensity of 0-1, 0-2 transitions. The pronounced changes in the optical absorption spectra suggest a strong electronic coupling of the perylene cores. Figure 4.4 shows the changes in absorption spectra for **44** upon aggregation in hexane. Similar changes in the absorption spectra were observed for the remaining three m-PTCI **41, 42** and **43.** Thus, we studied the formation of aggregates for the **41-44** using hexane as a poor solvent.
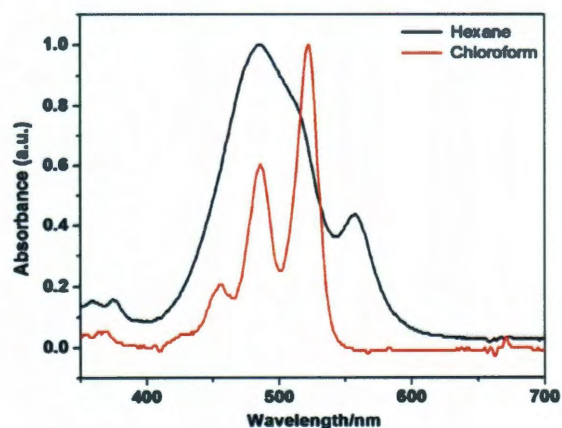
Figure 4.4 UV-Visible absorption spectra of **44** upon aggregation using hexane. A homogeneous solution of **44** in chloroform was rapidly dispersed in hexane and the spectrum was recorded.

4.4 Self-assembly of m-PTCI by phase transfer high temperature method

The self-assembly of m-PTCI molecules has been achieved by a modified two layer phase transfer method used previously to achieve 1D self-assembly (see chapter 3) of perylene diimides (PTCDI). The m-PTCI has far less solubilities in comparison to the corresponding PTCDI having the same number of carbon atoms in the alkyl side chain. Even a small change in the volume (because of evaporation) of the homogeneous chloroform stock solution leads to spontaneous formation of aggregates, thus preventing control over the formation of ordered structure. To this end, the previously developed phase-transfer method at high temperature can be a very viable method to not only allow for increased solubility of the PTCI molecules but also for the controlled growth of organized structures when an appropriate non-solvent is carefully added. Therefore, the phase-transfer at high temperature (2L-HT) was carried out for the formation of organized assemblies of the m-PTCI.

Briefly, a homogeneous stock solution of corresponding m-PTCI in chloroform (0.8 mg in 25 ml CHCl$_3$) was prepared by sonicating the solution in glass vial and placing the glass vial in a hot water bath set at 60°C. Separately, hexane (the non-solvent) is taken in glass vial and equilibrated at 60°C in a hot water bath. Once the homogeneous solution exhibiting green fluorescence of m-PTCI in chloroform is formed, a small amount of this solution is placed in glass tube and this tube is maintained at 60°C by placing in hot water bath. Then, the pre-equilibrated hexane at 60°C is carefully added in excess on top of the m-PTCI solution in chloroform maintained at 60°C. For atleast 2 h, there is no sign of aggregation and the solution of m-PTCI remains very homogeneously dissolved in chloroform. Hexane is added at regular time intervals to compensate for loss due to

evaporation. After 3 h, there are few aggregates formed at the interface which continue to grow with time. After total 6 h, all the m-PTCI molecules aggregate from chloroform solution and there is no fluorescence emission observed from free molecules when the tube is excited using hand held UV lamp (366 nm). When methanol was explored as poor solvent, no aggregation of m-PTCI was observed and at $60^{\circ}C$ a very homogenous solution was formed in methanol chloroform mixture. This is because of the H-bonding interactions between methanol and open mono-anhydride end of the m-PTCI. Thus, the aggregates were formed exclusively using hexane as poor solvent for all the four m-PTCI and were further examined for their morphology and the properties associated with the aggregates.

4.5 Characterization of the aggregates

4.5.1 Scanning and transmission electron microscopy

The aggregates formed using the 2L-HT method for all the four individual m-PTCI using hexane as poor solvent were separately cast on silicon wafer and examined by SEM after the drying of the solvent. The SEM investigations revealed that all four m-PTCI irrespective of the length of side chain attached to the perylene core led to the formation of 2D sheets (Figures 4.5-4.8). The observed morphology of the aggregates is very different from those observed for the PTCDI using the same method (as shown in chapter 3). The sheets made from different m-PTCI appear non-rectangular and in most cases with at least one of the corners of the sheet having an extremely tapering end. Furthermore, there is wide size disparity of the sheets formed. Despite the size disparity most of the sheets are no longer or wider than 30 μm. The best quality sheets could be

obtained only when m-PTCI **42, 43,** and **44** were employed. For **41,** the aggregates appear to be a mixture of sheets and long ribbons.

The self-assembly of m-PTCI was also investigated using other conditions and was found to produce entirely different morphology. 1D nanofibers were obtained by evaporation of the homogeneous solution of m-PTCI in chloroform (Figure 4.9). Since, 1D assembly has widely been performed for these molecules observation of 2D ordered assembly was found to be more interesting and is the first example for the formation of such structure because of the unique packing of these m-PTCI molecules.
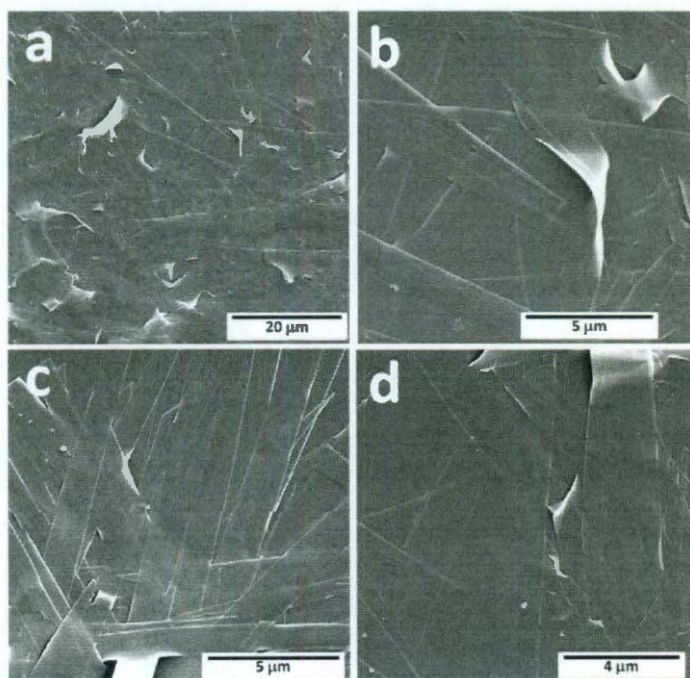
Figure 4.5 Morphology of aggregates of **41** by 2L-HT process using hexane
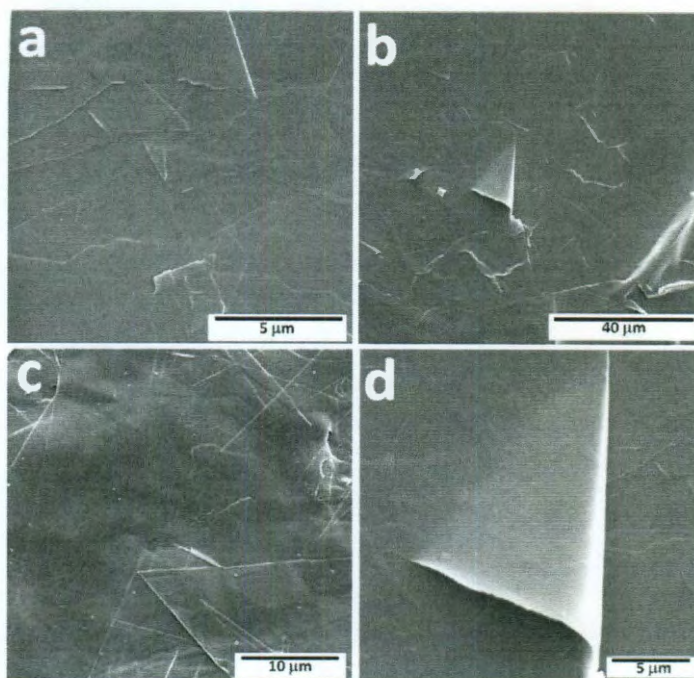
Figure 4.6 Morphology of aggregates of **42** by 2L-HT process using hexane.
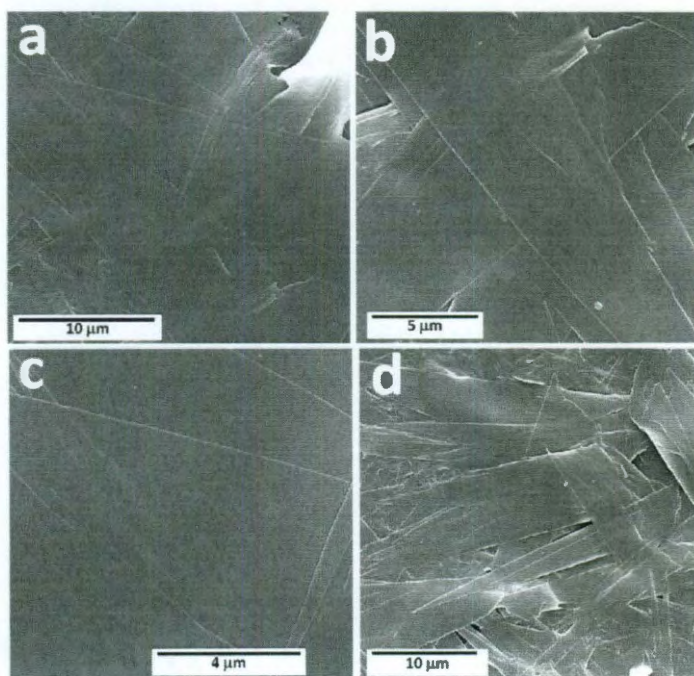
Figure 4.7 Morphology of aggregates of **43** by 2L-HT process using hexane.
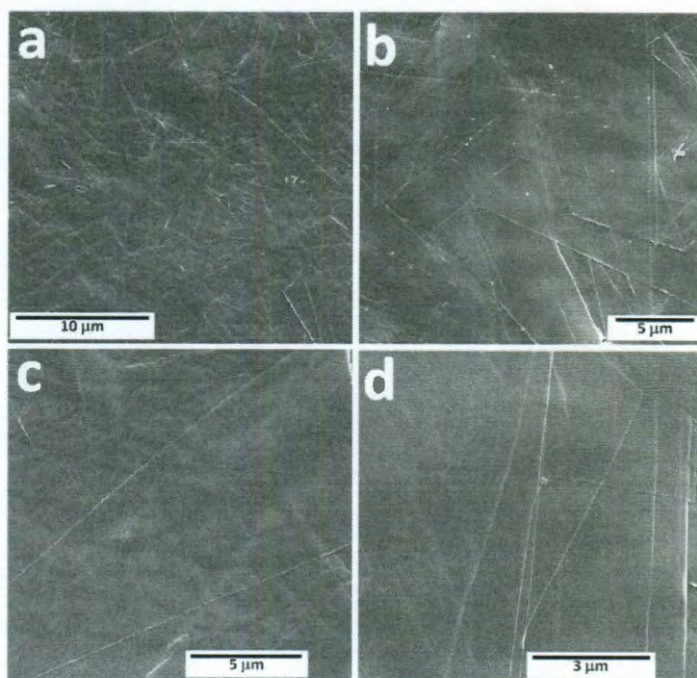
Figure 4.8 Morphology of aggregates of **44** by 2L-HT process using hexane.
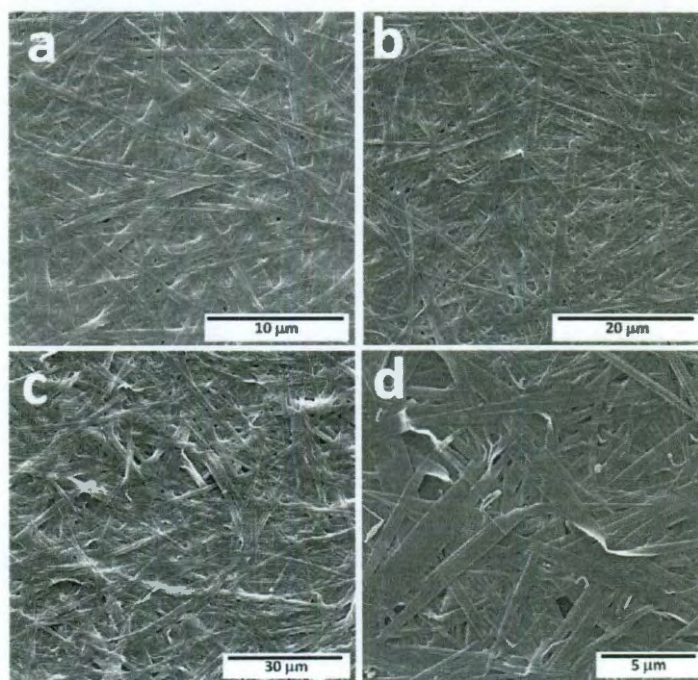
Figure 4.9 Morphology of aggregates of (a) 41, (b) 42, (c) 43 and (d) 44 by slow evaporation of homogeneous stock solution in chloroform.

In order to improve the size disparity of these 2D sheets the concentration of the initial stock solution was reduced. This should allow for formation of fewer sheets by self-assembly and indeed fewer sheets resulted because of the dilution effect. However, the size disparity still remains. The sheets grown from dilute stock solution were cast on Cu-TEM grid (400 mesh) and were imaged. Due to the presence of fewer sheets, a single sheet of m-PTCI can be imaged and characterized by SAED. Figure 4.10 shows the TEM image of single sheet of **44** grown by 2L-HT method using a diluted stock solution.

The 2D arrangements of these molecules are rather intriguing. It is likely a direct result of two sets of packing promoted by the processing conditions and the structural characteristics of the m-PTCI. These systems can be envisioned to be comprised of two half-units of PTCDA and PTCDI, each of which imparts unique non-covalent interaction possibilities e.g. H-bonding, π-stacking and side-chain interdigitation along with hydrophobic effects. To further understand the implication of the 2D sheet formation the optical as well as structural properties were studied.
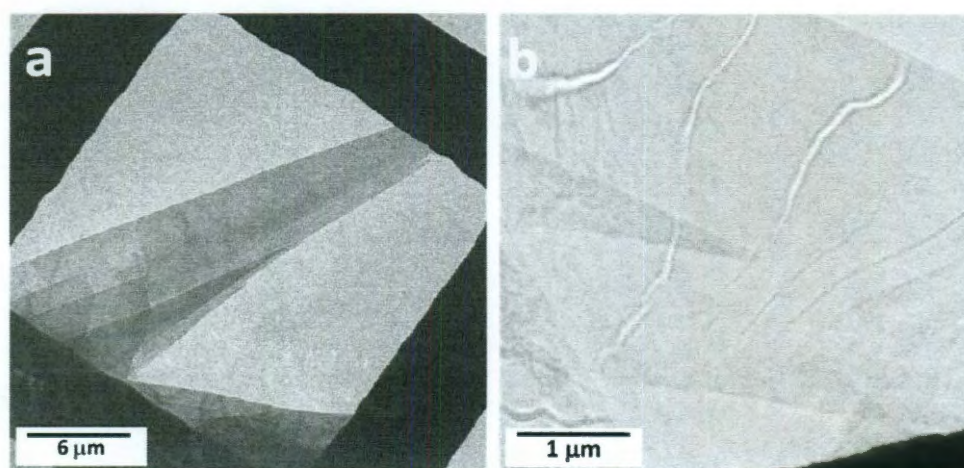
Figure 4.10 TEM image at different magnifications of single sheet of **44** grown from dilute stock solution of **44** using 2L-HT method.

4.5.2 Optical properties of the 2D sheets

The optical properties of the m-PTCI in solution are already discussed in the above section. The free molecule absorption changes significantly (0-1, and 0-2 transitions dictate over the 0-0) upon transferring them to hexane and a new peak at longer wavelengths (570 nm) is observed. This shows that electronic coupling exists between the m-PTCI molecules upon aggregation. To study the optical properties of the 2D sheets formed by the self-assembly process the aggregates were cast onto pre-cleaned glass substrates for the measurement of the solid state features. The UV-Visible spectra (Figure 4.11) obtained for the assemblies of **41-44** in the solid state matches well with those obtained for the aggregates in hexane, implying that the same structure is responsible for the formation of such assemblies.
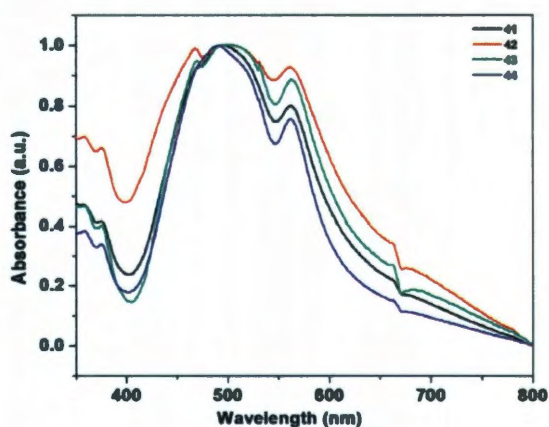
Figure 4.11 Solid state ensemble UV visible absorption spectroscopy of the 2D sheets of **41-44** cast on the glass slide.

The fluorescence spectra obtained for the assemblies show two well resolved peaks at 625 nm and 667 nm, respectively, in their emission spectra which is well red shifted (by 108 nm and 149 nm) in comparison to the free molecule 0-0 emission peak (Figure 4.12). It is interesting to note here that the sheets obtained for the four different

m-PTCI molecules show the same emission characteristics when excited in the wavelength range of 490-560 nm. Furthermore, large stokes shifts (131 nm, and 173 nm) could be measured for the m-PTCI sheets, which implies a rather profound structural characteristic of the sheets. Moreover, the excitation spectra (Figure 4.12, Right) obtained at 630 nm ad 700 nm emission wavelengths matched with the absorption spectra suggesting that this emission is from the aggregated state of mono-PTCI and is an excimeric emission.
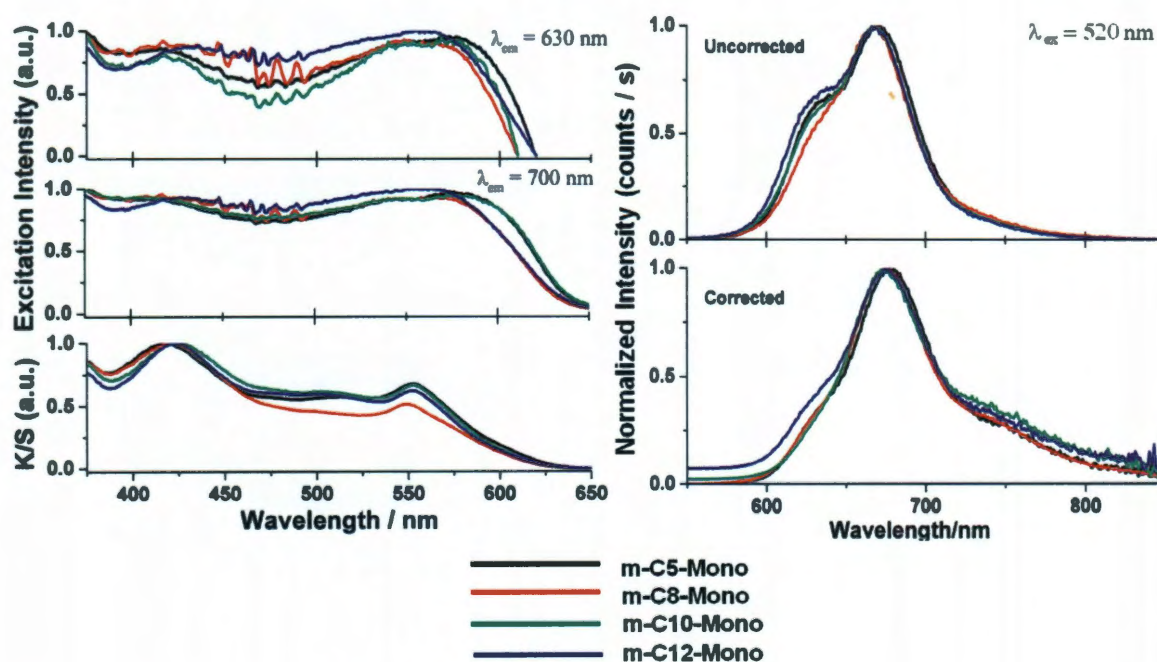
Figure 4.12 Solid state ensemble fluorescence emission spectra (Right) and the absorption, excitation spectra (Left) from the 2D aggregates of **41**(a), **42**(b), **43**(c) and **44**(d).

Such large stokes shifts have previously been observed by Wurthner et al.[187] for a liquid crystalline PTCDI with extremely bulky side chains. In this particular PTCDI case, described for the bulky liquid crystalline PTCDI, a large rotational offset could also be deciphered leading to allowed transitions from the coupled ground state. Also, for the

parent PTCDA molecules extremely close contact between the molecules has allowed for the formation of charge-transfer excitons. It is therefore interesting to observe two unique excimer like emission characteristics in case of m-PTCI. Thus, in the sheets it is likely that the two observed excimer like emission peaks are because of the allowed exciton transitions arising from the profound organization of the molecule.

4.5.3. Structural properties of sheets of m-PTCI

A highly ordered structure could be observed by the powder X-ray diffraction (XRD) measurements of the sheets of m-PTCI cast on glass substrate. The XRD of the sheets show far fewer and much sharper peaks than the powder patterns of the corresponding m-PTCI.
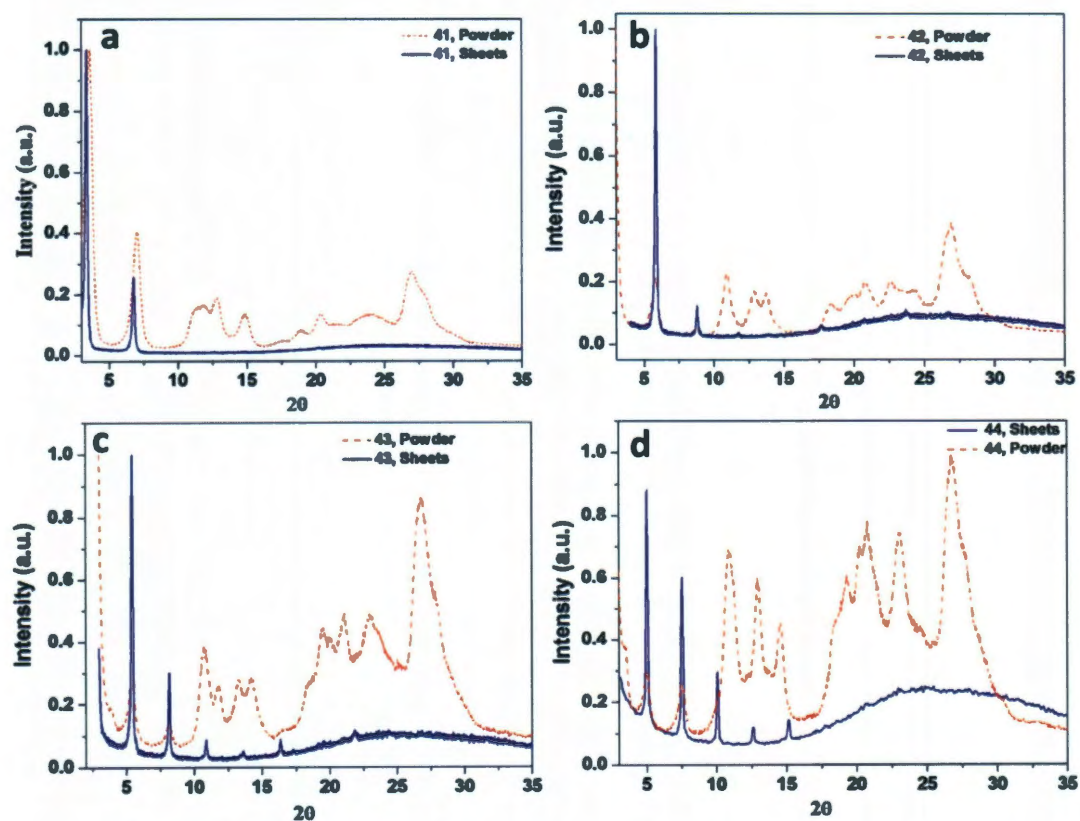
Figure 4.13 XRD of the ensemble of sheets of **41-44** on glass slide and its comparison with the powder of **41-44**.

The powder XRD patterns obtained for the as synthesized m-PTCI molecules represents the typical patterns of those expected for the general m-PTCI molecules and belong to the characteristic triclinic system. The XRD patterns (Figure 4.13) obtained for the sheets corroborate a very uniform packing of the molecules. Furthermore, the selected area electron diffraction pattern performed on different regions within the sheet and over different sheets show the same single-crystalline pattern (Figure 4.14). Such a pattern is consistent with those observed for some of the flip-flop organized PTCDI molecules showing single-crystal behavior[151]. In these flip-flop (large rotational offsets) systems that demonstrated the 1D morphology, large rotational displacement was responsible for extremely strong fluorescence emission. Both the optical and structural property features imply the rotational offsets within the structure along with significant lateral offsets and therefore result in the formation of 2D sheets.
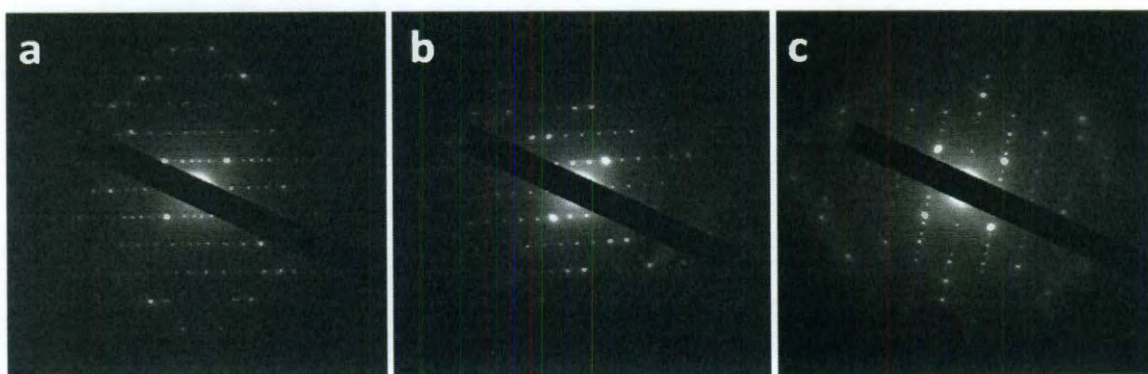
Figure 4.14 Single area electron diffraction (SAED) pattern for a single sheet of **44** from different regions in the sheet. The diffractions pattern remains the same irrespective of the region in the sheet, thus indicating that the sheets are single crystalline in nature.

4.6 Conclusion

The m-PTCI with their unique structural characteristics allow for the formation of fluorescent (excimeric) 2D self-assembly by using the phase-transfer at high temperature

method. The increased solubility of the m-PTCI molecules in the homogeneous chloroform solutions, because of the high temperature, allows for the control of the organization of the molecules resulting in the formation of single-crystalline sheets of the m-PTCI. These fluorescent, single-crystalline sheets are expected to find application in sensors, OLED and OPV devices.

Chapter 5

Chemical reaction mediated self-assembly of PTCDA into nanofibers

5.1 Introduction

Perylene-3,4,9,10-tetracarboxylic dianhydride (PTCDA), a n-type organic semiconducting molecule, has received wide spread attention in electronic and opto-electronic devices.[206] This molecule has been used as the parent molecule for the formation of PTCDI and m-PTCI. Early studies on this molecule were geared towards obtaining high quality, organized thin-films using vapor phase methods.[206] It has been found that close contact between the molecules by π–stacking and H-bonding allow for efficient charge propagation and are therefore well suitable for use in electronic and opto-electronic devices.[45,48,96,180,207] To enhance the charge-propagation and transport characteristics in organic semiconductors emphasis has largely shifted towards creating more organized 1D nanomaterials such as wires and belt which are more conducive to allow expedient movement of charges across the electrodes.[180,208] Largely, vapor based methods have been adopted for the successful assembly of PTCDA and related insoluble perylene based compounds into organized 1D nanostructures.[208-214] Recently, chemical vapor deposition (Ti-CVD) was used to realize nanofiber assembly of the PTCDA primarily driven by π–stacking interaction.[209] However, such 1D structure grown by Ti-CVD were found to be amorphous. In organic semiconductors, crystallinity of the assemblies are known to have pronounced effects towards charge-transport characteristics.[36,112,215,216] Generally, better transport characteristics can be attributed to increased crystallinity. For example, it has been demonstrated that using single-crystalline pentacene[217] and rubrene[218] extremely large hole-mobilities could be attained.

In general, for large-scale adoption of the organic materials in the area of electronic and opto-electronic devices arguments are based on the ability to use cost effective solution based approaches rather than expensive and intensive vapor based methods.[180,215] Thus, it is essential to find suitable solution based methods that can lead to the formation of highly crystalline 1D nanostructures for PTCDA.

The assemblies of the parent PTCDA using solution based processing are rather challenging, owing to intrinsic insolubility, and are therefore chemically converted to more soluble precursors by reacting with corresponding amine to yield perylene tetracarboxylic diimides (PTCDI)[97] for realizing solution based 1D assemblies. To date several elegant examples for the solution processed self-assembly of PTCDI into 1D nanostructures such as belts and wires have been demonstrated. [142,180] The insolubility of the PTCDI molecules in certain solvents have made them amenable to generate 1D assemblies either at the interface of the soluble and in-soluble solvents or by rapidly transferring them from soluble to insoluble solvents. The formation of the organized 1D assemblies in non-solvents is promoted largely because of the strong π–stacking interaction amongst the perylene cores and side-chain interdigitation.[97,141] Often, the side-chains attached to obtain sufficient solubility are comprised of insulating linear alkyl-chains. Despite the insulating side-chains attached to the perylene core in PTCDI, it has been possible to create materials with moderate charge-transport properties using vapor based techniques.[29] For example, electron mobility >0.5 $cm^2/V.s$[106] in thin-film of PTCDI, derived using vapor based approach, have been reported. However, the measurements on 1D assemblies derived using solution based processing shows only a fraction of the electron mobility in comparison.[67] This is likely due to the charge-traps

within the 1D assemblies as the major forces driving the self-assembly rely on both π—stacking and side-chain interdigitation interactions. It is therefore essential to find new solution based pathways to yield the 1D assemblies of the parent PTCDA which are devoid of such side-chains and concomitantly are expected to lead to materials with enhanced charge-transport characteristics. Such explorations will allow for fundamental understanding of the choice of materials for use in opto-electronic applications.

5.2 Choice of precursor for chemical reaction mediated self-assembly

We hypothesize that if an appropriate perylene precursor having functional groups, allowing reasonable solubility in certain organic solvents, and amenable to chemical modification to yield PTCDA, is designed, it may be possible to provide a solution based medium for successful 1D assembly of insoluble PTCDA. Indeed, such a precursor exists, namely, the perylene-3,4,9,10-tetracarboxylic acid (PTCA), **45** (Figure 5.1) which is highly soluble in dimethylformamide (DMF) and the acid groups can be favorably chemically transformed to yield PTCDA using carbodiimide chemistry (Figure 5.2). While, co-crystallization of PTCA with amines has been attempted and show remarkable propensity to strongly form crystals by H-bonding interactions,[219] to the best of our knowledge, solution based chemical transformation methods to obtain 1D assemblies of PTCDA have yet not been explored.
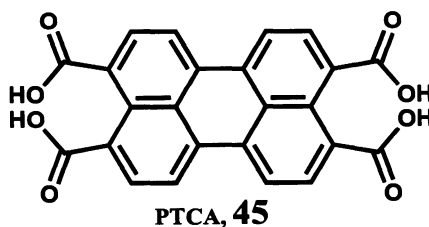
Figure 5.1 Chemical structure of perylene-3,4,9,10-tetracarboxylic acid (PTCA).

5.3 Protocol for the formation of 1D fibers of PTCDA

All the starting materials were obtained from commercial suppliers and used without further purification. Perylene-3,4,9,10-tetracarboxylic-3,4,9,10-dianhydride (PTCDA), N, N'-dimethylformamide (DMF) were purchased from Sigma Aldrich. Deionized (DI) water was used for all the experiments.

5.3.1 Synthesis of standard perylene tetracarboxylic acid (PTCA)

The synthetic protocol developed by Gregg et al.[220] has been adopted for the synthesis of PTCA. In a typical synthesis, 1 g of PTCDA powder (2.54 mmoles) was dispersed in ~500 ml water and 715 mg of KOH (12.74 mmoles) was added to this dispersion. This dispersion was heated on hot plate at $80^{\circ}C$ for 1 h to form a homogeneous aqueous fluorescent green solution of K_4PTCA. The solution was allowed to cool and filtered so as to remove trace amount of unreacted PTCDA, if any, and then 1M HCl was added dropwise to this fluorescent green solution at room temperature. There was precipitation of highly water immiscible PTCA in the solution. 1M HCl was kept on adding until all the K_4PTCA is converted into PTCA and there was complete disappearance of green fluorescence in the solution. This dispersion of PTCA was stirred at room temperature for further 1 h. This dispersion was then filtered using a 0.2 μm pore size filter paper and given several washings with water until the pH of the washings was neutral. The reddish orange solid PTCA powder was dried under vacuum and kept away from heat. Yield = 99%. IR (KBr) vmax 3618, 3122, 1774, 1696, 1586, 1410, 1300, 1296, 857 cm-1.

5.3.2 Synthesis of 4-(dimethylamino) pyridinium 4-toluene sulfonate (DPTS)

In order to carry carbodiimide reaction of PTCA, DPTS was synthesized. 61 g (0.5 moles) of 4-dimethylaminopyridine (DMAP) was dissolved in around 200 ml THF with vigorous stirring. A clear solution was obtained by occasionally sonicating and heating slightly with the heat gun. Then separately 95.11 g (0.5 moles) of p-toluenesulfonic acid monohydrate (PTSA.H$_2$O) was dissolved in around 200 ml THF with stirring, sonication and slight heating. Both these solutions are then cooled to room temperature. These two solutions are then mixed together and subjected to shaking of the flask by hand. The white aggregates of 4-(dimethylamino) pyridinium 4-toluene sulfonate (DPTS) immediately precipitates out of the solution. This precipitate is allowed to settle and filtered and dried under vacuum. (Yield: 100%).

5.3.3 Protocol for the conversion of PTCA to 1D nanofibers of PTCDA

(a) Chemical reaction of PTCA in DMF

7 mg (16 μmoles) of PTCA powder was taken in a 40 ml glass vial. ~ 35 ml dimethylformamide (DMF) was added to this vial and the resulting solution was sonicated for 15 minutes to form a clear homogeneous orange solution. A bright yellow fluorescence was observed when the solution was excited with hand-held UV lamp (365 nm) Figure 5.3. Then 35 mg (116 μmoles) of DPTS was added to this vial and was dissolved in this solution with slight sonication. The resulting solution was then stirred on the stir plate using a small teflon covered stir bar (10 mm long). Then, 230 mg (0.28 ml, 1.78 mmoles) N,N'-diisopropylcarbodiimide (DIPC) was added dropwise to this stirring solution. After 30 minutes addition of DIPC, the initial homogeneous solution started becoming turbid indicating aggregation. After 24 h of stirring, the color of the dispersion

became dark red and a very weak fluorescence was observed (Figure 5.3). This fluorescence did not disappear after stirring for additional few hours. Hence, the reaction was stopped at this stage.
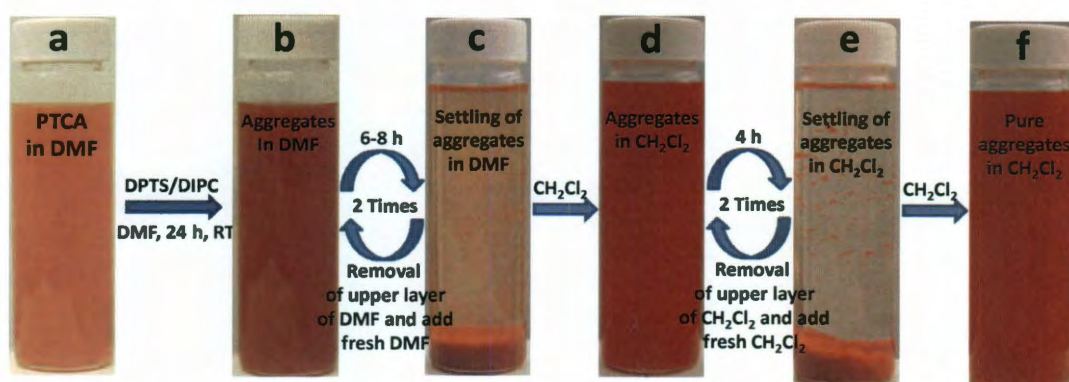
Scheme 5.1 Protocol followed for the formation of 1D nanofibers of PTCDA. The chemical reaction of homogeneous orange solution PTCA in DMF (a) leads to formation of red colored aggregates after 24 h (b). Unreacted PTCA was removed by two times extractions using DMF as shown in (b) and (c) above. DPTS, DIPC and DMF were removed from the system by two times extractions using CH_2Cl_2 as shown in (d) and (e). Finally, the pure fibers were dispersed in CH_2Cl_2.

(b) Removal of unreacted PTCA

After the reaction the stirring was stopped and the resulting dispersion was allowed to stand undisturbed for 12 h. All the red colored aggregates settled at the bottom of the vial leaving behind almost colorless layer of DMF on the top which when observed under UV light showed slight yellow fluorescence. This top layer of DMF was discarded carefully using a pipette and the lower settled portion of aggregates was again dispersed in DMF. The aggregates were again allowed to settle and the top portion of DMF was again discarded carefully using a pipette.

(c) Removal of DMF, DPTS, DIPC and dispersion of aggregates in dichloromethane

The settled aggregates after removal of top layer of DMF were then dispersed in dichloromethane (CH_2Cl_2). The vial was left undisturbed for 4 h. Again the settling of aggregates was observed and the upper top portion of CH_2Cl_2 was discarded and fresh CH_2Cl_2 was then added for second extraction. Totally, two such extractions were carried out so as to remove all the DMF, DPTS and DIPC from the system and all the fibers are finally suspended in CH_2Cl_2.

5.4 Carbodiimide chemistry mediated self-assembly

The carbodiimide chemistry has been widely used for the esterification reaction between carboxylic acid and an alcohol.[221-223] It has been established that this reaction proceeds via formation of acid anhydride.[221,222] In the absence of an alcohol, monocarboxylic acid undergoes *intermolecular* reaction yielding acid anhydride. Whereas, the dicarboxylic acid in which the carboxylic acid groups are separated by two or three methylene groups undergoes *intramolecular* reaction yielding cyclic anhydride.[222] Moreover, the rate of this reaction increases with solvent polarity and is expected to be higher in DMF. Thus, PTCA matches quite well the requirements of an *ideal* precursor, chemically reactive and soluble.
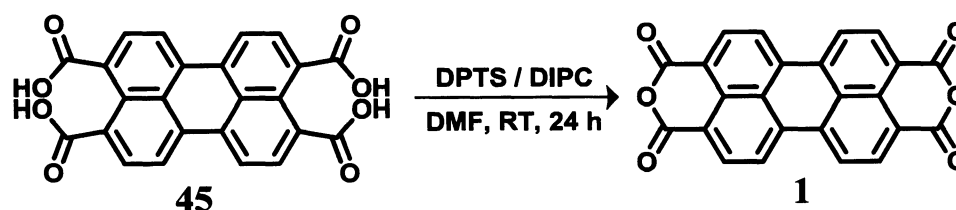
Figure 5.2 Synthesis of PTCDA from PTCA by carbodiimide chemistry.

Our goals were to explore, firstly, the chemical synthesis of PTCDA from PTCA (Figure 5.2) and finally, attempt to understand if such a chemical synthesis going from a highly soluble form of PTCA to the highly insoluble PTCDA would lead to any in-situ growth of 1D nanostructures with the final assemblies being composed of PTCDA molecules. The PTCA was synthesized using the known methods from the parent PTCDA.[220] This PTCA powder is highly soluble in DMF and exhibits a bright orange-yellow fluorescence when excited with a hand-held UV lamp (365 nm) (Figure 5.3). To perform the chemical transformation of PTCA using carbodiimide chemistry, homogeneous solution of PTCA was formed in DMF by sonication. Then, 4-(dimethylamino) pyridinium 4-toluene sulfonate (DPTS, synthesis protocol mentioned above) was added to this vial and further sonicated. The addition of DPTS prevents the formation of unreactive N-acylurea as the by-product and the reaction proceeds via the formation of O-acylisourea intermediate.[224] This was then followed by the addition of 1,3-diisopropylcarbodiimide (DIPC) and the solution was stirred slowly at room temperature.
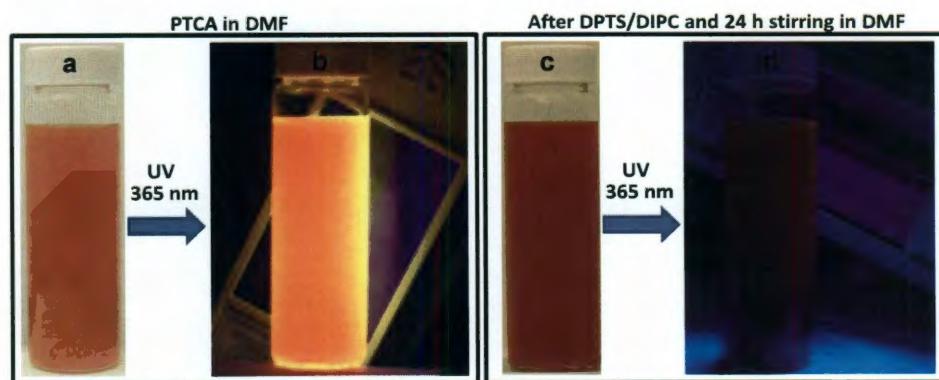
Figure 5.3 (a) Homogeneous orange solution of PTCA in DMF. (c) Red aggregates in DMF after 24 h of reaction and removal of unreacted PTCA. (b), (d) Yellow orange fluorescence and no fluorescence observed upon excitation of (a) and (c) respectively with UV light of 365 nm.

Within 1 h, the solution became turbid red indicating some aggregation. When this solution was now excited with the hand-held UV-lamp, there was large amount of fluorescence from the unreacted PTCA which considerably quenched after 24 h of the reaction leading to dark red colored aggregates in solution (Figure 5.3). The residual weak fluorescence can be attributed to the trace amount of unreacted PTCA in this aggregated dispersion in DMF. This unreacted PTCA was removed by allowing the aggregates to settle and the upper solution layer of the residual PTCA in DMF was discarded. This process was repeated by addition of fresh DMF and allowing the aggregates to settle until the upper clear solution showed no detectable fluorescence. Typically, this took about 2-3 washings in DMF.

5.5 Characterization of the product

Transmission electron microscopy (TEM) was performed on JEOL 1230 (acceleration voltage 120 kV), and JEOL 2010 (acceleration voltage 200kV) electron microscope using carbon-coated copper grid which were purchased from Electron Microscopy Sciences (EMS). The sample for TEM using dispersion of fibers in DMF was prepared by casting a droplet of this dispersion on the TEM grid placed on filter paper. The DMF spreads on filter paper and the aggregates remain on the TEM grid. The TEM sample from dispersion of fibers in dichloromethane was also prepared in the similar way.

5.5.1 Transmission Electron Microscopy (TEM)

In general, the chemical products obtained after synthesis are often found to be powdery substances. However, for the products (aggregates in DMF) mentioned above it

was interesting to note that the transmission electron microscopy (TEM) revealed the formation of bundles of uniform 1D nanofiber having widths of 50 nm and lengths of 2-3 µm as shown in Figure 5.4
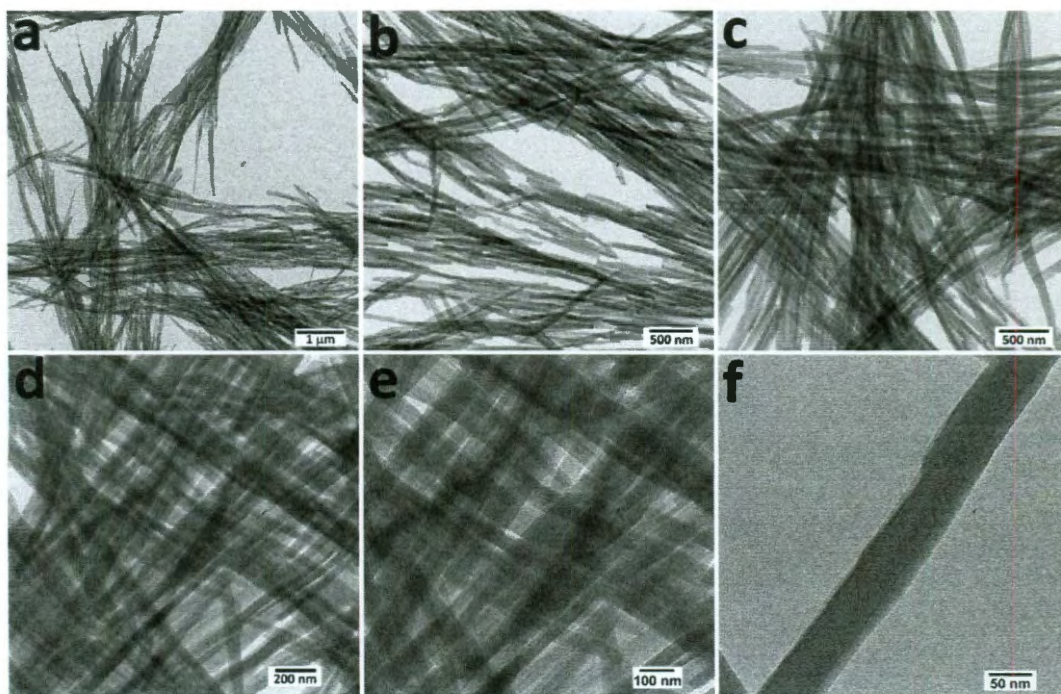
Figure 5.4 (a-e) TEM images of fibers of PTCDA from DMF dispersion at different magnifications. (f) High magnification TEM image of single fiber of PTCDA.

Intrigued by the observation of such morphology, we set on to understand the chemical species responsible for such a 1D assembly as the reaction proceeds via the formation of stable urea by-product. Purification of the product was done using a series of extractions in CH_2Cl_2, after the aggregates were extracted in DMF (Scheme 5.1). The series of extractions ensures only the removal of starting reagents (PTCA, DPTS, and DIPC) along with the stable urea by-product. This purified product now in CH_2Cl_2 was then again analyzed using TEM (Figure 5.5). Similar morphological characteristics are retained as those observed in DMF (Figure 5.4).
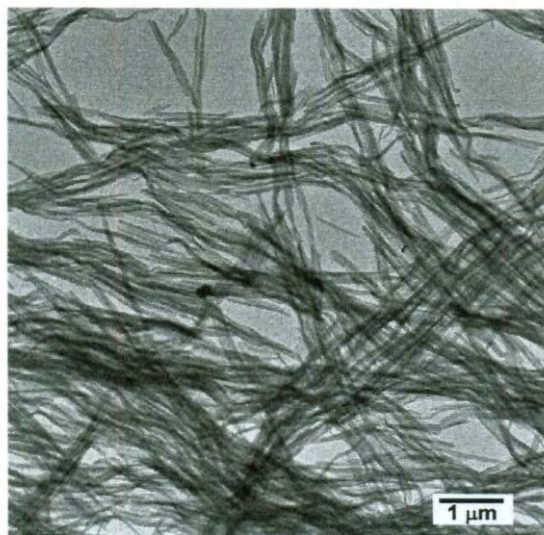
Figure 5.5 TEM image of fibers obtained by casting the fibers dispersed in dichloromethane. No change in morphology of fibers was observed.

To probe if chemical reaction has occurred, a TEM sample was prepared by casting the aggregates from CH_2Cl_2. The aggregates left on this TEM grid were then immersed into a potassium carbonate (K_2CO_3) solution for at least 2 minutes. Following the drying, TEM morphological inspection of the samples were carried out and it was found that there was no destruction in the morphology (Figure 5.6) and the aggregates were found to retain their original 1D nanostructure (in terms of both widths and lengths). At room temperature, PTCA powder is highly soluble in K_2CO_3, whereas PTCDA is not. This qualitatively suggests that indeed the reactants have been consumed and the fibers might be composed of PTCDA.
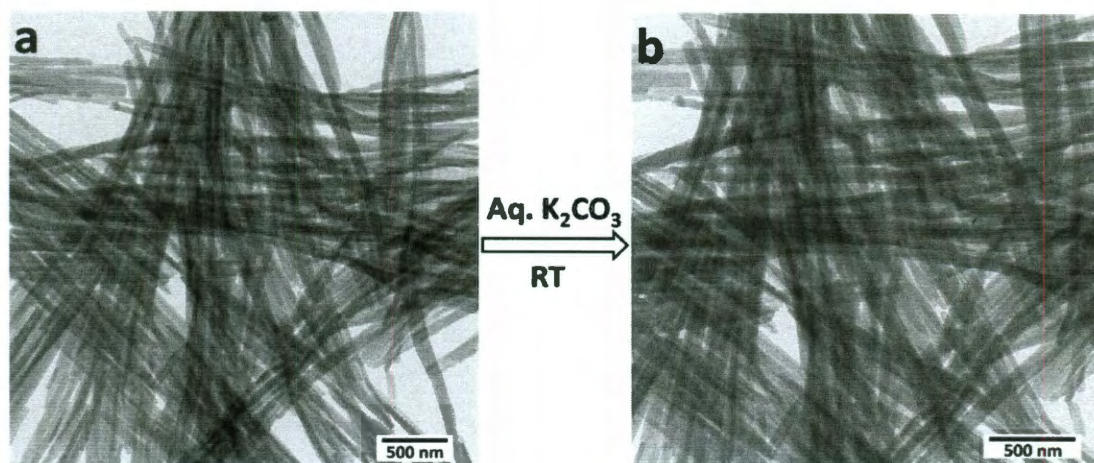
Figure 5.6. TEM image of fibers of PTCDA (a) before and (b) after treating with aqueous solution of K_2CO_3. For this purpose, a particular region on the TEM grid was identified and was imaged. This grid was then dipped in aqueous solution of K_2CO_3 for 2 minutes. The grid was then dried and then the same region was identified and imaged again. There was no destruction of fibers and the morphology of the fibers remained intact. This further proved that the PTCA was converted to fibers of PTCDA after the chemical reaction.

5.5.2 Fourier Transform Infrared Spectroscopy (FTIR)

To obtain the chemical entities responsible for the formation of 1D assembly, FTIR of the final fiber products were performed and compared to the starting PTCA and the parent PTCDA (standard). All the Fourier transform infrared spectra (FTIR) were obtained on FTIR-8400S Shimadzu instrument by grounding the solid powder of the samples with KBr powder. The FTIR spectra of the fibers obtained after reaction showed a distinct sharp vibrational modes corresponding to the carboxylic dianhydride which consisted of $\nu(C=O)$ at 1770 cm-1, $\nu(C-O-C)$ at 1299, 1234 cm-1 and $\nu(-CO-O-CO-)$ at 1022 cm^{-1} and matches very well with the commercially available PTCDA powder, and is different from the starting material PTCA (Figure 5.7).[225] Thus, from the FTIR data it

was very clear that the free carboxylic acid groups in PTCA upon reaction gets converted into dianhydride groups leading to the formation of PTCDA.
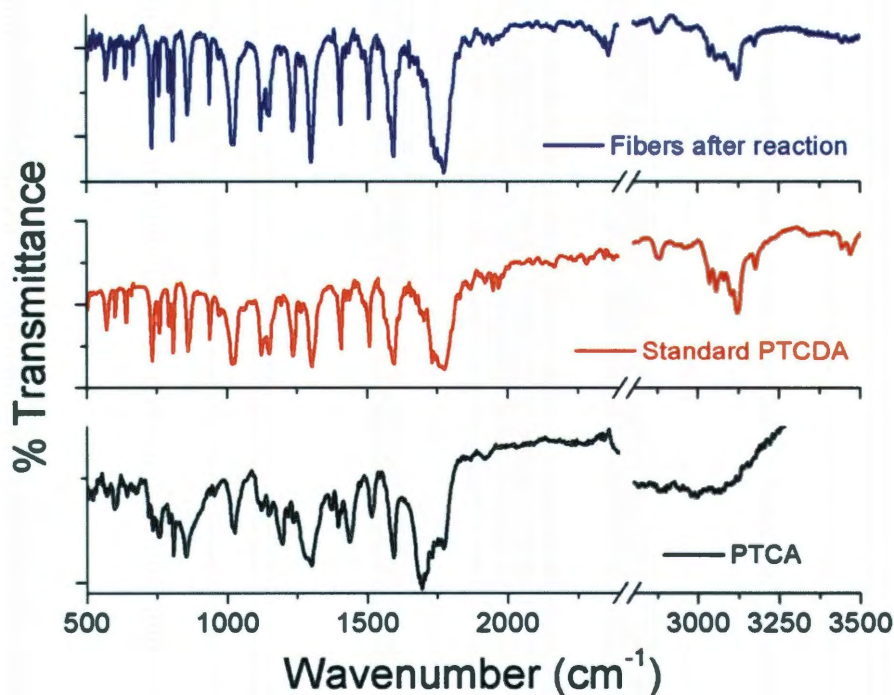
Figure 5.7 FTIR spectra of (a) standard PTCA powder (b) fibers of PTCDA obtained after chemical reaction by protocol mentioned in this paper (c) commercially available PTCDA powder. All the vibrational bands are labeled in each spectrum. In (a) there are strong vibrational bands corresponding to free carboxylic acid groups in PTCA whereas in (b) there are strong vibrational bands corresponding to anhydride group in PTCDA. The spectrum (b) matched exactly with the spectrum of commercially available PTCDA powder (c).

5.5.3 Mass Spectrocopy

Samples were analyzed by chemical ionization on a Waters Autospec Premier double-focusing magnetic sector mass spectrometer using methane as the reagent gas and internal calibration with perfluorokerosene (Courtesy: Dr. Karin Keller, UT-Austin). Solid samples were introduced using a direct exposure technique: a small amount of solid

material was packed into a glass melting point capillary, which was scored approximately

20 mm from the closed end and placed upright into a coil of 0.006″ tantalum wire

mounted on an insertion probe. The capillary was broken along the score, and the

probe/capillary assembly was inserted into the source. Approximately 1.6 amps of current

were run through the tantalum wire to heat the capillary and vaporize the sample. A

100% relative abundance peak for m/z at 393 corresponding to (PTCDA+H$^+$) and

matches perfectly with the standard PTCDA powder (Figure 5.8). Further, there are no

peaks observed at higher molecular weight range suggesting that there is no

polymerization and the species present in final 1D fiber is monomeric PTCDA.
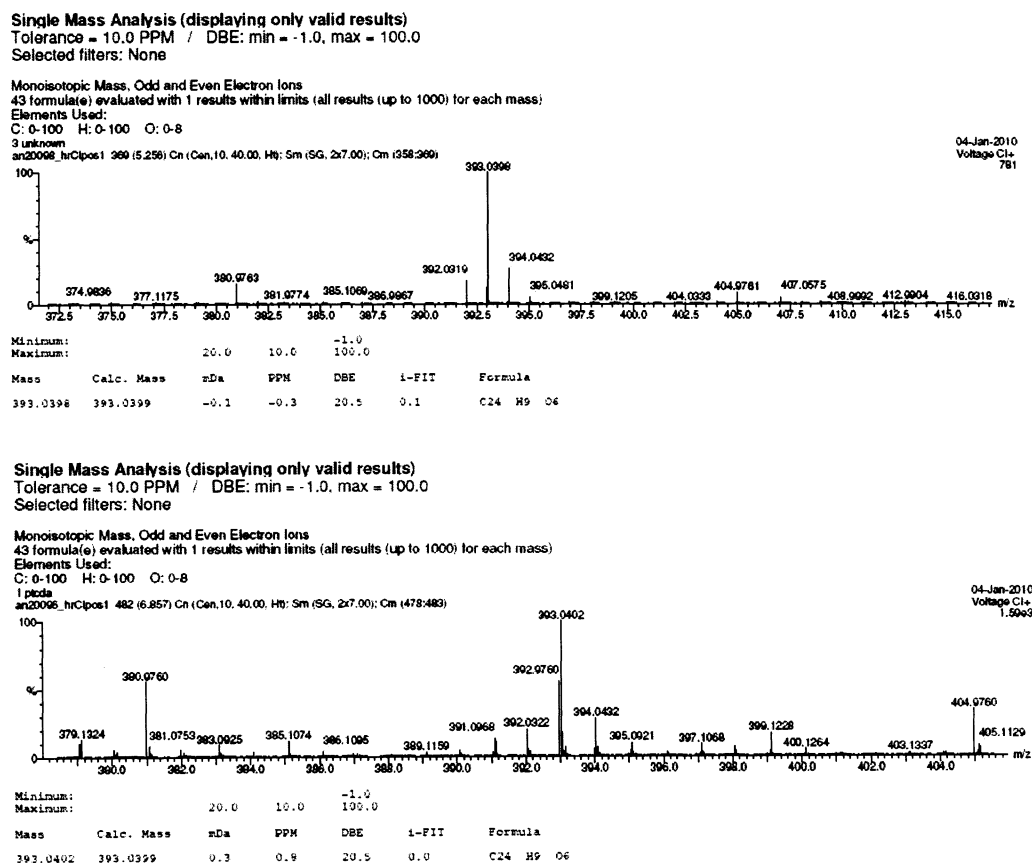
Figure 5.8 Mass spectra of fibers after reaction and its comparison with the mass spectra of standard PTCDA powder. Both the spectra shows a 100% relative abundance peak at 393.04 suggesting that the species in fiber is PTCDA.

The chemical analysis by FTIR and mass spectroscopy clearly demonstrate the fact that the fibers are indeed composed of PTCDA molecules.

5.5.4 X-ray Diffraction (XRD)

Powder X-ray Diffraction (XRD) was done on Rigaku D/Max Ultima II Powder XRD instrument using Cu Kα X-ray beam of wavelength 1.54 Å. Samples for XRD were prepared by drying the respective aggregates from chloroform dispersion on the glass slides resulting in thick film of uniform thickness. The data was collected by using 5 mm slit width and a scan rate of 0.5 degree/minute.
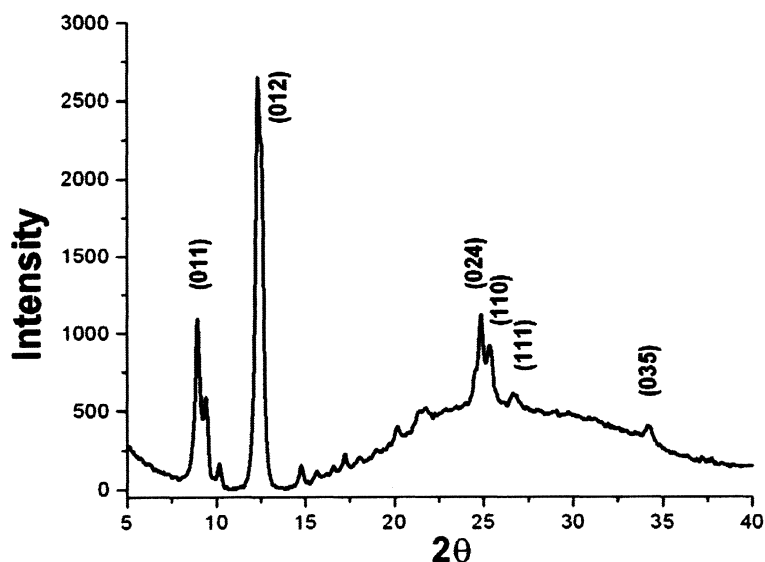
Figure 5.9. X-Ray Diffraction (XRD) of PTCDA fibers.

The X-ray diffraction (XRD) pattern from the bundles of fibers of PTCDA shows that the assemblies are highly crystalline in nature. The peaks obtained could be indexed by matching with standard PTCDA powder (Figure 5.9).[210]

5.6 Plausible Mechanism

5.6.1 Conversion of PTCA to PTCDA by carbodiimide chemistry
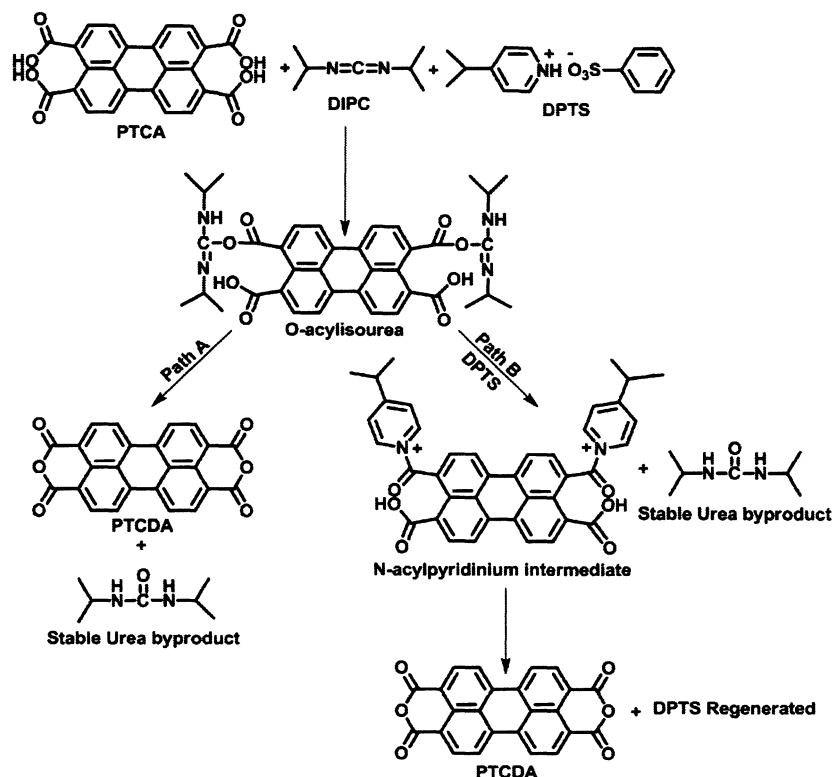
Figure 5.10 Perylene-3,4,9,10-tetracarboxylic acid (PTCA) can react with 1,3-diisopropylcarbodiimide (DIPC) in presence of 4-(dimethylamino) pyridinium 4-toluene sulfonate (DPTS) leading to the formation of o-acylisourea intermediate. This intermediate can react via two paths. Path A: O-acylisourea groups can undergo intramolecular reaction with their neighboring carboxylic acid groups leading to formation of perylene-3,4,9,10-tetracarboxylic-3,4,9,10-dianhydride (PTCDA) and stable urea product. Path B: N-acylpyridinium intermediate can be formed from O-acylisourea in presence of DPTS, which undergo reaction with their neighboring carboxylic acid groups leading to PTCDA and stable urea product.

5.6.2 Formation of crystalline 1D fibers of PTCDA

The exact mechanism for the formation of the fibers of PTCDA by this chemical reaction mediated self assembly is not very clear at the moment. It is likely that various intermolecular forces like π–π interactions, hydrogen bonding and dipolar interactions

play a critical role, as observed in small size aggregates of PTCDA from vapor phase, when the intermediates are converted to the final fiber product (PTCDA).[206,208,219,226,227] One plausible explanation is that the insoluble PTCDA seeds formed upon the reaction initiation might allow for controlled assembly as more and more PTCA molecules get converted to PTCDA in DMF leading to highly crystalline 1D assemblies.

5.7 Conclusion

Thus, in conclusion we have for the first time demonstrated a carbodiimide based chemical reaction mediated self assembly of PTCDA into 1D nanofibers using PTCA as a starting material. The fibers prepared by this approach are highly crystalline in nature and can be readily transferred to volatile organic solvents. The chemical compositions of the fibers were confirmed by FTIR and mass spectroscopy analysis. This kind of in-situ self assembly by a chemical reaction, leads to the expedient formation of organized 1D nanostructures of PTCDA under ambient conditions, which are otherwise impossible by any other solution processing technique. This generic protocol of the carbodiimide chemistry can be further extended to similar π–conjugated chemical systems, with carboxylic acids, to yield the assembled structures of the π–conjugated cores without any side-chains. The comparison of the electrical performance from these 1D nanofibers with those obtained in thin-films, and vapor phase methods for PTCDA, and the fibers and films of the well known PTCDI, with side-chains, will be crucial for the advancement of these materials in the electronic and opto-electronic applications. The electrical and optical properties of these 1D nanofibers are under investigation and will be reported in due course.

Chapter 6

Self-assembly of tetrapotassium salts of perylene tetracarboxylic acid

6.1 Introduction

The synthesis and self-assembly of perylene-3,4,9,10-tetracarboxylic dianhydride (PTCDA) based n-type organic semiconducting molecules into ordered structures has gained a lot of interest in the fabrication of nano-scale devices having applications in electronics, opto-electronics and sensing.[97,180] Besides the inherent π-π interactions between the perylene cores, the alkyl side chain interdigitation,[68,69,141,142,151,153] hydrogen bonding,[159-163] electrostatic,[172-175] solvophobic,[149] metal-ligand interactions[97,168-171] have also been utilized to create ordered structures by the design and synthesis of appropriate functional groups to the perylene core. Various self assembling methods like dispersion or phase transfer using an appropriate solvent that leads to aggregation (poor solvent), are used to achieve 1D nanostructures.[68,180] A key challenge in creating ordered multi-functional materials relies on the ability to control the organization of the components with high precision. To this end, there is also a need to explore the possibilities for the formation of assemblies in a range of solvent to allow for compatibility with other components. Presently, the chemical conversion of PTCDA into PTCDI and other related compounds has allowed for realization of assemblies mainly in organic solvents, owing primarily to their solubility in these solvent.[115] However, by introducing appropriate side chains it has also been possible to attain sufficient solubility in aqueous conditions.[182,228-230] We hypothesize that instead of utilizing these substituted PTCDI amenable for aqueous processing it must possible to attain sufficient solubility by creating salts from PTCDA. In order to attain sufficient solubility in aqueous solvents salts of the perylene

tetracarboxylic acids were created. These salts show high solubility in water and therefore act as an appropriate precursors for exploring the self-assembly of these salts. Furthermore, given the known chemical reactions that can be used to convert the salts into different compounds,[117,220] the chemical transformations of the self-assembled structures are also explored.

Recently, the electrostatic interaction between a double hydrophilic block copolymer - Poly(ethylene glycol)-*block*-branched-poly(ethyleneimine) (PEG-b-PEI) and tripotassium salt of 3,4,9,10-perylenetetracarboxylic acid (PTCAPS) from water/ethanol mixture, has been reported for the formation of very uniform ultralong hierarchically structured PTCAPS fluorescent microbelts.[228] At an appropriate pH the cationic PEI interacts with the anionic carboxylate ions of PTCAPS and allows for controlled crystallization of PTCAPS along the polymer chain by π–π interactions. These fibers showed significant improvement in the electrical conductivity upon doping with hydrazine as compared to the organic nanobelts of PTCDI, acenes, phthalocyanine and undoped C_{60}. This was attributed to the meso-porous crystal structure of the fibers thus leading to efficient electron donation by hydrazine and subsequently efficient charge transfer along the long direction of the fibers. A colloidal method has also been developed by Kang et.al.[231] for obtaining assemblies of the bare perylene molecules. In this chemical process the perylene perchlorate (salt) undergoes reduction due to the Br^- present in the cetyl trimethyl ammonium bromide (CTAB) in solution leading to the formation of uniform perylene nanoparticles having a protective layer of CTA^+ around them. Under appropriate conditions these perylene nanoparticles self-organize themselves into hierarchical square nanorods and nanobelts because of the templating provided by

the lamellar micellar structure of CTA$^+$. In both the above mentioned cases, a directing agent has been utilized for the formation of organized assemblies. In this chapter, the self-assembly of alkali metal salts of perylene tetracarboxylic acid (M$_4$-PTCA) has been explored. These salts are highly soluble in water and therefore are ideally suited to form organized assemblies.

6.2 Synthesis of tetrapotassium salt of PTCA (K$_4$-PTCA)

All the starting materials were obtained from commercial suppliers and used without further purification. Perylene-3,4,9,10-tetracarboxylic-3,4,9,10-dianhydride (PTCDA), Tetrahydrofuran (THF) (99.9% without any preservatives), n-propanol, Dimethylformamide (DMF), Lithium hydroxide monohydrate (LiOH.H$_2$O) were purchased from Sigma Aldrich. Potassium hydroxide (KOH) and Sodium hydroxide (NaOH) were purchased from Fischer Scientific. Deionized (DI) water was used for all the experiments.

The highly water miscible fluorescent green solution of tetrapotassium salt of PTCA (K$_4$-PTCA) is obtained by reacting PTCDA powder with potassium hydroxide (KOH) in water at high temperature (90°C).
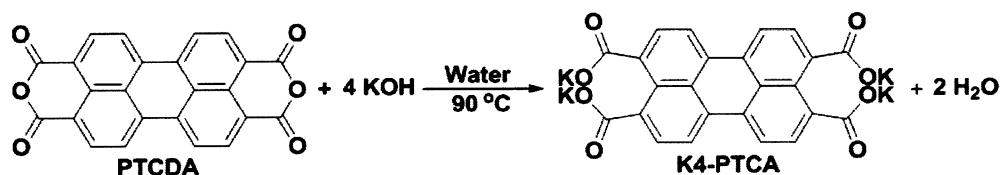
Figure 6.1 Synthesis of highly water miscible K$_4$-PTCA.

Briefly, 7 mg (17.84 μmoles) dark red PTCDA powder was taken in 40 ml vial. Separately, 5 mg/ml stock solution of KOH in water was prepared. Exactly 1 ml of this

stock solution (exactly 5 equivalents of KOH) was added to the previously weighed PTCDA powder. Additionally, 2.5 ml of water was added to this vial to make the total volume of the water 3.5 ml. The vial was sonicated so as to homogeneously disperse the solid PTCDA powder. This red dispersion was then heated on a hot plate at $80^{o}C$ for 30 minutes. A highly water miscible fluorescent yellowish green solution of K_4-PTCA was formed. This solution was also occasionally sonicated during heating so as to ensure that all the PTCDA is converted into K_4-PTCA. This solution was then allowed to cool at room temperature. Thus, a 3.5 ml aqueous solution of ~ 3 mg/ml of K_4-PTCA was ready for the self-assembly process.

6.3 Self-assembly of K_4-PTCA

6.3.1 Role of solvent used for aggregation

In order to study the self-assembly of K_4-PTCA by nucleation and growth process, several solvents that can be miscible with water in all proportions were screened. Solvents such as tetrahydrofuran (THF), ethanol, methanol, n-propanol, acetone, dimethylformamide (DMF), dimethylsulfoxide (DMSO) were attempted to aggregate these salts. We found that only the dropwise addition of THF (~ 35ml) to 3.5 ml aqueous solution of K_4-PTCA (~ 3 mg/ml) with stirring leads to the formation of very uniform 1D nanostructures of K_4-PTCA. Scheme 6.1 depicts the various stages of assembly process. When a drop of this dispersion (in THF) was cast on the glass slide and observed under the optical microscope, the bundles of 1D fibers were seen floating in the solution. As soon as THF starts evaporating, the concentration of water increases and the fibers being highly soluble in water gets completely destroyed. In order to form stable fibers of K_4-PTCA the removal of THF and water was considered to be a critical step. This was

achieved by extracting the pre-aggregated fibers of K_4-PTCA (in THF) in n-propanol. This procedure effectively removes water and THF from the medium, and n-propanol being non-volatile solvent renders stability to the fibers upon drying. The morphology of these fibers was then analyzed by the SEM and TEM investigation.

The K_4-PTCA in water used for the formation of fibers was also aggregated by using other poor solvents like n-propanol, methanol and ethanol. The detailed protocol is mentioned in the experimental section. The resulting aggregates were then extracted in n-propanol so as to retain the stability and were further analyzed by the SEM.

6.3.2 Protocol for the self-assembly of K_4-PTCA into 1D nanofibers

THF was added dropwise to the stirring solution of the previously made 3.5 ml of ~3 mg/ml of K_4-PTCA in water in a 40 ml vial. There was uniform mixing and the solution remained homogeneous up to about 10 ml THF addition. With further dropwise addition of THF, there was an onset of aggregation and yellowish orange fluffy precipitate started forming in the solution. When the specimen in the vial was excited using a hand held UV lamp the aggregates were seen to be dispersed in fluorescent green solution. This fluorescence was attributed to the unassembled K_4-PTCA, which remained homogenously dissolved in solution. As more and more THF was added, more and more molecules of K_4-PTCA self-assembled. The complete aggregation of the entire salt occurs upon addition of ~35 ml THF, confirmed by complete quenching of the fluorescence. The yellowish-orange fluffy aggregates of K_4-PTCA were found to be uniformly dispersed in the THF : water mixture.
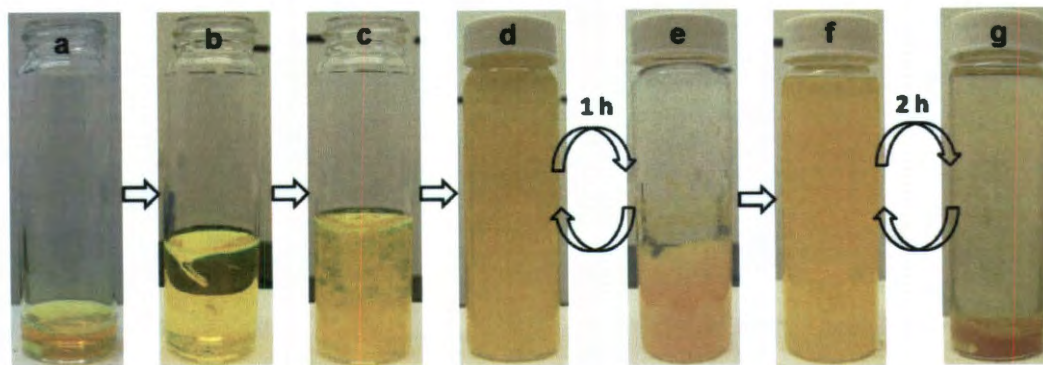
Scheme 6.1 Detailed experimental protocol followed for the self-assembly of K_4-PTCA into 1D stable fibers by the solution based self-assembly process. A 3.5 ml homogeneous solution of K_4-PTCA in water (a). THF was added dropwise to the stirring solution of K_4-PTCA in water (b) and there was an onset of aggregation (c). As more THF was added, all the K_4-PTCA molecules self-assembled (d) and there was fluorescence quenching. In order to remove water, the fibers were allowed to settle, the upper portion of THF was discarded using pipette and fresh THF was added. Two such extractions were carried out using THF to remove water (d, e). Then THF was removed completely (method not shown here but explained in detail in the experimental protocol) and these fibers were then suspended in n-propanol (f). The fibers were made devoid of residual water and THF by final 3 extractions using n-propanol by settling the fibers, removing the upper clear layer of n-propanol and re-dispersing in fresh n-propanol (f,g) . Finally, the fibers were then dispersed in n-propanol for further characterization.

In order to form stable fibers of the K_4-PTCA, the removal of water and THF from the system was an essential process. Since, water is highly miscible in THF; several extractions were initially carried out in THF. For this purpose, the vial containing the fibers of K_4-PTCA dispersed in THF and water mixture was allowed to stand undisturbed for an hour. The bundles of fibers slowly settle down in a period of 1 h and a clear layer of THF water mixture was formed at the top. This top portion of clear THF:water mixture was removed carefully using a pipette and then the fibers were again dispersed in fresh THF. Again the fibers were allowed to settle, the upper clear layer of THF was discarded using a pipette and the fibers were dispersed in fresh THF. This process was repeated

atleast three times. After final extractions in THF, the fibers at this stage were suspended in ~10 ml THF. In order for the stabilization of the fibers, the extraction process was now again carried out using n-propanol in a similar way as mentioned above. Upon removal of THF the aggregates remain dispersed in n-propanol. Casting of this suspension now allows for obtaining the self-assembled fibers composed of K_4-PTCA salts. The extraction using n-propanol is repeated three times to obtain stable fibers. The morphology of this sample was then examined by SEM and TEM.

6.3.3 Morphology of the aggregates of K_4-PTCA

The SEM and TEM investigation of the aggregates using the THF as poor solvent and subsequent extraction in n-propanol revealed the formation of very well-defined fibers of nearly uniform diameter (~100 nm). The lengths of the fibers were between 8-10 μm (Figure 6.2).

We also found that instead of THF, when self assembly was carried out using n-propanol or methanol (procedure mentioned in the experimental section), 3D faceted crystals were formed whereas ethanol lead to the formation of 2D sheets (Figure 6.3, 6.4 and 6.5). These experiments (assembly in different solvents) highlight the importance of solvent towards controlling the molecular interactions responsible for the formation of morphologically defined structures.
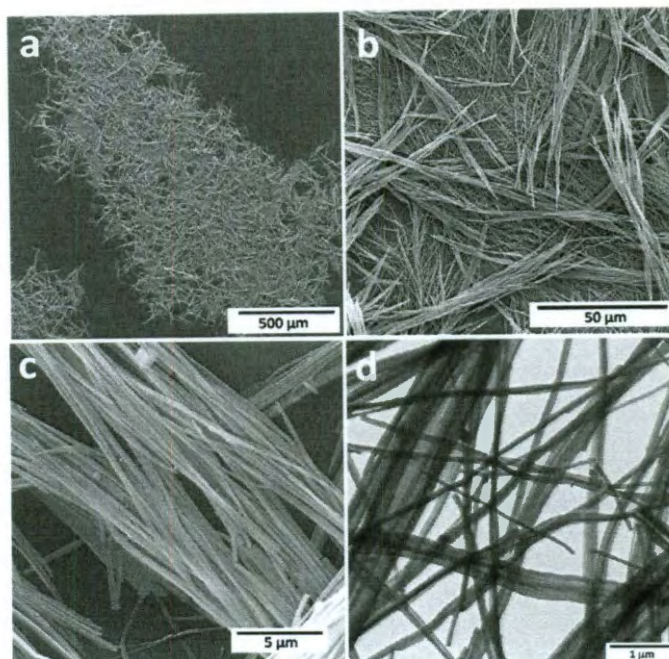
Figure 6.2 Fibers of K4-PTCA formed by dropwise addition of THF to the aqueous solution of K4-PTCA and subsequent extraction in n-propanol. (a) (b) (c) SEM images at different magnifications (d) TEM image of bundles of fibers.
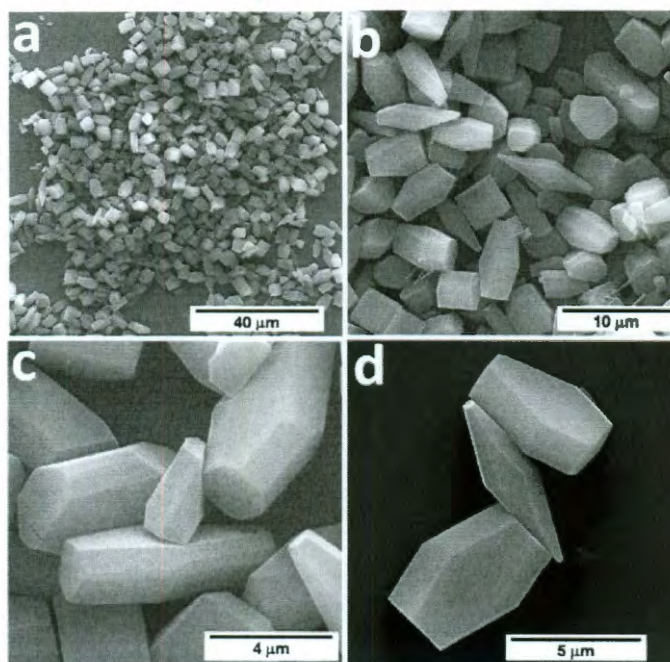
Figure 6.3 3D faceted crystals of K4-PTCA formed by dropwise addition of n-propanol to the solution of K4-PTCA in water and subsequent extraction in n-propanol. (a-d) SEM images at different magnifications. Samples were prepared by casting a drop of the dispersion on the silicon wafer.
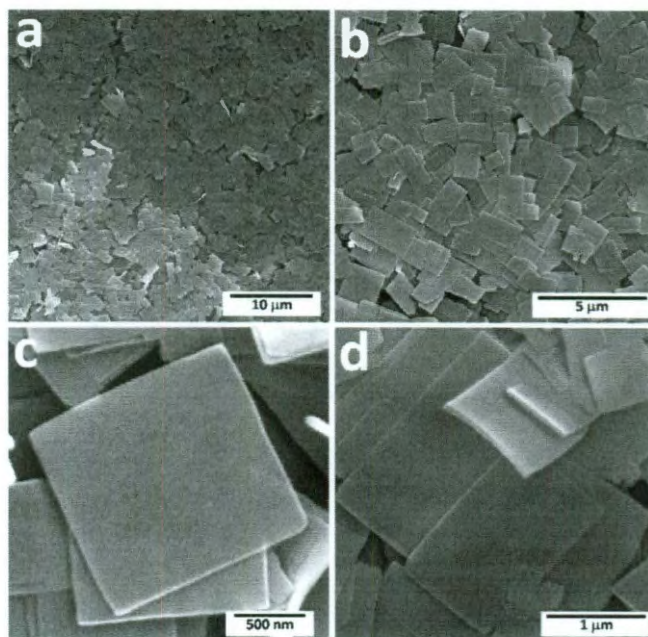
Figure 6.4 2D Sheets of K₄-PTCA formed by dropwise addition of ethanol to K₄-PTCA in water and extraction in n-propanol. (a-d) SEM images at different magnifications. Samples were prepared by casting a drop of the dispersion on the silicon wafer.
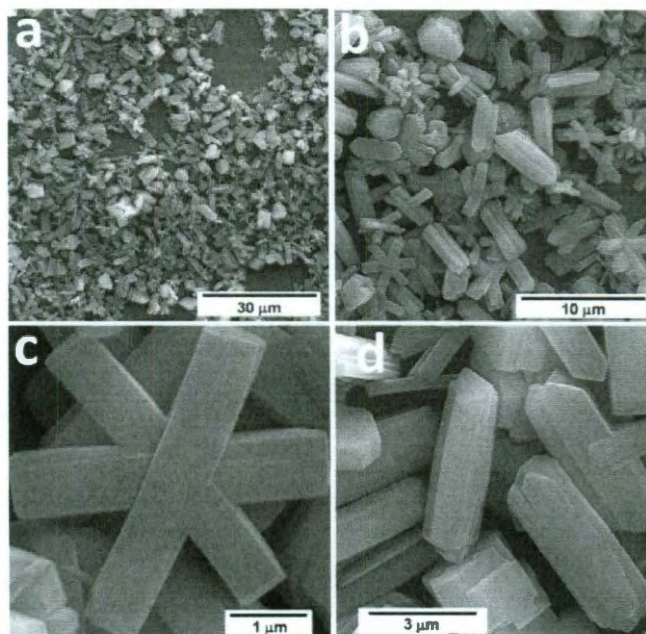
Figure 6.5 Rod and flower like crystals of K₄-PTCA formed by dropwise addition of methanol to the solution of K₄-PTCA in water and subsequent extraction in n-propanol. (a-d) SEM images at different magnifications. Samples were prepared by casting a drop of the dispersion on the silicon wafer.

6.3.4 Factors affecting the self-assembly of K_4-PTCA

The sequence and manner of addition of THF, amount of KOH and water in the initial solution was also found to be critical to obtain very uniform diameter 1D nanofibers of K_4-PTCA.

6.3.4.1 Sequence and manner of addition:

When THF was directly poured into this 3.5 ml aqueous solution of K_4-PTCA without any stirring, there was immediate onset of aggregation and within few minutes the entire solution was aggregated. THF and water were removed from the system completely and all the fibers were finally dispersed in n-propanol. When a drop of this solution was cast on silicon wafer and examined under SEM, large size distribution in the dimensions of the fibers was observed (Figure 6.6).
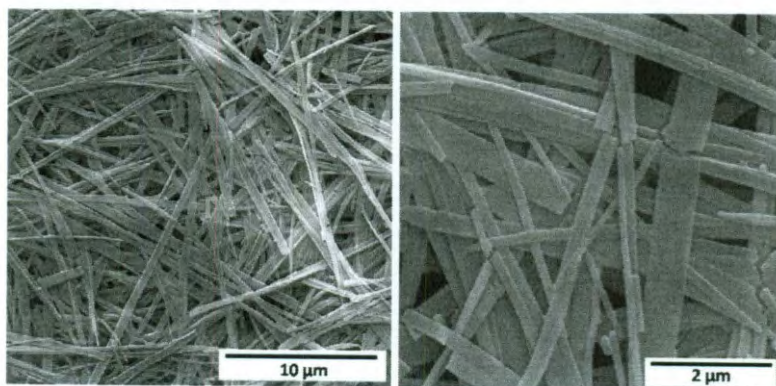
Figure 6.6 Effect of rapid addition of THF to the homogeneous solution of K_4-PTCA in water without any stirring.

If 3.5 ml aqueous solution of K_4-PTCA was dropwise added to excess THF (~ 35 ml) with stirring, there was rapid formation of yellowish orange aggregates. Water and THF were removed from these aggregates and the sample was then cast on silicon wafer and examined under SEM. The SEM revealed the formation of mixture of non-uniform

diameter fibers and ill-defined seeds (Figure 6.7). The diameter of these fibers ranged from few nanometers to few microns. This was due to rapid non-uniform aggregation upon dropwise addition of K_4-PTCA to a huge excess of poor solvent (THF).
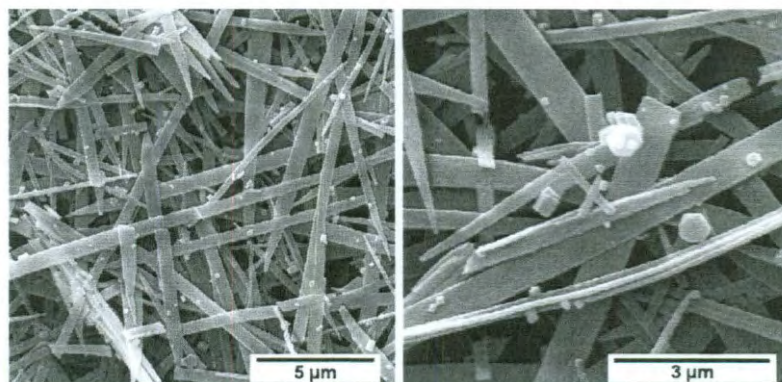
Figure 6.7 Effect of dropwise addition of K_4-PTCA salt in water to ~35 ml THF with stirring.

Only the dropwise addition of THF to the stock solution resulted in the formation of uniform diameter self assembled 1D nanofibers of K_4-PTCA.

6.3.4.2 Amount of water and KOH in the K_4-PTCA solution

When the amount of water was decreased to less than 3.5 ml for the same amount of K_4-PTCA used in previous experiments, the rate of aggregation upon addition of THF was faster and there was non-uniform growth of fibers. Also, if the amount of KOH used to form K_4-PTCA from PTCDA (7 mg) was increased in the same volume of water (3.5 ml), then best quality fibers were formed until 5 mg KOH. Beyond 5 mg KOH, there was formation of approximately 1:1 mixture of large size distribution 1D fibers and random seeds. This was probably because of increase in solubility of the K_4-PTCA in water and hence inefficient aggregation in THF, which upon extraction in n-propanol lead to the formation 3D crystals along with fibers (Figure 6.8). Thus, it was very important to use

exactly 5 equivalents of KOH while forming K$_4$-PTCA from 7 mg PTCDA in 3.5 ml water, which on self assembly leads to very uniform diameter fibers.
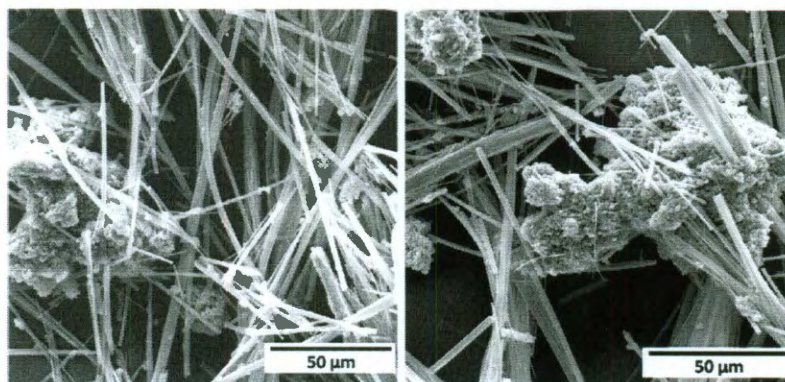
Figure 6.8 Effect of KOH on the self-assembly of K$_4$-PTCA. For this purpose, 7 mg KOH was used instead of 5 mg to form K$_4$-PTCA in water starting from 7 mg PTCDA and this solution was self-assembled leading to mixture of large size distribution fibers and seeds.

6.3.5 Role of potassium ion on the self-assembly of K$_4$-PTCA

In order to study the effect of metal ion on the self-assembly of tetra alkali metal salt of PTCA, two other highly water miscible salt of PTCA namely tetralithium salt of PTCA (Li$_4$-PTCA) and tetrasodium salt of PTCA (Na$_4$-PTCA) were synthesized. As explained above for K$_4$-PTCA, the Li$_4$-PTCA and Na$_4$-PTCA in water were prepared as follows: Using a 1 ml syringe, 0.75 ml of 5 mg/ml solution of LiOH.H$_2$O in water (exactly 5 equivalents of LiOH.H$_2$O, 89.2 μmoles) was added to 7 mg PTCDA (17.84 μmoles) in a 40 ml vial. The total volume of water in this vial was made 3.5 ml by adding extra 2.75 ml water and this red dispersion was heated at 80°C for 30 min to get a 3.5 ml aqueous solution of Li$_4$-PTCA. Similarly, 0.71 ml of 5 mg/ml solution of NaOH in water (exactly 5 equivalents of NaOH) was added to 7 mg PTCDA (17.84 μmoles) in a 40 ml vial using a 1 ml syringe. Additional 2.79 ml of water was added to this vial to make the

total volume of water as 3.5 ml and this red dispersion was heated at 80°C for 30 min to get 3.5 ml aqueous solution of Na$_4$-PTCA. These solutions were cooled at room temperature and then used further for self-assembly process.

The aqueous solutions of Li$_4$-PTCA and Na$_4$-PTCA were assembled in the similar way as that of K$_4$-PTCA and extracted in n-propanol as explained above for fibers of K$_4$-PTCA. The SEM of these samples revealed only spherical, ill-defined morphology and not single fiber morphology was observed in both the cases (Figure 6.9). Moreover, similar morphology was obtained irrespective of the solvent used (THF, methanol, ethanol and n-propanol). These experiments suggest the critical role of the K$^+$ for the formation of ordered 1D nanostructures.
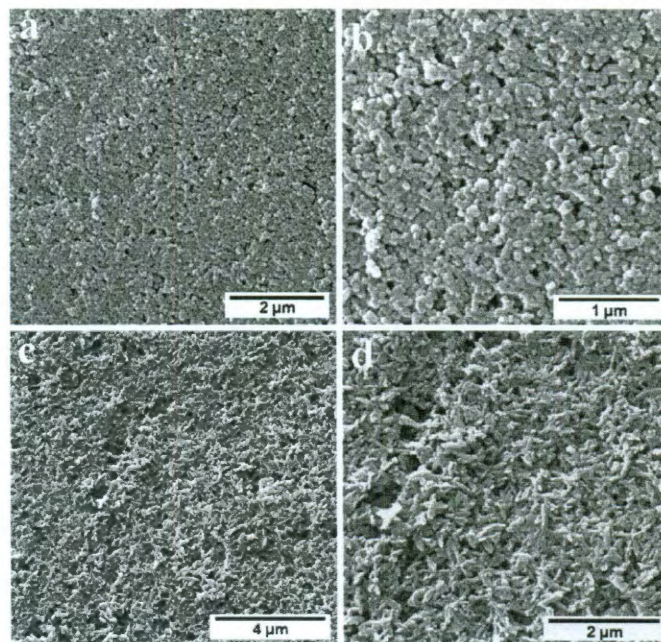
Figure 6.9 (a), (b) Random spherical morphology formed by dropwise addition of THF to the Li$_4$-PTCA in water and subsequent extraction in n-propanol at different magnifications. (c) ,(d) Random ill-defined aggregates formed due to the dropwise addition of THF to the Na$_4$-PTCA in water and subsequent extraction in n-propanol at different magnification. There was complete absence of 1D fiber in case of self-assembly of both the Li$_4$-PTCA and Na$_4$-PTCA salts in water using THF.

6.4 Optical properties of K_4-PTCA in solution

The UV-visible spectrum of aqueous solution of K_4-PTCA exhibits the 0-0, 0-1, 0-2 transition at 466, 438 and 412 nm respectively. The fluorescence spectrum showed the same peak structure in mirror image to that of the absorption. However, upon aggregation in THF the 0-1, 0-2 transitions were enhanced in comparison to the 0-0 transitions in the UV-spectra. Furthermore, a small red shift in the 0-0 transition is observed. These changes imply electronic coupling among the individual K_4-PTCA molecules. The coupling could also be inferred by the strong quenching of the fluorescence signals upon aggregation in THF (Figure 6.10).
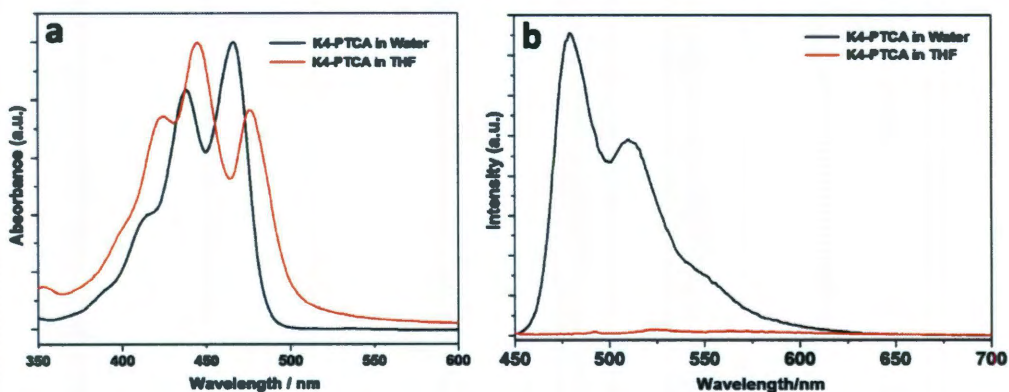
Figure 6.10 UV-visible absorption (a) and florescence (b) spectra of K_4-PTCA (5 µM) in homogeneous solution (water) and poor solvent (THF).The fluorescence spectra was obtained by excitation at 430 nm. The absorption and fluorescence spectra are both normalized at the 0-0 transition maximum.

6.5 Importance of interactions and environment in the self-assembly

A key challenge in the self-assembly of 1D structures lies in the ability to control the organization in a specific directions. In most organic systems there are more than one possible molecular interaction and thus the control for the formation lies in the ability to

allow favorable interactions along the long axis of the 1D structure rather than the lateral associations that can lead to the disruption of the structures. For e.g., in case of PTCDI the formation of 1D structure have been found to be a balance between the packing of the molecules by π-stacking interactions and the lateral side-chain association.[141] In case of the perylene salts explored here there are again more than one possible molecular interaction. The key molecular interactions responsible for the ordered structures are hydrophobic, π-stacking, and electrostatic interactions (ion-dipole, ion-solvent, and ion-molecule) interactions. The roles of the interactions and the environments responsible for the formation of the ordered structures are discussed below.

The role of environment for the formation of stable assembly has also been found to be critical. Though the 1D fiber structure was already formed in THF, upon evaporation the fiber morphology was destroyed because of the evaporative- cooling effect. However, the fiber morphology could be stabilized in the n-propanol solvent likely because no free molecules of the salt were present. The removal of THF and water further facilitates the ordered morphology to be stable in n-propanol and the evaporation does not allow for the destruction of the morphology (since the boiling point of n-propanol is closer to water).

Furthermore, the role of ion has also been found to be critical. Most of the studies thus far on the formation of ion-perylene structures have been performed using vapor phase methods wherein the perylene molecules are vaporized and deposited onto salt surfaces (e.g. NaCl, KCl etc.).[206,232] In these structures it has been found that the metal ions coordinate with the O-atoms in the carbonyl groups and allow for the formation of a square phase. In case of solution based environments the situation is rather different. The

ions are strongly solvated in an aqueous environment.[233,234] In order for stabilizing the molecular interactions the aggregating solvent must first overcome massive solvation energies before allowing the molecular interactions to occur. Thus, the choice of the solvent for aggregation also becomes very critical. THF being highly non-polar and miscible with water in all proportions allows for maximizing the molecular interactions. On the other hand solvents such as methanol, ethanol, and n-propanol also interact with water molecules via H-bonding interactions and are therefore unable to overcome the solvation energy of the ions. The specific cases of K-salts for the morphology control in different solvents are discussed below. The formation of ordered 1D structure is best facilitated in THF solvent. Furthermore, the solvation energy is the most for Li and least for K.[233,234] The aggregation in the aqueous medium will be most favored for the K ions, owing the subtle balance between the size of the ion and the solvation energy. The sizes of the ions have also been found to be critical for the realization of organized assemblies. The rates of aggregation are the most for Li > Na > K > Cs, as observed by the time it takes for the precipitation to occur upon addition of the THF solvent. In case of Cs the addition of THF does not lead to any precipitation at all implying a very stable salt at all concentrations. This is because of the extremely large size of the Cs^+ ion. The Cs-salt used here as a control was synthesized and processed by the same protocols mentioned above. However, in case of Li and Na the aggregation was almost instantaneous and the extreme precipitation of the molecules likely results in disordered structures as observed by the morphological investigations. The aqueous environments are mainly responsible for the increased hydrophobic and π-stacking interactions amidst the π-rich perylene cores.

The formation of 1D wire structures from THF, sheets from the K-salts from ethanol, and 3D crystals from methanol and n-propanol further substantiate the role of solvents used in the self-assembly. The formation of sheets in ethanol has been observed for the tripotassium salt of PTCA by Colfen et al.[228] when no additive (responsible for 1D structure) was used. Such an observation further corroborates the fact that the THF solvent is playing a vital role in not only stabilizing the molecular interactions but also participating in the formation of the assembled structures. In the previously shown case of wires from PTCAPS the additive played a pivotal role of directing the self-assembly by π-stacking interactions leading to formation of 1D structures.[228] It has been previously found that solvent molecules can form complex with rigid π-structures (such as anthracene and perylene) thereby leading to controlled crystallization of the π-rich structures.[235] Indeed, THF molecules can be trapped within the wires and act as a directing agent leading to the formation of the 1D structures.

6.6 Chemical modifications of fibers of K_4-PTCA

The next step was to investigate if it was possible to chemically modify the fibers of K_4-PTCA and study the changes in morphology. Any changes in the dimension of the fibers after the chemical modification can be attributed to the processing condition employed and the interaction between the new chemical species generated in the fiber morphology. Typically, the self-assembled materials often would revert back to molecular state or when converted lead to destruction of the morphology. In order to carry out the chemical transformation of the 1D structures of K-PTCA the known chemistry was used Figure 6.11. Two different sets of conditions were adopted for the chemical transformation of the assembled salt structures. To this end, here the assembled

fibers of the salt were reacted with acid to observe the morphology and the chemical entities responsible for the formation of the ordered structures.

Initially, concentrated hydrochloric acid (HCl) was explored for chemical modification of fibers of K_4-PTCA and heating the resulting dispersion at $80^\circ C$. Usually, this step in the case of homogeneous solution of K_4-PTCA in water, leads to the formation of PTCA and subsequently to PTCDA because of the ring closing at high temperature.[220] But as soon as HCl was added to the dispersion of fibers in n-propanol, because of the presence of water in HCl, all the fibers destroyed. Thus, this strategy of modification of the fibers was found to be inappropriate for this system.

The synthesis of perylene-3,4,9,10-tetracarboxylic acid monoanhydride mono-potassium salt from K_4-PTCA in water has been widely studied.[117] In the synthesis of perylene-3,4,9,10-tetracarboxylic acid monoanhydride mono-potassium salt, glacial acetic acid was added dropwise to the homogeneous solution of K_4-PTCA in water at 80°C. The Bordeaux colored perylene-3,4,9,10-tetracarboxylic acid monoanhydride mono-potassium salt, 4 being highly immiscible in water precipitated out of the solution which was then filtered and washed. Thus, glacial acetic acid was added to the K_4-PTCA fibers in propanol and studied under two set of conditions.
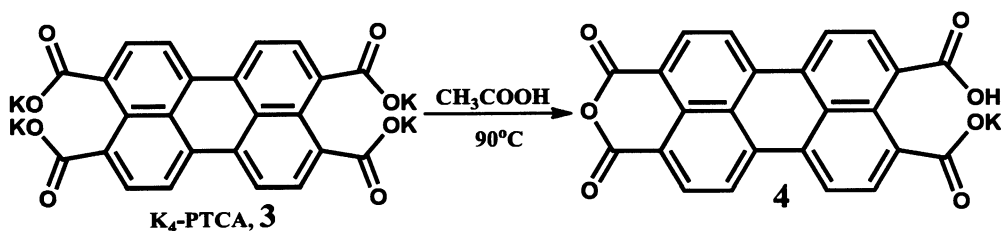
Figure 6.11 Scheme for the synthesis of perylene-3,4,9,10-tetracarboxylic acid monoanhydride mono-potassium salt, 4.

Following the extractions and obtaining stable fibers of K_4-PTCA, the weight of K_4-PTCA fibers was ~10 mg which were dispersed in ~15 ml n-propanol, 40 μl of glacial acetic acid (8 times excess) was added. The color of the dispersions at this stage changes from yellowish orange to dark orange. This reaction mixture was then processed using two set of condition. In the first condition, the reaction mixture was stirred at room temperature (RT) and in the other the reaction mixture was stirred at higher temperature, 80°C (HT) by immersing the vial in an oil bath (Figure 6.12). After 48 h of RT and HT processing, the resulting morphologies were examined by SEM and TEM. The difference in the colors of the initial K_4-PTCA fibers, final RT and HT processing fibers suggested that all these fibers were composed of entirely different chemical species (Figure 6.12). The resulting aggregates were studied for their morphological changes by SEM and TEM.
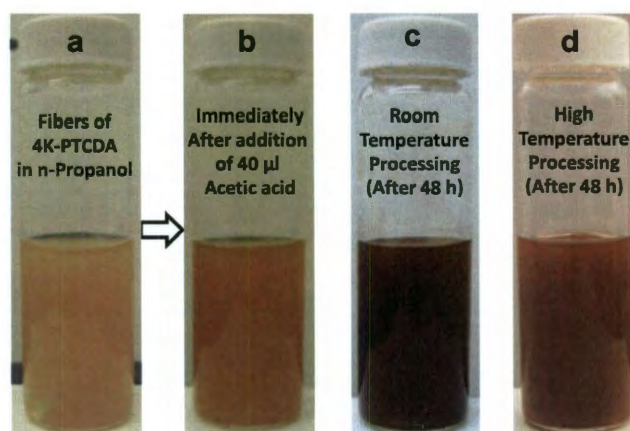
Figure 6.12 (a) Fibers of K_4-PTCA dispersed in n-propanol, (b) After addition of 40 μl glacial acetic acid there is change in color from yellowish orange to dark orange, (c) Dispersion of fibers in n-propanol obtained by room temperature processing after 48 h. The color changes to dark brown indicating some chemical transformation. (d) Dispersion of fibers in n-propanol by high temperature processing (80°C) after 48 h. The color of the dispersion is red indicating that completely different chemical species is formed as compared to room temperature processing.

In case of RT processing, the diameter of the fibers remained unchanged (100 nm) but the cross section of these fibers became more circular in nature, in comparison to the original K_4-PTCA morphology. Whereas, in case of HT processing the initial 100 nm fibers gets transformed into very uniform 20 nm diameter fibers (Figure 6.13). A time dependent study was carried out to see the changes in the morphology due to addition of acetic acid in the course of 48 h under room temperature (RT) and high temperature (HT) processing conditions. For this purpose, samples were cast on silicon wafer at different time intervals after the addition of acetic acid in case of both the processing conditions.
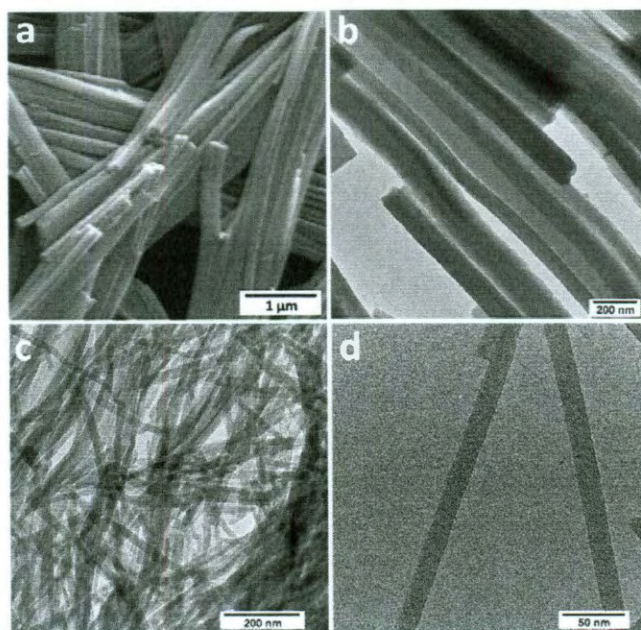
Figure 6.13 (a) SEM image and (b) TEM image of the fibers obtained by RT processing after 48 h. The diameter of the fibers remained unchanged however, the cross section of the fibers became more circular in nature. (c), (d) TEM images of the fibers obtained by HT processing after 48 h. The diameter of the fibers changed to 20 nm.

6.6.1 HT processing of fibers of K$_4$-PTCA

The time dependent TEM images for HT processing are shown in Figure 6.14. In case of HT processing (80°C), immediately after 5 minutes of glacial acetic acid addition, there is destruction of the columnar aggregate with seeds appearing on the fiber structure (Figure 6.14b). At this stage the width of the structures are comparable to those of the original fibers of the K$_4$-PTCA. After about 5 h, TEM investigations reveal the formation of small 20 nm fibers emerging out of the broken columnar bundles of 100 nm fibers (Figure 6.14c). At this stage there was mixture of 20 nm and 100 nm broken columnar bundles of fibers. When the TEM of the same dispersion of fibers was taken after 24 h heating at 80°C, almost 95% of the fibers were 20 nm in diameter (Figure 6.14d). The dispersion was allowed to stir at this temperature for further 24 h. When the TEM of this dispersion of fibers was taken after total 48 hour of acetic acid addition and heating at 80°C, there were exclusively 20 nm fibers in all the areas of the TEM grid (Figure 6.14e). The diameter of the fibers changed from 100 nm to 20 nm and the length also changed to less than a micron under these HT processing conditions. The color of the dispersion of fibers in n-propanol after 48 h heating in presence of acetic acid was dark red. When a drop of this dispersion was suspended in water, there was no destruction of fiber morphology. In order to check the susceptibility of the fibers towards water, a sample was casted on TEM grid and allowed to dry and this grid was then dipped in water for 5 minutes and dried. When this grid was examined under the TEM, there was no destruction of fibers observed and all the fibers were still 20 nm in diameter (Figure 6.14f).
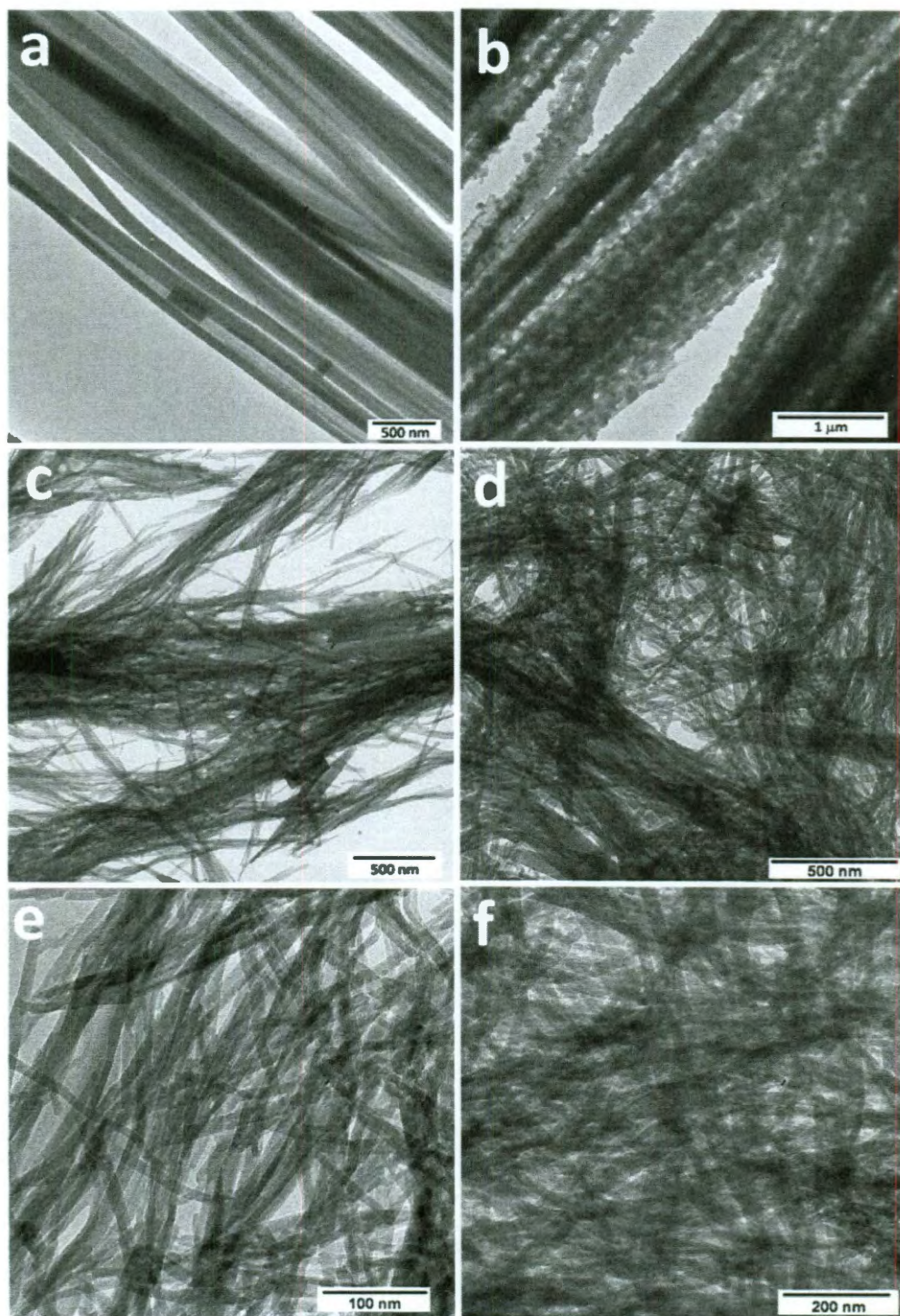
Figure 6.14 TEM Images of (a) K$_4$-PTCA fibers before acetic acid addition, (b) after 5 min, (c) after 5 h, (d) after 24 h, (e) after 48 h acetic acid addition, (f) after dipping and drying the TEM grid casted with sample in water.

The 20 nm fibers obtained by HT processing of the K_4-PTCA salt were completely destroyed in DMF and a homogenous fluorescent green solution of the species present in the fibers was formed. PTCDA powder and perylene-3,4,9,10-tetracarboxylic acid monoanhydride mono-potassium salt are completely immiscible in DMF. This suggested that the final components formed in 20 nm fibers due to HT processing of K_4-PTCA fibers were not composed of either of these two components. Thus, the ring closing did not take place under these HT conditions. This is obvious because, the dissociation constant of acetic acid in n-propanol as against water is very low and K_4-PTCA fibers are already in aggregated form in n-propanol. This is contrary to the reaction of acetic acid with the homogenous solution of K_4-PTCA in water at 80°C leading to the formation of perylene-3,4,9,10-tetracarboxylic acid monoanhydride mono-potassium salt. Thus, the ring closing failed in case of aggregated fibers of K_4-PTCA in n-propanol under HT processing conditions upon addition of acetic acid. In order to explore the chemical species present in these 20 nm fibers we synthesized PTCA by a standard procedure as mentioned in chapter 5 and compared its FTIR and UV visible spectrum with the fibers made by HT processing. The standard PTCA powder was highly miscible in DMF. When UV visible spectra of this solution in DMF was recorder it showed the presence of 0-0 transitions at 517 nm, 0-1 transitions at 483 nm, 0-2 transitions at 451 nm. This UV visible spectrum exactly matched with the spectrum of the homogeneous solution of the species present in HT processing fibers in DMF (Figure 6.15).This suggested that the components present in the HT processing fibers might be PTCA.
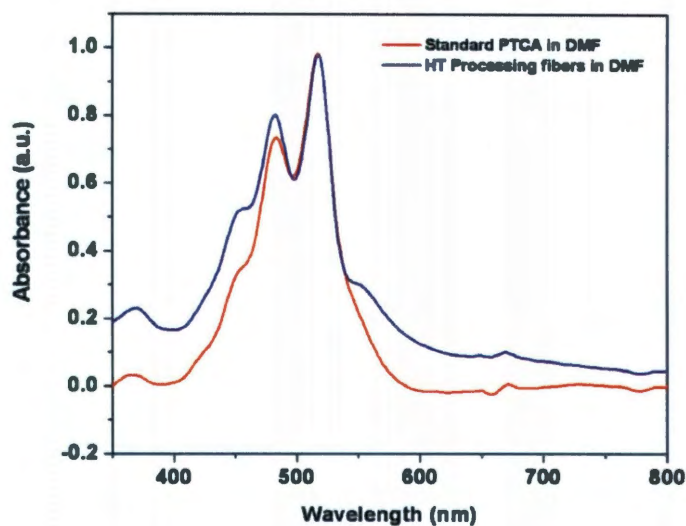
Figure 6.15 UV-Visible spectra of the homogeneous solution of species present in HT processing fibers in DMF and standard PTCA solution in DMF. Both the spectra match with each other suggesting that the species present in HT fibers is PTCA.

To further confirm the presence of PTCA in the structure of 20 nm fibers, FTIR was carried out. The solid powders of fibers of K_4-PTCA, standard PTCA and fibers after HT processing were separately grounded with KBr powder and their FTIR was recorded (Figure 6.16). The carbonyl of the carboxylate ions should appear at lower wavenumber whereas the carbonyl of the free carboxylic acid should appear at higher wavenumber. The FTIR of K_4-PTCA showed the carbonyl stretching at around 1538 cm^{-1} and 1391 cm^{-1} (narrow) whereas the FTIR of fibers obtained at HT processing showed the carbonyl stretching at around 1771 cm^{-1} (broad). Moreover, the FTIR spectra of standard PTCA matches exactly with of the fibers obtained after HT processing. Both of them show distinctive carbonyl stretch at 1771 cm^{-1} (broad) and OH stretching of the free carboxylic acids at 3122 cm^{-1} (narrow) and 3600 cm^{-1} (broad). Thus, it can be concluded that the chemical transformation of the K_4-PTCA fibers (100 nm, widths) under HT conditions results in the formation of the fibers of PTCA with a width of 20 nm. This is likely

because the PTCA molecules can now, as they are formed, undergo H-bonding interactions in addition to the hydrophobic and the p-stacking interactions leading to the formation of organized 1D nanostructures. These results highlight the first example for the use of self-assembled structures of perylene salts in order to achieve a chemical product which is different from the bulk reactions of the salts under same conditions.
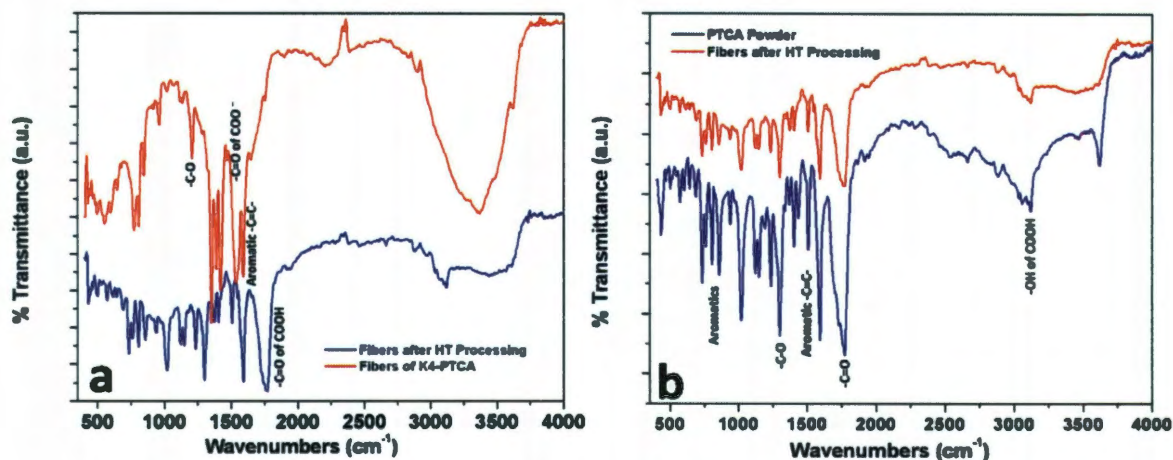
Figure 6.16 (a) FTIR spectra of the HT processing fibers and its comparison with the FTIR spectra of fibers of K_4-PTCA. (b) FTIR spectra of standard PTCA powder and its comparison with the FTIR spectra of Fibers after HT Processing.

6.6.2 RT processing of fibers of K_4-PTCA

The time dependent SEM images for RT processing are shown in Figure 6.17. In case of RT processing, immediately after 5 min addition of acetic acid, the SEM revealed the formation of small rod shaped seeds on the surface of the fibers indicative of some chemical transformation. The entire surface of these fibers was densely decorated with these rod shaped seeds (Figure 6.17b). These rods grow orthogonal to the long axis of the K_4-PTCA fiber axis. After 1 h of glacial acetic acid addition, the density of these seeds on the surface of the fibers decreased and the shape of the seeds became more spherical
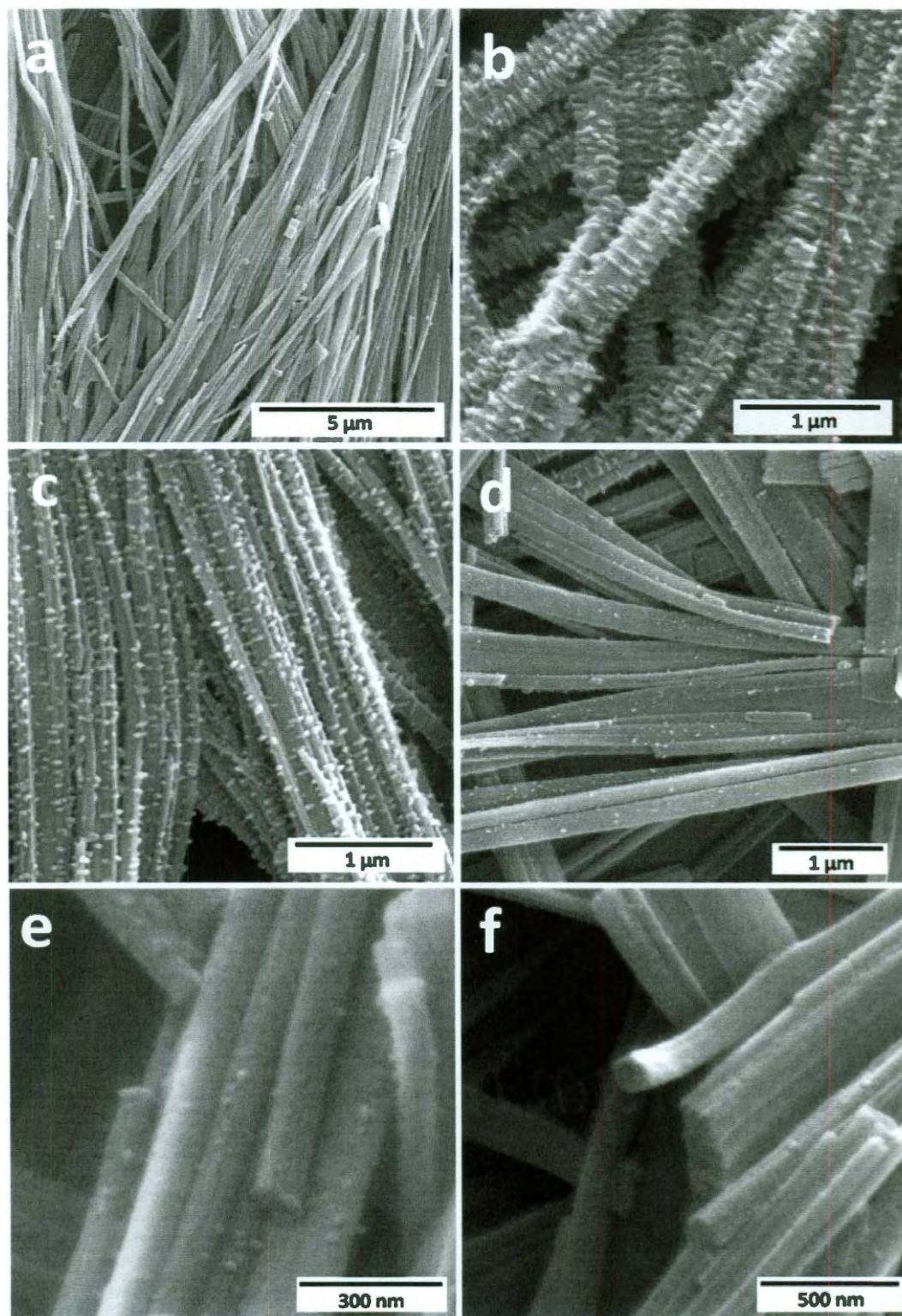
Figure 6.17 SEM Images of (a) K_4-PTCA fibers before acetic acid addition, (b) after 5 min, (c) after 1 h, (d) after 5 h, (e) after 24 h and (f) after 48 h acetic acid additions.

(Figure 6.17c). After 5 h of glacial acetic acid addition, the size and the density of these seeds decreased drastically (Figure 6.17d). Even after 24 h stirring in presence of glacial acetic acid (Figure 6.17e), there were some seeds present on fibers which completely disappeared after 48 h stirring (Figure 6.17f). The surface of the fibers after 48 h stirring in presence of acetic acid became very smooth and uniform. The lengths and widths of the fibers remain unchanged. However, the width of these fibers became circular (100 nm) as opposed to the rectangular width of the K_4-PTCA fibers. After 48 h addition of acetic acid to the dispersion of fibers of K_4-PTCA, the color slowly changed from dark orange to dark brown.

Upon casting a drop of the RT processing dispersion is suspended in water the fibers morphology was completely destroyed as the species present in these fibers dissolved in water. When immediately observed under the UV lamp, this homogeneous solution exhibited a green fluorescence, expected for the homogeneous dissolved molecules. However, within a minute the fluorescence of this suspension in water suddenly disappeared and some insoluble material was formed. This is because of the use of excess acetic acid in the initial condition. The fiber product was washed with large amount of propanol to remove all of the excess acid. The resulting residue retains the morphology of the aggregates after RT processing and homogeneously dissolved in water exhibiting a green fluorescence. This fluorescence did not disappear and remained permanent and there was no insoluble material formed. These observations suggested that the components present in the fibers obtained after RT processing were still in the form of some kind of potassium salt.

The dark brown colored K_2-PTCA (synthesized, see experimental) had color similar to the RT processing fibers. When UV visible spectra of this standard K_2-PTCA in water was recorder it showed the presence of 0-0 transitions at 467 nm, 0-1 transitions at 440 nm, 0-2 transitions at 415 nm. This UV visible spectrum exactly matched with the homogeneous aqueous solution of species present in the solid powder of RT processing fibers (Figure 6.18). This suggested that the components present in the fibers by room temperature processing might be K_2-PTCA.
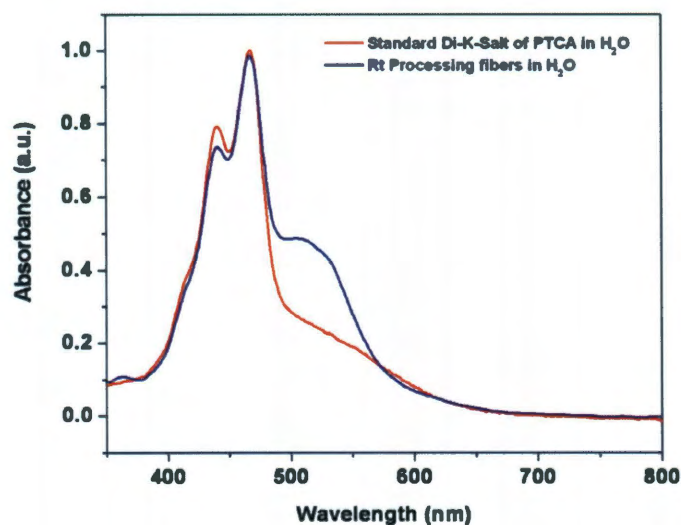
Figure 6.18 UV-Visible spectra of the homogeneous solution of species present in RT processing fibers in water and standard K_2-PTCA solution in water. Both the spectra match with each other suggesting that the species present in RT fibers might be K_2-PTCA.

To further confirm the presence of K_2-PTCA in the structure of 100 nm fibers, FTIR of standard K_2-PTCA powder and RT processing solid powder of fibers was carried out by grounding them separately in KBr powder (Figure 6.19).The FTIR spectrum of solid powder of standard K_2-PTCA showed the presence of –OH stretch of free carboxylic acid at around 3416 cm^{-1} (broad) and two bands of carbonyl stretching at

around 1759 cm^{-1} and 1724 cm^{-1}. These two carbonyl stretching bands are observed due to the presence of carboxylate and free carboxylic acid groups both present in the structure of K$_2$-PTCA. The protonation of the K$_4$-PTCA fibers allows for the H-bonding interactions within the resulting acidic structure. Thus, the chances of acetic acid protonating two carboxylate ions present on the opposite sides of the perylene core are very high. This position and nature of carbonyl stretching was completely different as compared to the K$_4$-PTCA which appeared at lower wavenumber. This further proved that the standard K$_2$-PTCA was indeed a di-potassium salt of PTCA (brown colored) which was highly miscible in water and not K$_4$-PTCA (yellow colored). The FTIR of the fibers obtained at RT processing showed similar carbonyl stretching's at around 1759 cm^{-1} and 1724 cm^{-1} and –OH stretching at around 3416 cm^{-1}. Thus the FTIR spectrum of standard K$_2$-PTCA was an exact match of the fibers obtained at RT processing.
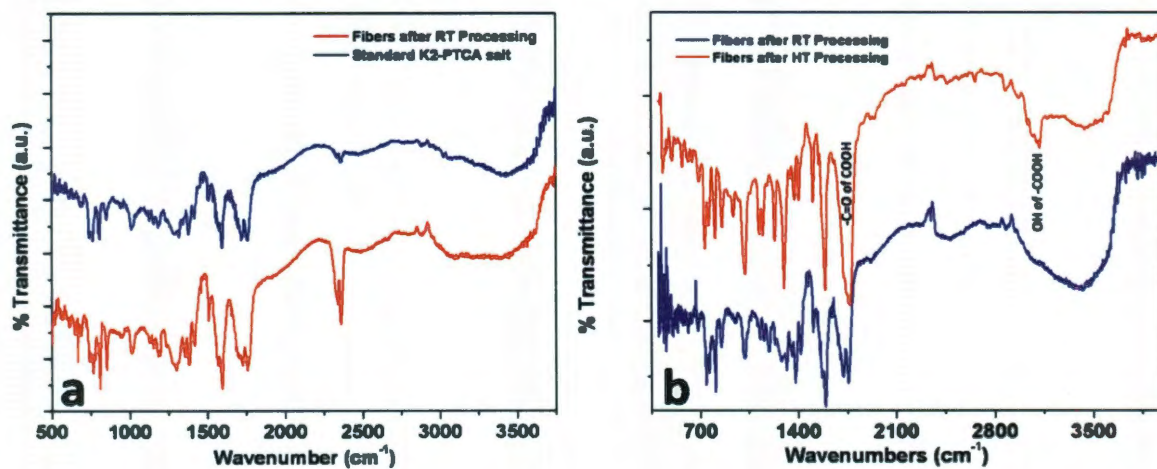
Figure 6.19 (a) FTIR spectra of the RT processing fibers and its comparison with the FTIR spectra of fibers of standard K$_2$-PTCA. (b) FTIR spectra of the RT processing fibers and its comparison with the FTIR spectra of fibers of the HT processing fibers.

Thus, from the UV visible and FTIR data it was confirmed that the species present in the RT processing fibers was K_2-PTCA whereas the species present in HT-processing fibers was PTCA.

6.7 Plausible mechanism for morphology evolution by RT and HT processing

In the RT and HT processing, glacial acetic acid was added to the dispersion of fibers of K_4-PTCA in n-propanol. The dissociation constant of glacial acetic acid is lower in n-propanol in comparison to water. After 48 h stirring in presence of acetic acid at RT, there is slow protonation of the carboxylate groups present in the fibers. The chance of both the carboxylate ions at 3, 4 or 9, 10 positions (i.e. on the same side) being protonated is very less. This is because, as soon as one carboxylate ion is protonated with acetic acid, the neighboring carboxylate-ion can immediately hydrogen bond with this free acid. Thus, only carboxylate ions present in the opposite sides of perylene core will get protonated to form free carboxylic acid and their adjacent carboxylate ions will immediately hydrogen bond with these free acids leading to formation of K_2-PTCA. This is a slow process and hence in the time dependant study, we observe seeds on the surface of the fibers even after 24 h. After 48 h, all the seeds on the surface of the fibers disappear indicating the completion of this chemical transformation (Figure 6.14). There is no change in the morphology or FTIR of the fibers after 48 h indicating that stable products have indeed been formed. The formation of seeds only on the surface of the original K_4-PTCA structure again highlights that the formation of assembly is driven by the co-existence of two different structures that are in strong interaction with each other. However, upon completion of the reaction the process leads to the formation of K_2-PTCA fibers with the cross section of the assembly being circular as opposed to rectangular.

However, in case of HT processing, the kinetics of the protonation of carboxylate ions due to acetic acid in n-propanol is very fast. This is the reason why within 2 h, the color of the HT processing dispersion becomes brown which was similar to RT processing fibers after 48 h. As this dispersion of fibers in n-propanol is further heated at 80°C, the remaining carboxylate ions are completely protonated. This is clearly seen in the time dependant morphology evolution study, wherein, after 5 h there are 20 nm fibers protruding outside the broken columnar bundles of fibers (Figure 6.17). After 48 h there is complete reorganization of the system via strong hydrogen bonding interaction between free carboxylic acids of PTCA, leading to the formation of small 20 nm diameter fibers.

6.8 Experimental Section

6.8.1 Characterization

The optical absorption spectra were obtained with a UV-3600 Shimadzu UV/Vis/NIR spectrophotometer. The fluorescence (or PL) data was obtained using a SPEX fluorimeter (Fluoromax-3 model). All the Fourier transform infrared spectra (FTIR) were obtained on FTIR-8400S Shimadzu instrument by grounding the solid powder of the samples with KBr powder. Scanning electron microscopy (SEM) for all the samples was done on FEI Quanta 400 ESEM FEG (ESEM2). The samples for SEM were prepared by drying the dispersion of the aggregates in n-propanol on the silicon wafer. The resulting samples were then coated with gold using CRC-150 sputter coater (40 s) for SEM imaging. Transmission electron microscopy (TEM) was performed on JEOL 1230 (acceleration voltage 120 kV), JEOL 2010 (acceleration voltage 200kV) electron microscope using carbon-coated copper grid which were purchased from Electron

Microscopy Sciences (EMS). All the samples for SEM/TEM were prepared by casting a droplet of dispersion of aggregates in n-propanol on silicon wafer or TEM grid and allowed to dry.

6.8.2 Self assembly of K_4-PTCA into 3D crystals

N-propanol (approximately 35 ml) was added dropwise to the stirring solution of aqueous 3.5 ml K_4-PTCA prepared as mentioned above. The solution remained homogeneous until 15 ml of n-propanol addition which showed an intense green fluorescence. On total 35 ml addition of n-propanol, the solution became turbid and there was complete quenching of fluorescence. Immediately there were no aggregates that precipitated out of solution at the bottom of the vial. The vial was left to stand undisturbed for 3 days when most of the aggregates settled at the bottom of the vial and formed a solid thick layer. The upper layer of n-propanol was discarded without disturbing the bottom layer of the aggregates. Slowly, n-propanol was then added to this vial and the bottom layer was rinsed carefully so as to remove all the water trapped inside the aggregates. This ensured that there would be no destruction of the morphology of the aggregates and they would be easily examined by SEM when dried on the silicon wafer. The bottom thick layer of the aggregates were then suspended uniformly in the 10 ml n-propanol by slightly shaking the vial and the resulting aggregates were examined by SEM

6.8.3 Self assembly of K_4-PTCA into 2D sheets

K_4-PTCA was self assembled using ethanol as a poor solvent as per the protocol mentioned for the self assembly using n-propanol as poor solvent above. After complete addition of n-propanol, the vial was allowed to stand for 2 days, which led to the formation of solid thick layer of aggregates at the bottom, which was rinsed carefully

several times with n-propanol so as to remove water and volatile ethanol and then aggregates were suspended in 10 ml n-propanol. The sample was then cast on the silicon wafer, dried and examined by SEM. Similarly, when K_4-PTCA was aggregated using methanol as poor solvent by the similar procedure mentioned in case of ethanol and the aggregates were extracted in n-propanol, 3D flower and rod like crystals were obtained.

6.8.4 Protocol for the self-assembly of Li$_4$-PTCA and Na$_4$-PTCA

THF (~35 ml) was added dropwise to the stirring solutions of previously prepared 3.5 ml solution of Li$_4$-PTCA and Na$_4$-PTCA in water respectively. After about 10 ml addition of THF, there was rapid aggregation and the entire solution turned turbid yellow in both the Li$_4$-PTCA and Na$_4$-PTCA. On further addition of THF, the entire solution in both the cases became bright yellow which when shined with UV light did not fluoresce indicating the completion of the aggregation process. The rate of aggregation in case of Li$_4$-PTCA and Na$_4$-PTCA was much faster as compared to K_4-PTCA. When a drop of these dispersions were casted on the glass slide and observed under optical microscope only random aggregates were observed floating in the solution and there was complete absence of fibers. The vials were then left undisturbed for about an hour when all the aggregates settled at the bottom. All these aggregates were then made devoid of THF and water and then extracted in n-propanol by the protocol mentioned above for the fibers of K_4-PTCA. A drop of these samples was then casted on the silicon wafers separately and examined by SEM.

6.8.5 Synthesis of standard PTCA and K_2-PTCA

In order to determine the chemical species present in the fibers made by room temperature and high temperature processing, standard PTCA and K_2-PTCA was synthesized as follows:

(a) Synthesis of standard perylene tetracarboxylic acid (PTCA)

1 g of PTCDA powder (2.54 mmoles) was dispersed in ~500 ml water and 715 mg of KOH (12.74 mmoles) was added to this dispersion. This dispersion was heated on hot plate at 80°C for 1 h to form a fluorescent green homogeneous solution of K_4-PTCA dissolved in water. The solution was allowed to cool and filtered so as to remove trace amount of unreacted PTCDA if any and then 1M HCl was added dropwise to this fluorescent green solution at room temperature. There was precipitation of highly water immiscible PTCA in the solution. 1M HCl was kept on adding until all the K_4-PTCA is converted into PTCA and there was complete disappearance of green fluorescence in the solution. This dispersion of PTCA was stirred at room temperature for further 1 h and kept away from heat. This dispersion was then filtered using a 0.2 μm pore size filter paper and given several washings with water until the pH of the washings was neutral. The reddish orange solid PTCA powder was dried under vaccum and kept away from heat. Yield = 99%. IR (KBr) v_{max} 3618, 3122, 1763, 1586, 1296, 857 cm^{-1}.

(b) Synthesis of dipotassium salt of PTCA (K_2-PTCA)

Briefly, 7 mg of previously synthesized standard PTCA powder was taken in a vial and exactly 2 equivalents of KOH (0.36 ml of 5M KOH solution) was added to it. Extra 2 ml water was added to this vial so as to form a highly water miscible homogeneous concentrated solution. This salt of K_2-PTCA homogeneously dissolved in

water was than precipitated using n-propanol. The dark brown colored K₂-PTCA settled

at the bottom of the vial in 1 day. The upper layer of the clear n-propanol was discarded

using a pipette and the solid residue at the bottom of the vial was filtered using a 0.2 μm

filter paper and given several washing with n-propanol. The filtered solid was then dried

under vacuum. This dried brown colored solid powder of K₂-PTCA was completely

miscible in water. The chances of this salt being a mixture of K₄-PTCA and free PTCA

was very less, because this product was not bright yellow in color (color of solid K₄-

PTCA is bright yellow) and neither it was miscible in DMF (PTCA is miscible in DMF

and immiscible in water). Thus, under the conditions in which it had been synthesized it

had to be K₂-PTCA. Yield = 98%. IR K₂-PTCA (KBr) v_{max} 3422, 1759, 1724, 1591, 813

cm^{-1}.

6.9 Conclusions

Thus in conclusion, the self-assembly of tetra potassium salt of PTCA into 1D

nanofibers in a controlled environment is reported for the first time. The self-assembly of

the K₄-PTCA salt is driven by hydrophobic, π-π stacking and ion-solvent interactions.

Furthermore, assembly was indeed an ion-mediated self-assembly and 1D nanostructures

are formed only in case of tetrapotassium salt of PTCA whereas the tetra lithium salt and

tetra sodium salt of PTCA lead to random morphology. Moreover, it was also possible to

chemically modified the fibers of tetrapotassium salt of PTCA into fibers of two different

species - perylene tetracarboxylic acid (PTCA) and di-potassium salt of PTCA (K₂-

PTCA) having 20 nm and 100 nm diameters respectively. These assemblies may have

better performances as compared to the fibers based on perylene diimides due to absence

of any insulating alkyl/aryl side chain attached to the perylene cores. This facile self-

assembly and chemical modification process leads to the formation of chemically active fiber surface which can be further chemically modified to generate various hybrid materials.

Chapter 7

Summary

Various perylene based n-type organic semiconducting molecules have been successfully synthesized and further self-assembled into very uniform ordered 1D (fibers, belts and wires), 2D (sheets) and 3D (crystals) structures. Different solution processing methods such as dispersion, two layer phase transfer at room temperature (2L-RT) and two layer phase transfer at high temperature (2L-HT) have been successfully utilized to generate these self-assembled structures. The perylene based molecules utilized for the self-assembly are perylene tetracarboxylic diimide (PTCDI), perylene-tetracarboxylic monoanhydride monoimides (m-PTCI), perylene-tetracarboxylic acid (PTCA) and tetrapotassium salt of PTCA (K_4-PTCA).

The self-assembly of PTCDI molecules with varying length of side chains attached to the perylene core have been studied in this thesis by the 2L-HT method. It was found that due to slow nucleation and growth process associated with this method very long (few millimeters) PTCDI wires could be obtained which show very intense excimeric emission. These observations were attributed to the two different packing (due to both strong π- stacking and distorted π- stacking) present in these wires which not only lead to 1D structures but also leads to very intense excimer like emission from a single wire. Moreover, due to the extremely large lengths associated with these wires, a single wire could be picked and placed easily for any device fabrication.

The 2L-HT method was also utilized for the self-assembly of sparingly soluble m-PTCI molecules with varying length of side chain. This method leads to the formation of highly crystalline and fluorescent 2D sheets. From the optical properties coupled with

the results obtained from XRD, it is evident that atleast two types of packing are responsible for such 2D structures. The H-bonding, π-stacking and hydrophobic interactions are the primary driving forces for such 2D packing in these molecules. The 2D structures developed in this thesis are the first examples of 2D self-assembly from m-PTCI and hold promised in electronic and optoelectronic applications. The 2L-HT method developed in this thesis can be utilized to not only improve the solubility of the sparingly soluble functional materials but at the same time control their rate of aggregation leading to formation of long range ordered structures. Future plans with the 2L-HT processing method includes the ability to co-assemble two different functional molecules (e.g. incorporation of p-type within the framework of the n-type assembly).

In order to achieve the 1D self-assembly of extremely insoluble perylene-3, 4, 9, 10-tetracarboxylic dianhydride (PTCDA) by solution processing, the chemical reaction mediated self-assembly has been demonstrated for the first time. In this process, carbodiimide chemistry has been utilized for the conversion of highly soluble PTCA precursor into highly insoluble PTCDA. The most intriguing aspect of this conversion is that, highly crystalline 1D nanofibers of highly insoluble PTCDA are formed due to this chemical transformation. Due to the absence of alkyl side chains, the H-bonding and π-stacking interactions are attributed to the formation of such organized structures. Thus, this method of self-assembly open doors for the formation of ordered structures from other highly insoluble functional organic molecules from appropriately designed precursors.

Further, in order to explore the self-assembly of perylene based molecules without any side chain modifications from aqueous solutions, various tetra alkali metal

salts of perylene tetracarboxylic acid (M_4-PTCA) were utilized for self-assembly process. It was found that the self-assembly in this system is an ion mediated and solvent mediated leading to the formation of 1D, 2D and 3D self-assembled structures. Different non-covalent interactions such as hydrophobic, π- stacking, and electrostatic interactions (ion-dipole, ion-solvent, and ion-molecule) were attributed for the formation of such ordered structures. Further, the 1D nanofibers were chemically modified in their aggregated into fibers of two different chemical species. This modification was found to lead no destruction of the morphology but there was change in the sizes of the resulting modified aggregates. The self-assembly for the salts of PTCA demonstrated in this work is a unique example for the formation of ordered structures utilizing these molecules. Moreover, the ability to chemically further change the characteristics is extremely promising for the incorporation of more complex structures to impart unique properties to these dimensionally controlled structures.

Thus, overall this thesis elucidates that by appropriately designing molecules with various functional groups, the favorable interactions can be controlled in an appropriate environment (solvent) leading to the ordered structures. Further, this thesis elaborates the role of the processing conditions which can control the rate of nucleation and growth, leading to the dimension control of the self-assembly from organic molecules. Some of the future work would entail the fabrication of novel electronic, opto-electronic devices from these materials.

Bibliography

(1)   Tang, C. W.; Vanslyke, S. A. *Appl. Phys. Lett.* **1987**, *51*, 913-915.

(2)   Horowitz, G.; Fichou, D.; Peng, X.; Xu, Z.; Garnier, F. *Solid State Commun.* **1989**, *72*, 381-384.

(3)   Tang, C. W. *Appl. Phys. Lett.* **1986**, *48*, 183-185.

(4)   Chesterfield, R. J.; Newman, C. R.; Pappenfus, T. M.; Ewbank, P. C.; Haukaas, M. H.; Mann, K. R.; Miller, L. L.; Frisbie, C. D. *Adv. Mater.* **2003**, *15*, 1278-1282.

(5)   Kozlov, V. G.; Bulovic, V.; Burrows, P. E.; Forrest, S. R. *Nature* **1997**, *389*, 362-364.

(6)   Peumans, P.; Bulovic, V.; Forrest, S. R. *Appl. Phys. Lett.* **2000**, *76*, 3855-3857.

(7)   Pope, M.; Swenberg, C. E. *Electronic Processes in Organic Crystals and Polymers*, **1999**.

(8)   Akamatu, H.; Inokuchi, H.; Matsunaga, Y. *Nature* **1954**, *173*, 168–169.

(9)   Mcneill, R.; Weiss, D. E.; Wardlaw, J. H.; Siudak, R. *Aust. J. Chem.* **1963**, *16*, 1056-1057.

(10) Epstein, A. J.; Etemad, S.; Garito, A. F.; Heeger, A. J. *Phys. Rev. B* **1972**, *5*, 952-977.

(11) Coleman, L. B.; Cohen, M. J.; Sandman, D. J.; Yamagishi, F. G.; Garito, A. F.; Heeger, A. J. *Solid State Commun.* **1973**, *12*, 1125-1132.

(12) McGinness, J.; Corry, P.; Proctor, P. *Science* **1974**, *183*, 853-855.

(13) Chiang, C. K.; Fincher, C. R.; Park, Y. W.; Heeger, A. J.; Shirakawa, H.; Louis, E. J.; Gau, S. C.; MacDiarmid, A. G. *Phys. Rev. Lett.* **1977**, *39*, 1098-1101.

(14) Shirakawa, H.; Louis, E. J.; MacDiarmid, A. G.; Chiang, C. K.; Heeger, A. J. *J. Chem. Soc., Chem. Commun.* **1977**, 578-580.

(15) Sirringhaus, H.; Ando, M. *MRS Bull.* **2008**, *33*, 676-682.

(16) Sirringhaus, H.; Tessler, N.; Friend, R. H. *Science* **1998**, *280*, 1741-1744.

(17)   Friend, R. H.; Gymer, R. W.; Holmes, A. B.; Burroughes, J. H.; Marks, R. N.; Taliani, C.; Bradley, D. D. C.; dos Santos, D. A.; Bredas, J. L.; Lglund, M.; Salaneck, W. R. *Nature* **1999**, *397*, 121-128.

(18)   Thompson, B. C.; Frechet, J. M. J. *Angew. Chem., Int. Ed.* **2008**, *47*, 58-77.

(19)   Someya, T.; Pal, B.; Huang, J.; Katz, H. E. *MRS Bull.* **2008**, *33*, 690-696.

(20)   Lewerenz, H. J.; Jungblut, H. *Photovoltaic – Grundlagen und Anwendungen Springer Berlin,Heidelberg, New York,* **1995**.

(21)   Sze, S. M. *Physics of Semiconductor Devices; Wiley and Sons,* **1982**.

(22)   Yu, P. Y.; Cardona, M. *Fundamentals of Semiconductors: Physics and Materials Properties, Springer,* **2001**.

(23)   Banerjee, S. K.; Streetman, B. G. *Solid State Electronic Devices,* **2005**.

(24)   Chan, K. Y.; Knipp, D.; Carius, R.; Stiebig, H. *MRS Bull.* **2008**, *1066*, 293-298.

(25)   O'Mara, W. C.; Hunt, L. P.; Herring, R. B. *Handbook of Semiconductor Silicon Technology; Noyes Publications,* **1990**.

(26)   Chen, H.-Z.; Shi, M.-M.; Aernouts, T.; Wang, M.; Borghs, G.; Heremans, P. *Sol. Energy Mater. Sol. Cells* **2005**, *87*, 521-527.

(27)   Hush, N. S. *Ann.N.Y.Acad. Sci.* **2003**, *1006*, 1-20.

(28)   Allegra, G.; Meille, S. V. *Macromol.* **2004**, *37*, 3487-3496.

(29)   Ling, M. M.; Bao, Z.; Erk, P.; Koenemann, M.; Gomez, M. *Appl. Phys. Lett.* **2007**, *90*, 093508.

(30)   Briseno, A. L.; Mannsfeld, S. C. B.; Jenekhe, S. A.; Bao, Z.; Xia, Y. *Mater. Today* **2008**, *11*, 38-47.

(31)   Forrest, S. *Nature (London)* **2004**, *428*, 911-918.

(32)   Naka, S.; Okada, H.; Onnagawa, H.; Tsutsui, T. A. P. L. *Appl. Phys. Lett.* **2000**, *76*, 197-199.

(33)   Stolka, M.; Yanus, J. F.; Pai, D. M. *J. Phys. Chem.* **1984**, *88*, 4707-4714.

(34) Roth, S. *One-Dimensional Metals Wiley-VCH, Weinheim*,**1995**.

(35) Horowitz, G. *Adv. Mater.* **1998**, *10*, 365-377.

(36) Coropceanu, V.; Cornil, J.; da Silva, D. A.; Olivier, Y.; Silbey, R.; Bredas, J. L. *Chem. Rev.* **2007**, *107*, 926-952.

(37) Jaiswal, M.; Menon, R. *Polym. Int.* **2006**, *55*, 1371-1384.

(38) Emin, D. *Adv. Phys.* **1975**, *24*, 305-348.

(39) Heeger, A. J. *Faraday Discuss. Chem. Soc.* **1989**, 203-211.

(40) Chabinyc, M. L.; Jimison, L. H.; Rivnay, J.; Salleo, A. *MRS Bull.* **2008**, *33*, 683-689.

(41) Reinhoudt, D. N.; Crego-Calama, M. *Science* **2002**, *295*, 2403.

(42) Lehn, J.-M. *Angew. Chem. Int. Ed.* **1988**, *27*, 89-112.

(43) Lehn, J. M. *Angew. Chem. Int. Ed. Engl.* **1990**, *29*, 1304-1325.

(44) Whitesides, G. M.; Grzybowski, B. *Science* **2002**, *295*, 2418-2421.

(45) Wu, J.; Pisula, W.; Mullen, K. *Chem. Rev.* **2007**, *107*, 718-747.

(46) Watson, M. D.; Fechtenotter, A.; Mullen, K. *Chem. Rev.* **2001**, *101, 1267-1300*.

(47) Hoeben, F. J. M.; Jonkheijm, P.; Meijer, E. W.; Schenning, A. P. H. J. *Chem. Rev.* **2005**, *105*, 1491-1546.

(48) Schenning, A. P. H. J.; Meijer, E. W. *Chem. Commun.* **2005**, 3245-3258.

(49) Meijer, E. W.; Schenning, A. P. H. J. *Nature* **2002**, *419*, 353-354.

(50) Curtis, M. D.; Cao, J.; Kampf, J. W. *J. Am. Chem. Soc.* **2004**, *126*, 4318-4328.

(51) Anthony, J. E. *Chem. Rev.* **2006**, *106*, 5028-5048.

(52) Cornil, J.; Beljonne, D.; Calbert, J. P.; Berdas, J. L. *Adv. Mater.* **2001**, *13*, 1053-1067.

(53) Schenning, A. P. H. J.; Meijer, E. W. *Chem. Commun.* **2005**, 3245-3258.

(54) Sandra , C. H.; Debangshu, C.; Wilfred, C.; Nosang, V. M.; Ashok, M. *Electroanalysis* **2007**, *19*, 2125-2130.

(55) Huang, J. X.; Virji, S.; Weiller, B. H.; Kaner, R. B. *J. Am. Chem. Soc.* **2003**, *125*, 314-315.

(56) Tang, Q.; Li, L.; Song, Y.; Liu, Y.; Li, H.; Xu, W.; Hu, W.; Zhu, D. *Adv. Mater.* **2007**, *19*, 2624-2628.

(57) Brien, G. A. O.; Quinn, A. J.; Tanner, D. A.; Redmond, G. *Adv. Mater.* **2006**, *18*, 2379-2383.

(58) Berson, S.; de Bettignies, R.; Bailly, S.; Guillerez, S. *Adv. Funct. Mater.* **2007**, *17*, 1377-1384.

(59) Ong, B. S.; Wu, Y.; Liu, P.; Gardner, S. *Adv. Mater.* **2005**, *17*, 1141-1144.

(60) Wanekaya, A. K.; Bangar, M. A.; Yun, M.; Chen, W.; Myung, N. V.; Mulchandani, A. *J. Phys. Chem. C* **2007**, *111*, 5218-5221.

(61) DeLongchamp, D. M.; Kline, R. J.; Lin, E. K.; Fischer, D. A.; Richter, L. J.; Lucas, L. A.; Heeney, M.; McCulloch, I.; Northrup, J. E. *Adv. Mater.* **2007**, *19*, 833-837.

(62) DeLongchamp, D. M.; Sambasivan, S.; Fischer, D. A.; Lin, E. K.; Chang, P.; Murphy, A. R.; Fréchet, J. M. J.; Subramanian, V. *Adv. Funct. Mater.* **2005**, *17*, 2340-2344.

(63) Aleshin, A. N. *Adv. Funct. Mater.* **2006**, *18*, 17-27.

(64) Merlo, J. A.; Frisbie, C. D. *J. Phys. Chem. B* **2004**, *108*, 19169-19179.

(65) Hoichang, Y.; Tae Joo, S.; Zhenan, B.; Chang, Y. R. *J.Polym. Sci., Part B: Polym. Phys.,* **2007**, *45*, 1303-1312.

(66) Merlo, J. A.; Frisbie, C. D. *J. Polym. Sci., Part B: Polym. Phys.* **2003**, *41*, 2674-2680.

(67) Briseno, A. L.; Mannsfeld, S. C. B.; Reese, C.; Hancock, J. M.; Xiong, Y.; Jenekhe, S. A.; Bao, Z.; Xia, Y. *Nano Lett.* **2007**, *7*, 2847-2853.

(68) Briseno, A. L.; Mannsfeld, S. C. B.; Lu, X.; Xiong, Y.; Jenekhe, S. A.; Bao, Z.; Xia, Y. *Nano Lett.* **2007**, *7*, 668-675.

(69) Datar, A.; Balakrishnan, K.; Yang, X.; Zuo, X.; Huang, J.; Oitker, R.; Yen, M.; Zhao, J.; Tiede, D. M.; Zang, L. *J. Phys. Chem. B* **2006**, *110*, 12327-12332.

(70) Sirringhaus, H. *Adv. Mater.* **2005**, *17*, 2411-2425.

(71) Katz, H. E.; Bao, Z. N.; Gilat, S. L. *Acc. Chem. Res.* **2001**, *34*, 359-369.

(72)   Chabinyc, M. L.; Salleo, A. *Chem.Mater.* **2004**, *16*, 4509-4521.

(73)   Kim, D. H.; Lee, D. Y.; Lee, H. S.; Lee, W. H.; Kim, Y. H.; Han, J. I.; Cho, K. *Adv. Mater.* **2007**, *19*, 678-682.

(74)   Tang, Q.; Li, H.; Liu, Y.; Hu, W. *J. Am. Chem. Soc.* **2006**, *128*, 14634-14639.

(75)   Minari, T.; Seto, M.; Nemoto, T.; Isoda, S.; Tsukagoshi, K.; Aoyagi, Y. *Appl. Phys. Lett.* **2007**, *91*, 123501-123504.

(76)   Jiang, H.; Yang, X. J.; Cui, Z. D.; Liu, Y. C.; Li, H. X.; Hu, W. P.; Liu, Y. Q.; Zhu, D. B. *Appl. Phys. Lett.* **2007**, *91*, 123505.

(77)   Sun, Y.; Tan, L.; Jiang, S.; Qian, H.; Wang, Z.; Yan, D.; Di, C.; Wang, Y.; Wu, W.; Yu, G.; Yan, S.; Wang, C.; Hu, W.; Liu, Y.; Zhu, D. *J. Am. Chem. Soc.* **2007**, *129*, 1882-1883.

(78)   Kraft, A.; Grimsdale, A. C.; Holmes, A. B. *Angew. Chem., Int. Ed.* **1998**, *37*, 402-428.

(79)   McCullough, R. D. *Adv. Mater.* **1998**, *10*, 93-116.

(80)   Martens, H. C. F.; Blom, P. W. M.; Schoo, H. F. M. *Phys. Rev. B* **2000**, *61*, 7489-7493.

(81)   Kemerink, M.; van Duren, J. K. J.; Jonkheijm, P.; Pasveer, W. F.; Koenraad, P. M.; Janssen, R. A. J.; Salemink, H. W. M.; Wolter, J. H. *Nano Lett.* **2003**, *3*, 1191-1196.

(82)   DiCesare, N.; Belletete, M.; Raymond, F.; Leclerc, M.; Durocher, G. *J. Phys. Chem. A* **1998**, *102*, 2700-2707.

(83)   Krebs, F. C.; Jorgensen, M. *Macromol.* **2003**, *36*, 4374-4384.

(84)   McCullough, R. D.; Tristram-Nagle, S.; Williams, S. P.; Lowe, R. D.; Jayaraman, M. *J. Am. Chem. Soc.* **1993**, *115*, 4910-4911.

(85)   Faid, K.; Cloutier, R.; Leclerc, M. *Macromol.* **1993**, *26*, 2501-2507.

(86)   Langeveld-Voss, B. M. W.; Janssen, R. A. J.; Christiaans, M. P. T.; Meskers, S. C. J.; Dekkers, H. P. J. M.; Meijer, E. W. *J. Am. Chem. Soc.* **1996**, *118*, 4908-4909.

(87)   Liu, J.; Sheina, E.; Kowalewski, T.; McCullough, R. D. *Angew. Chem., Int. Ed.* **2002**, *41*, 329-332.

(88) Jonkheijm, P.; Hoeben, F. J. M.; Kleppinger, R.; Van Herrikhuyzen, J.; Schenning, A. P. H. J.; Meijer, E. W. *J. Am. Chem. Soc.* **2003**, *125*, 15941-15949.

(89) Kastler, M.; Pisula, W.; Wasserfallen, D.; Pakula, T.; Mullen, K. *J. Am. Chem. Soc.* **2005**, *127*, 4286-4296.

(90) Duati, M.; Grave, C.; Tcbeborateva, N.; Wu, J.; Müllen, K.; Shaporenko, A.; Zharnikov, M.; Kriebel, J. K.; Whitesides, G. M.; Rampi, M. A. *Adv. Mater.* **2006**, *18*, 329-333.

(91) Tyutyulkov, N.; Müllen, K.; Baumgarten, M.; Ivanova, A.; Tadjer, A. *Synt. Met.* **2003**, *139*, 99-107.

(92) van de Craats, A. M.; Stutzmann, N.; Bunk, O.; Nielsen, M. M.; Watson, M.; Mllen, K.; Chanzy, H. D.; Sirringhaus, H.; Friend, R. H. *Adv. Mater.* **2003**, *15*, 495-499.

(93) Yamamoto, Y.; Fukushima, T.; Suna, Y.; Ishii, N.; Saeki, A.; Seki, S.; Tagawa, S.; Taniguchi, M.; Kawai, T.; Aida, T. *Science* **2006**, *314*, 1761-1764.

(94) van de Craats, A. M.; Warman, J. M.; Mullen, K.; Geerts, Y.; Brand, J. D. *Adv. Mater.* **1998**, *10*, 36-38.

(95) Van De Craats, A. M.; Warman, J. M.; Fechtenktter, A.; Brand, J. D.; Harbison, M. A.; Mullen, K. *Adv. Mater.* **1999**, *11*, 1469-1472.

(96) Hill, J. P.; Jin, W.; Kosaka, A.; Fukushima, T.; Ichihara, H.; Shimomura, T.; Ito, K.; Hashizume, T.; Ishii, N.; Aida, T. *Science* **2004**, *304*, 1481-1483.

(97) Wurthner, F. *Chem. Commun.* **2004**, 1564-1579.

(98) Schmidt-Mende, L.; Fechtenkotter, A.; Mullen, K.; Moons, E.; Friend, R.; H.; MacKenzie, J. D. *Science* **2001**, *293*, 1119-1122.

(99) Peeters, E.; Van Hal, P. A.; Meskers, S. C. J.; Janssen, R. A. J.; Meijer, E. W. *Chem. Eur. J.* **2002**, *8*, 4470-4474.

(100) Law, K. Y. *Chem. Rev.* **1993**, *93*, 449-486.

(101) Muthukumaran, K.; Loewe, R. S.; Kirmaier, C.; Hindin, E.; Schwartz, J. K.; Sazanovich, I. V.; Diers, J. R.; Bocian, D. F.; Holten, D.; Lindsey, J. S. *J. Phys. Chem. B* **2003**, *107*, 3431-3442.

(102) Van der Boom, T.; Hayes, R. T.; Zhao, Y.; Bushard, P. J.; Weiss, E. A.; Wasielewski, M. R. *J. Am. Chem. Soc.* **2002**, *124*, 9582-9590.

(103) Schenning, A. P. H.; Herrikhuyzen, J. V.; Jonkheijm, P.; Chen, Z.; Wurthner, F.; Meijer, E. W. *J. Am. Chem. Soc.* **2002**, *124*, 10252-10253.

(104) Chesterfield, R. J.; McKeen, J. C.; Newman, C. R.; Ewbank, P. C.; da Silva Filho, D. A.; Bredas, J. L.; Miller, L. L.; Mann, K. R.; Frisbie, C. D. *J. Phys. Chem. B* **2004**, *108*, 19281-19292.

(105) Chesterfield, R. J.; McKeen, J. C.; Newman, C. R.; Frisbie, C. D.; Ewbank, P. C.; Mann, K. R.; Miller, L. L. *J. Appl. Phys.* **2004**, *95*, 6396-6405.

(106) Malenfant, P. R. L.; Dimitrakopoulos, C. D.; Gelorme, J. D.; Kosbar, L. L.; Graham, T. O.; Curioni, A.; Andreoni, W. *Appl. Phys. Lett.* **2002**, *80*, 2517-2519.

(107) Horowitz, G.; Kouki, F.; Spearman, P.; Fichou, D.; Nogues, C.; Pan, X.; Garnier, F. *Adv. Mater.* **1996**, *8*, 242-245.

(108) Langhals, H. *Heterocycles* **1995**, *40*, 477-500.

(109) Zollinger, H. *Color Chemistry,* **2003**.

(110) Herbst, W.; Hunger, K. *Industrial Organic Pigments: Production, Properties, Applications,* **1997**.

(111) Lee, S. K.; Zu, Y.; Herrmann, A.; Geerts, Y.; Mullen, K.; Bard, A. J. *J. Am. Chem. Soc.* **1999**, *121*, 3513-3520.

(112) Dimitrakopoulos, C. D.; Malenfant, P. R. L. *Adv. Mater.* **2002**, *14*, 99-117.

(113) Struijk, C. W.; Sieval, A. B.; Dakhorst, J. E. J.; van Dijk, M.; Kimkes, P.; Koehorst, R. B. M.; Donker, H.; Schaafsma, T. J.; Picken, S. J.; van de Craats, A. M.; Warman, J. M.; Zuihof, H.; Sudholter, E. J. R. *J. Am. Chem. Soc.* **2000**, *122*, 11057-11066.

(114)   Langhals, H. *Chem. Ber.* **1985**, *118*, 4641-4645.

(115)   Langhals, H. *Helv. Chim. Acta* **2005**, *88*, 1309-1343.

(116)   Langhals, H.; Jaschke, H.; Ring, U.; von Unold, P. *Angew. Chem., Int. Ed.* **1999**, *38*, 201-203.

(117)   Troster, H. *Dyes Pigm.* **1983**, *4*, 171-177.

(118)   Kaiser, H.; Lindner, J.; Langhals, H. *Chem. Ber.* **1991**, *124*, 529-535.

(119)   Nagao, Y.; Misono, T. *Bull.Chem.Soc.Jpn.* **1981**, *54*, 1269-1270.

(120)   Nagao, Y.; Tanabe, Y.; Misono, T. *Nippon Kagaku Kaishi* **1979**.

(121)   Seybold, G.; Wagenblast, G. *Dyes Pigm.* **1989**, *11*, 303-317.

(122)   Sandrai, M.; Hadel, L.; Sauers, R. R.; Husain, S.; Krogh-Jespersen, K.; Westbrook, J. D.; Bird, G. R. *J. Phys. Chem.* **1992**, *96*, 7988-7996.

(123)   Bohm, A.; Arms, H.; Henning, G.; Blaschka, P.; German Pat, n. *Chem. Abstr.* **1997**, *127*, 96569g.

(124)   Rohr, U.; Kohl, C.; Mullen, K.; van de Craats, A.; Warman, J. *J. Mater. Chem.* **2001**, *11*, 1789-1799.

(125)   Rohr, U.; Schlichting, P.; Bohm, A.; Gross, M.; Meerholz, K.; Bruchle, C.; Mullen, K. *Angew. Chem., Int. Ed.* **1998**, *37*, 1434-1437.

(126)   Wurthner, F.; Stepaneko, V.; Chen, Z.; Saha-Moller, C.; Kocher, N.; Stalke, D. *J. Org. Chem.* **2004**, *69*, 7933-7939.

(127)   Fan, L.; Xu, X.; Tian, H. *Tetrahedron Lett.* **2005**, *46*, 4443-4447.

(128)   Chao, C. C.; Leung, M.; Su, Y. O.; Chiu, K. Y.; Lin, T. H.; Shieh, S. J.; Lin, S. C. *J. Org. Chem.* **2005**, *70*, 4323-4331.

(129)   Ahrens, M. J.; Fuller, M. J.; Wasielewski, M. R. *Chem. Mater.* **2003**, *15*, 2684-2686.

(130)   Zhao, Y.; Wasielewski, M. R. *Tetrahedron Lett.* **1999**, *40*, 7047-7050.

(131)   Lukas, A. S.; Zhao, Y.; Miller, S. E.; Wasielewski, M. R. *J. Phys.Chem. B* **2002**, *106*, 1299-1306.

(132) Chen, S.; Liu, Y.; Qiu, W.; Sun, X.; Ma, Y.; Zhu, D. *Chem.Mater.* **2005**, *17*, 2208-2215.

(133) Klok, H. A.; Becker, S.; Schuch, F.; Pakula, T.; Müllen, K. *Macromol. Chem. Phys.* **2002**, *203*, 1106-1113.

(134) Qu, J.; Zhang, J.; Grimsdale, A. C.; Mullen, K.; Jaiser, F.; Yang, X.; Neher, D. *Macromol.* **2004**, *37*, 8297-8306.

(135) Rademacher, A.; Markle, S.; Langhals, H. *Chem. Ber.* **1982**, *115*, 2927.

(136) Wurthner, F.; Thalacker, C.; Diele, S.; Tschierske, C. *Chem. Eur. J.* **2001**, *7*, 2245-2253.

(137) Gvishi, R.; Reisfeld, R.; Burshtein, Z. *Chem. Phys. Lett.* **1993**, *213*, 338-344.

(138) Klebe, G.; Graser, F.; Hadicke, E.; Berndt, J. *Acta Crystallogr.* **1989**, *B45*, 69-77.

(139) Hadicke, E. H.; Graser, F. *Acta Crystallogr., Sect. C: Cryst. Struct. Commun.* **1986**, *C42*, 189-195.

(140) Kazmaier, P. M.; Hoffmann, R. *J. Am. Chem. Soc.* **1994**, *116*, 9684-9691.

(141) Balakrishnan, K.; Datar, A.; Naddo, T.; Huang, J.; Oitker, R.; Yen, M.; Zhao, J.; Zang, L. *J. Am. Chem. Soc.* **2006**, *128*, 7390-7398.

(142) Balakrishnan, K.; Datar, A.; Oitker, R.; Chen, H.; Zuo, J.; Zang, L. *J. Am. Chem. Soc.* **2005**, *127*, 10496-10497.

(143) Chen, Z.; Baumeister, U.; Tschierske, C.; Wurthner, F. *Chem. Eur. J.* **2007**, *13*, 450-465.

(144) Chen, Z.; Debije, M. S.; Debaerdemaeker, T.; Osswald, P.; Wurthner, F. *ChemPhysChem* **2004**, *5*, 137-140.

(145) Wurthner, F.; Sautter, A.; Schilling, J. *J. Org. Chem.* **2002**, *67*, 3037-3044.

(146) Jones, B. A.; Facchetti, A.; Wasielewski, M. R.; Marks, T. J. *J. Am. Chem. Soc.* **2007**, *129*, 15259-15278.

(147) Zugenmaier, P.; Duff, J.; Bluhm, T. L. *Cryst. Res. Technol.* **2000**, *35*, 1095-1115.

(148) Dehm, V.; Chen, Z.; Baumeister, U.; Prins, P.; Siebbeles, L. D. A.; Wuerthner, F. *Org. Lett.* **2007**, *9*, 1085-1088.

(149) Che, Y.; Datar, A.; Balakrishnan, K.; Zang, L. *J. Am. Chem. Soc.* **2007**, *129*, 7234-7235.

(150) Che, Y.; Yang, X.; Liu, G.; Yu, C.; Ji, H.; Zuo, J.; Zhao, J.; Zang, L. *J. Am. Chem. Soc.* **2010**, *132*, 5743-5750.

(151) Che, Y.; Yang, X.; Balakrishnan, K.; Zuo, J.; Zang, L. *Chem.Mater.* **2009**, *21*, 2930-2934.

(152) Datar, A.; Oitker, R.; Zang, L. *Chem. Commun.* **2006**, 1649-1651.

(153) De Luca, G.; Liscio, A.; Maccagnani, P.; Nolde, F.; Palermo, V.; Müllen, K.; Samorì, P. *Adv. Funct. Mater.* **2007**, *17*, 3791-3798.

(154) Oh, J. H.; Lee, H. W.; Mannsfeld, S.; Stoltenberg, R. M.; Jung, E.; Jin, Y. W.; Kim, J. M.; Yoo, J. B.; Bao, Z. N. *Proc. Natl. Acad. Sci.* **2009**, *106*, 6065-6070.

(155) Luo, Y.; Lin, J.; Duan, H.; Zhang, J.; Lin, C. *Chem.Mater.* **2005**, *17*, 2234-2236.

(156) Lu, Y.; Huisheng, P.; Kun, H.; Joel, T. M.; Hexing, L.; Yunfeng, L. *Adv. Funct. Mater.* **2008**, *18*, 1536-1535.

(157) Ren, X.; Sun, B.; Tsai, C.-C.; Tu, Y.; Leng, S.; Li, K.; Kang, Z.; Horn, R. M. V.; Li, X.; Zhu, M.; Wesdemiotis, C.; Zhang, W.-B.; Cheng, S. Z. D. *J.Phys. Chem. B* **2010**, *114*, 4802-4810.

(158) Yu, L.; Ke-Rang, W.; Dong-Sheng, G.; Bang-Ping, J. *Adv. Funct. Mater.* **2009**, *19*, 2230-2235.

(159) Theo , E. K.; Hao, W.; Vladimir, S.; Frank, W. *Angew. Chem., Int. Ed.* **2007**, *46*, 5541-5544.

(160) Wurthner, F.; Thalacker, C.; Sautter, A.; Schartl, W.; Ibach, W.; Hollricher, O. *Chem. Eur. J.* **2000**, *6*, 3871-3886.

(161) Liu, Y.; Xiao, S.; Li, H.; Li, Y.; Liu, H.; Lu, F.; Zhuang, J.; Zhu, D. *J.Phys. Chem. B* **2004**, *108*, 6256-6260.

(162) Yang, L.; Junpeng, Z.; Huibiao, L.; Yuliang, L.; Fushen, L.; Haiyang, G.; Tonggang, J.; Ning, W.; Xiaorong, H.; Daoben, Z. *ChemPhysChem* **2004**, *5*, 1210-1215.

(163) Marta , E. C.-V.; Wende, X.; Daniel, W.; Klaus, M.; Harald, B.; Johannes , V. B.; Roman, F. *Angew. Chem. Int. Ed.* **2007**, *46*, 1814-1818.

(164) Syamakumari, A.; Schenning, A. P. H. J.; Meijer, E. W. *Chem.Eur. J.* **2002**, *8*, 3353-3361.

(165) Liu, Y.; Li, Y.; Jiang, L.; Gan, H.; Liu, H.; Li, Y.; Zhuang, J.; Lu, F.; Zhu, D. *The J. Org. Chem.* **2004**, *69*, 9049-9054.

(166) Jancy, B.; Asha, S. K. *Chem. Mater.* **2008**, *20*, 169-181.

(167) Shiki, Y.; Tomohiro, S.; Takashi, K.; Akihide, K.; Frank, W. *Angew. Chem. Int. Ed.* **2008**, *47*, 3367-3371.

(168) Dobrawa, R.; Wurthner, F. *Chem. Commun.* **2002**, 1878-1879.

(169) Frank, W.; Vladimir, S.; Armin, S. *Angew. Chem. Int. Ed.* **2006**, *45*, 1939-1942.

(170) You, C.-C.; Wurthner, F. *J.Am.Chem.Soc.* **2003**, *125*, 9716-9725.

(171) Chang-Cheng, Y.; Catharina, H.; Matthias, G.; Frank, W. *Chem. Eur. J.* **2006**, *12*, 7510-7519.

(172) Guan, Y.; Zakrevskyy, Y.; Stumpe, J.; Antonietti, M.; Faul, C. F. J. *Chem. Commun.* **2003**, 894-895.

(173) Ying, G.; Shu-Hong, Y.; Markus, A.; Christoph, B.; Charl, F. J. F. *Chem. Eur. J.* **2005**, *11*, 1305-1311.

(174) Franke, D.; Vos, M.; Antonietti, M.; Sommerdijk, N. A. J. M.; Faul, C. F. J. *Chem. Mater.* **2006**, *18*, 1839-1847.

(175) Ma, T.; Li, C.; Shi, G. *Langmuir* **2007**, *24*, 43-48.

(176) Xie, A.; Liu, B.; Hall, J. E.; Barron, S. L.; Higgins, D. A. *Langmuir* **2005**, *21*, 4149-4155.

(177) Everett, T. A.; Twite, A. A.; Xie, A.; Battina, S. K.; Hua, D. H.; Higgins, D. A. *Chem. Mater.* **2006**, *18*, 5937-5943.

(178) Popovic, Z. D.; Loutfy, R. O.; Hor, A.-M. *Can. J. Phys.* **1985**, *63*, 134.

(179) Wurthner, F.; Sautter, A.; Schmid, D.; Weber, P. J. A. *Chem. Eur. J.* **2001**, *7*, 894-902.

(180) Zang, L.; Che, Y.; Moore, J. S. *Acc. Chem. Res.* **2008**, *41*, 1596-1608.

(181) Spillmann, C. M.; Naciri, J.; Anderson, G. P.; Chen, M.-S.; Ratna, B. R. *ACS Nano* **2009**, *3*, 3214-3220.

(182) Zhang, X.; Rehm, S.; Safont-Sempere, M. M.; Wurthner, F. *Nature Chem.* **2009**, *1*, 623-629.

(183) Che, Y.; Yang, X.; Loser, S.; Zang, L. *Nano Lett.* **2008**, *8*, 2219-2223.

(184) Bao, Z. L., J., *Organic Field-Effect Transistors.* CRC Press, Boca Raton, FL **2007**.

(185) Vura-Weis, J.; Ratner, M. A.; Wasielewski, M. R. *J.Am.Chem.Soc.***2010**, *132*, 1738-1739.

(186) Delgado, M. C. R.; Kim, E.-G.; Filho, D. A. d. S.; Bredas, J.-L. *J.Am.Chem.Soc.* **2010**, *132*, 3375-3387.

(187) Wurthner, F.; Chen, Z.; Dehm, V.; Stepanenko, V. *Chem. Commun.* **2006**, 1188-1190.

(188) Suhrit, G.; Xue-Qing, L.; Vladimir, S.; Frank, W. *Chem. Eur. J.* **2008**, *14*, 11343-11357.

(189) Zhijian, C.; Ute, B.; Carsten, T.; Wurthner, F. *Chem. Eur. J.* **2007**, *13*, 450-465.

(190) Zhijian, C.; Vladimir, S.; Volker, D.; Paulette, P.; Laurens , D. A. S.; Joachim, S.; Philipp, M.; Volker, E.; Frank, W. *Chem. Eur. J.* **2007**, *13*, 436-449.

(191) Xue-Qing, L.; Xin, Z.; Suhrit, G.; Wurthner, F. *Chem. Eur. J* **2008**, *14*, 8074-8078.

(192) Langhals, H.; Krotz, O.; Polborn, K.; Mayer, P. A. *Angew. Chem., Int. Ed.* **2005**, *44*, 2427-2428.

(193) Seibt, J.; Winkler, T.; Renziehausen, K.; Dehm, V.; Wurthner, F.; Meyer, H. D.; Engel, V. *J. Phys. Chem. A* **2009**, *113*, 13475-13482.

(194) Wurthner, F. *Pure Appl. Chem.* **2006**, *78*, 2341-2350.

(195) Yagai, S.; Seki, T.; Karatsu, T.; Kitamura, A.; Wurthner, F. *Angew. Chem., Int. Ed.* **2008**, *47*, 3367-3371.

(196) Cicoira, F.; Santato, C.; Rosei, F. *Top. Curr. Chem.* **2008**, *285*, 203-267.

(197) Piot, L.; Silly, F.; Tortech, L.; Nicolas, Y.; Blanchard, P.; Roncali, J.; Fichou, D. *J. Am. Chem. Soc.* **2009**, *131*, 12864-12865.

(198) Barth, J. V.; Costantini, G.; Kern, K. *Nature* **2005**, *437*, 671-679.

(199) Xu, L. P.; Yan, C. J.; Wan, L. J.; Jiang, S. G.; Liu, M. H. *J. Phys. Chem. B* **2005**, *109*, 14773-14778.

(200) Mougous, J. D.; Brackley, A. J.; Foland, K.; Backer, R. T.; Patrick, D. L. *Phys.Rev.Lett.* **2000**, *84*, 2742-2745.

(201) Piot, L.; Marchenko, A.; Wu, J.; Mullen, K.; Fichou, D. *J. Am. Chem. Soc.* **2005**, *127*, 16245-16250.

(202) Lei, S.; Tahara, K.; Schryver, D.; C., F.; Van der Auweraer, M.; Tobe, Y.; De Feyter, S. *Angew. Chem. Int. Ed.* **2008**, *47*, 2964-2968.

(203) Li, C. J.; Zeng, Q. D.; Liu, Y. H.; Wan, L. J.; Wang, C.; Wang, C. R.; Bai, C. L. *ChemPhysChem* **2003**, *4*, 857-859.

(204) Treossi, E.; Liscio, A.; Feng, X.; Palermo, V.; Mullen, K.; Samori, P. *Small* **2009**, *5*, 112-119.

(205) Lei, Y.; Liao, Q.; Fu, H.; Yao, J. *J. Phys. Chem. C* **2009**, *113*, 10038-10043.

(206) Forrest, S. R. *Chem. Rev.* **1997**, *97*, 1793-1896.

(207) van Hameren, R.; Schoen, P.; van Buul, A. M.; Hoogboom, J.; Lazarenko, S. V.; Gerritsen, J. W.; Engelkamp, H.; Christianen, P. C. M.; Heus, H. A.; Maan, J. C.; Rasing, T.; Speller, S.; Rowan, A. E.; Elemans, J. A. A. W.; Nolte, R. J. M. *Science* **2006**, *314*, 1433.

(208) Treier, M.; Nguyen, M.-T.; Richardson, N. V.; Pignedoli, C.; Passerone, D.; Fasel, R. *Nano Lett.* **2008**, *9*, 126-131.

(209) Suen, S.-C.; Whang, W.-T.; Hou, F.-J.; Dai, B.-T. *Org. Elect.* **2007**, *8*, 505-512.

(210) Ostrick, J. R.; Dodabalapur, A.; Torsi, L.; Lovinger, A. J.; Kwock, E. W.; Miller, T. M.; Galvin, M.; Berggren, M.; Katz, H. E. *J. Appl. Phys.* **1997**, *81*, 6804-6808.

(211) A. Tekiel; S. Godlewski; J. Budzioch; M. Symonski *Nanotechnol.* **2008**, *19*, 495304.

(212) M. Eremtchenko; J. A. Schaefer; Tautz, F. S. *Nature* **2003**, *425*, 602-605.

(213) Sarah, A. B.; Jeffrey, M. L.; Jessica, M. T.; Shawn, F.; Peter, G. *Adv. Mater.* **2009**, *21*, 2029-2033.

(214) Liu, H.; Li, Y.; Xiao, S.; Gan, H.; Jiu, T.; Li, H.; Jiang, L.; Zhu, D.; Yu, D.; Xiang, B.; Chen, Y. *J. Am. Chem. Soc.* **2003**, *125*, 10794-10795.

(215) S. Liu; W. M. Wang; A. L. Briseno; S. C. B. Mannsfeld; Bao, Z. *Adv. Mater.* **2009**, *21*, 1217-1232.

(216) R. W. I. d. Boer; M. E. Gershenson; A. F. Morpurgo; Podzorov, V. *physi. status solidi* **2004**, *201*, 1302-1331.

(217) V. Podzorov; S. E. Sysoev; E. Loginova; V. M. Pudalov; Gershenson, M. E. *Appl. Phys. Lett.* **2003**, *83*, 3504-3506.

(218) A. F. Stassen; R. W. I. de Boer; N. N. Iosad; Morpurgo, A. F. *Appl. Phys. Lett.* **2004**, *85*, 3899-3901.

(219) J.-R. Li; Y. Tao; Q. Yu; Bu, X.-H. *Cryst. Growth Des.* **2006**, *6*, 2493-2500.

(220) Ferrere, S.; Zaban, A.; Gregg, B. A. *J. Phys. Chem. B* **1997**, *101*, 4490-4493.

(221) Mikolajczyk, M.; Kielbasinski, P. *Tetrahedron* **1981**, *37*, 233-284.

(222) Williams, A.; Ibrahim, I. T. *Chem. Rev.* **1981**, *81*, 589-636.

(223) Moore, J. S.; Stupp, S. I. *Macromol.* **1990**, *23*, 65-70.

(224) DeTar, D. F.; Silverstein, R. *J. Am. Chem. Soc.* **1966**, *88*, 1013-1019.

(225) Hara, M.; Satoh, A.; Takami, N.; Ohsaki, T. *J. Phys. Chem.* **1995**, *99*, 16338-16343.

(226) Silly, F.; Weber, U. K.; Shaw, A. Q.; Burlakov, V. M.; Castell, M. R.; Briggs, G. A. D.; Pettifor, D. G. *Phys. Rev. B* **2008**, *77*, 201408.

(227) Kafer, D.; El Helou, M.; Gemel, C.; Witte, G. *Cryst. Growth Des.* **2008**, *8*, 3053-3057.

(228) Huang, M.; Schilde, U.; Kumke, M.; Antonietti, M.; Colfen, H. *J. Am. Chem. Soc.* **2010**, *132*, 3700-3707.

(229) Fu, G.; Wang, M.; Wang, Y.; Xia, N.; Zhang, X.; Yang, M.; Zheng, P.; Wang, W.; Burger, C. *New Journal of Chemistry* **2009**, *33*, 784-792.

(230) Huang, Y.; Quan, B.; Wei, Z.; Liu, G.; Sun, L. *J. Phys. Chem. C* **2009**, *113*, 3929-3933.

(231) Kang, L.; Wang, Z.; Cao, Z.; Ma, Y.; Fu, H.; Yao, J. *J. Am. Chem. Soc.* **2007**, *129*, 7305-7312.

(232) Weiss, C.; Wagner, C.; Temirov, R.; Tautz, F. S. *J. Am. Chem. Soc.* **2010**, *132*, 11864-11865.

(233) Lee, H. M.; Tarakeshwar, P.; Park, J.; Koaski, M. R.; Yoon, Y. J.; Yi, H.-B.; Kim, W. Y.; Kim, K. S. *J. Phys. Chem. A* **2004**, *108*, 2949-2958.

(234) Glendening, E. D.; Feller, D. *J. Phys. Chem.* **1995**, *99*, 3060-3067.

(235) Bock, H.; Gharagozloo-Hubmann, K.; Sievert, M.; Prisner, T.; Havlas, Z. *Nature* **2000**, *404*, 267-269.

Appendices

Appendix A. Abbreviations used

PTCDA : Perylene-3,4,9,10-tetracarboxylic dianhydride

PTCDI : Perylene-3,4,9,10-tetracarboxylic diimides

m-PTCI : Perylene-3,4,9,10-tetracarboxylic monoanhydride monoimides

PTCA : Perylene-3,4,9,10-tetracarboxylic acid

DPTS : 4-(dimethylamino) pyridinium 4-toluene sulfonate (DPTS)

DIPC : N,N'-diisopropylcarbodiimide

K_4-PTCA : Tetrapotassium salt of perylene-3,4,9,10-tetracarboxylic acid

Li_4-PTCA : Tetralithium salt of perylene-3,4,9,10-tetracarboxylic acid

Na_4-PTCA : Tetrasodium salt of perylene-3,4,9,10-tetracarboxylic acid

K_2-PTCA : Dipotassium salt of perylene-3,4,9,10-tetracarboxylic acid

2L-RT : Two layer phase transfer at room temperature

2L-HT : Two layer phase transfer at high temperature

SEM : Scanning electron microscopy

TEM : Transmission electron microscopy

XRD : X-Ray diffraction

SAED : Single area electron diffraction

FTIR : Fourier transform infrared spectroscopy

TEM : Transmission electron microscopy